UNIVERSITY OF OKLAHOMA

GRADUATE COLLEGE

FIBER-OPTIC INFRARED SPECTROELECTROCHEMISTRY OF SOME DINITROSYL IRON PHOSPHINE COMPLEXES AND AN NMR KINETICS AND EQUILIBRIUM STUDY OF AN ORGANIC NITROSO COMPOUND IN VARIOUS SOLVENTS

A DISSERTATION

SUBMITTED TO THE GRADUATE FACULTY

in partial fulfillment of the requirements for the

Degree of

DOCTOR OF PHILOSOPHY

By

MYRON WAYNE JONES
Norman, Oklahoma
2010

Downloaded from SHAREOK. Persistent Handle URL: https://hdl.handle.net/11244/319209

FIBER-OPTIC INFRARED SPECTROELECTROCHEMISTRY OF SOME DINITROSYL IRON PHOSPHINE COMPLEXES AND AN NMR KINETICS AND EQUILIBRIUM STUDY OF AN ORGANIC NITROSO COMPOUND IN VARIOUS SOLVENTS

A DISSERTATION APPROVED FOR THE
DEPARTMENT OF CHEMISTRY AND BIOCHEMISTRY

BY

_____
Dr. George B. Richter-Addo, Chair

_____
Dr. Richard W. Taylor

_____
Dr. C. Leroy Blank

_____
Dr. Robert L. White

_____
Dr. Mark A. Nanny

© Copyright by MYRON WAYNE JONES 2010
All Rights Reserved.

In Memory of My Grandfather

Wilson Jones

(1924 - 2005)

Acknowledgments

It would not have been possible for me to complete this work without the support of many individuals along the way. It would certainly be proper to thank each of them individually, but it is only possible to acknowledge a small fraction of them here.

First, I would like to thank God for blessing me with my life and my family. I know that it is only through his grace that I am able to do anything at all. Thanks to my son Solomon and my daughter Elizabeth for putting up with those times Dad was not able to be with you. I love you both. Thanks to my wife of 14 years. Laura, I truly appreciate all your sacrifices and for helping me to stay the course. I love you. I could not have done this without you.

I would like to express my sincere appreciation to my research advisor and Ph.D. advisory committee chair, Dr. George B. Richter-Addo. Thank-you for your guidance and support over the years I've spent at OU. I know that I will continue to benefit from your counsel as my career progresses in the future.

Thank-you to Drs. Richard W. Taylor, C. Leroy Blank, Robert L. White, Mark A. Nanny and Melissa M. Rieger for serving on my advisory committee. Counsel from each one of you has at one time or another been instrumental in guiding me through the Ph.D. program. I truly appreciate your invaluable help.

Thank-you to Dr. Douglas Powell for the X-ray analyses he provided on my compounds. Thanks to Dr. Susan Nimmo for assistance with my variable temperature NMR experiments. Thanks to Jim Cornell for making some of my custom glassware.

Thanks to the Department of Chemistry and Biochemistry for providing me with financial support in the form of teaching assistantships and as a United States Department

of Education GAANN fellow. Thanks to the National Science Foundation (NSF) and the National Institutes of Health (NIH) for funding which made much of this work possible.

I would be remiss if I did not also thank my former advisors Drs. Gregory J. Grant of the University of Tennessee at Chattanooga, Gregory H. Robinson of the University of Georgia (formerly at Clemson University) and Gary P. Wulfsberg of Middle Tennessee State University. I am grateful to have had these professors as my mentors. I thank each one of them for their valuable influence on my career path.

Thanks to the faculty and students of the department's Analytical Divison. I am glad I chose to be among such great people. Thanks to Dr. Glenn Dryhurst for his thought provoking questions during Analytical seminar. Thanks to all the members of Dr. Richter-Addo's research group with whom I've worked (past and present) including: Dr. Lin Cheng, Dr. Li Chen, Dr. Jonghyuk Lee, Dr. Shawn Carter, Dr. Dan Copeland, Keeshaloy Thompson, Dr. Nan Xu, Dr. Lillian Chooback, Dr. Zaki Zahran, Dr. Jun Yi, Dr. Carolina Salazar-Ballesteros, Christal Sohl, Adam Warhausen, Victoria Nittler, Adam Campbell, Ye Guan, Dennis Awasabisah and our groups collaborator Dr. Michael J. Shaw of Southern Illinois University – Edwardsville. My interactions with each one of these individuals have been priceless. I am glad to know all of them as my friends.

Thanks to my in-laws Dr. Charles and Ms. Helen Bailey for all they have done to support my family and me during our time here in Oklahoma. Thanks to my brother-in-law Omari. Thanks to my sisters Carlotta and Heather. I hope you both know that I love and admire you. Thanks to my Grandparents the late Wilson Jones, Billie L. Jones and Arizola Welch. And finally, thanks to my parents Rev. E. Wayne and Annie L. Jones. Your love and unwavering support has meant the world to me.

Table of Contents

Chapter 1. Introduction 1

Chapter 2. Fiber-optic Infrared Reflectance Spectroelectrochemical Studies of Some Dinitrosyl Iron Diphosphine Complexes, $Fe(NO)_2L_2$ ($L = P(C_6H_4X)_3$)

2.1. Introduction 5

2.2. Experimental 8

2.2.1 General 8

2.2.2 Chemicals 9

2.2.3 Instrumentation 9

2.2.4 Synthesis 10

2.2.4.1 $Fe(NO)_2(P(C_6H_4$-*p*-$OCH_3)_3)_2$ 11

2.2.4.2 $Fe(NO)_2(P(C_6H_4$-*p*-$CH_3)_3)_2$ 11

2.2.4.3 $Fe(NO)_2(P(C_6H_4$-*m*-$CH_3)_3)_2$ 12

2.2.4.4 $Fe(NO)_2(PPh_3)_2$ 12

2.2.4.5 $Fe(NO)_2(P(C_6H_4$-*p*-$F)_3)_2$ 12

2.2.4.6 $Fe(NO)_2(P(C_6H_4$-*p*-$Cl)_3)_2$ 13

2.2.4.7 $Fe(NO)_2(P(C_6H_4$-*p*-$CF_3)_3)_2$ 13

2.2.5 X-ray Crystallography 14

2.2.5.1 $Fe(NO)_2(P(C_6H_4$-*p*-$OCH_3)_3)_2$ 14

2.2.5.2 $Fe(NO)_2(P(C_6H_4$-*p*-$CH_3)_3)_2$ 15

2.2.5.3 $Fe(NO)_2(P(C_6H_4$-*p*-$F)_3)_2$ 16

2.2.5.4 $Fe(NO)_2(P(C_6H_4$-*p*-$Cl)_3)_2$ 16

2.2.5.5 $Fe(NO)_2(P(C_6H_4$-*p*-$CF_3)_3)_2$ 17

2.3. Results 19

2.3.1 Synthesis 19

2.3.2 Infrared Spectroscopy 20

2.3.3 ^{31}P NMR Spectroscopy 25

2.3.4 X-ray crystallography 27

2.3.5 Electrochemistry 34

2.3.6 Infrared Spectroelectrochemistry 38

2.4. Discussion 42

2.4.1 Synthesis 42

2.4.2 Infrared Spectroscopy 43

2.4.3 ^{31}P NMR spectroscopy 55

2.4.4 X-ray Crystallography 59

2.4.5 Electrochemistry 62

2.4.6 Infrared Spectroelectrochemistry 65

2.5. Conclusion 66

2.6. References 69

Chapter 3. The Behavior of 2-Methyl-2-nitrosopropane in Several Solvents: A Kinetics and Equilibrium Study Using ^{1}H NMR Spectroscopy

3.1. Introduction 76

3.2. Experimental 79

3.2.1 Chemicals 79

3.2.2 Instrumentation 79

3.2.3 Variable Temperature NMR in Different Solvents 80

3.3. Results 81

3.3.1 Equilibrium Constants for the Dissociation of the 2-Methyl-2-Nitrosopropane Dimer in Various Solvents 81

3.3.2 Rate Constants for the Dissociation of 2-Methyl-2-Nitrosopropane Dimer in Various Solvents 88

3.3.3 Calculation of Thermodynamic and Kinetic Parameters. 91

3.4. Discussion 102

3.4.1 Solvent Effects on Equilibrium and Rate Constants 102

3.4.2 Solvent Polarity 104

3.4.3 Correlations with Relative Permittivity, ε_r, (the dielectric constant) 106
3.4.4 Solvatochromism 109
3.4.5 Correlations with the Kosower *Z* scale 109
3.4.6 Correlations with the $E_T(30)$ and E_T^N scales 112
3.4.7 Correlations with the Gutmann Donor Number 115
3.4.8 Correlations with the Gutmann Acceptor Number 119
3.4.9 Kamlet-Taft Analysis 122
3.4.10 Correlations with Thermodynamic and Kinetic Parameters 131
3.5. Conclusion 133
3.6. References 136

Epilogue 142

List of Tables

Table		Page
2.1	Crystallographic Collection and Refinement Parameters for the $Fe(NO)_2(PAr_3)_2$ Products	18
2.2	Colors and Isolated Yields of the $Fe(NO)_2(PAr_3)_2$ Products	20
2.3	Infrared Data for the $Fe(NO)_2(PAr_3)_2$ Products	24
2.4	$^{31}P\{^1H\}$ NMR data for the $Fe(NO)_2(PAr_3)_2$ Products	25
2.5	Selected Bond Angles (°) for the $Fe(NO)_2(PAr_3)_2$ Products	27
2.6	Selected Bond Distances (Å) for the $Fe(NO)_2(PAr_3)_2$ Products	28
2.7	Formal Electrode Potentials (V vs. Fc/Fc^+) and Related Electrochemical Data for the $Fe(NO)_2(PAr_3)_2$ Products in CH_2Cl_2 (scan rate = 0.1 V s^{-1})	36
2.8	Infrared Spectroelectrochemical Data Obtained for the $Fe(NO)_2(PAr_3)_2$ Products in CH_2Cl_2	38
2.9	Hammett Parameters (σ) for Substituents on Substituted PAr_3 and pK_a Values for the Corresponding Acids	44
2.10	Solvent Acceptor and Donor numbers	51
3.1	Equilibrium Constants, K_{eq} (M) for the Dissociation of 2-Methyl-2-Nitrosopropane Dimer in Various Solvents	87
3.2	Rate Constants for the 2-Methyl-2-Nitrosopropane Dimer-Monomer Equilibrium in Various Solvents	90

3.3	Gibbs Free Energies ($\Delta G°$, kJ mol^{-1}) for the Dissociation of 2-Methyl-2-Nitrosopropane Dimer in Various Solvents	92
3.4	Standard Changes in Enthalpy, $\Delta H°$, and Entropy, $\Delta S°$, for the 2-Methyl-2-Nitrosopropane Dimer-Monomer Dissociation Reaction in Various Solvents	94
3.5	Activation Energies for the 2-Methyl-2-Nitrosopropane Dimer-Monomer Dissociation Reaction in Various Solvents	96
3.6	Activation Parameters for the 2-Methyl-2-Nitrosopropane Dimer Monomer Equilibrium in Various Solvents	99
3.7	Free Energies of Activation for the 2-Methyl-2-Nitrosopropane Dimer Monomer Equilibrium in Various Solvents	101
3.8	Relative Permittivity, Viscosity and Various Empirical Scales of Solvent Polarity	105

List of Figures

Figure		Page
2.1	Reaction scheme (unbalanced) depicting the oxidation of bis(nitrosyl) iron dimers by molecular oxygen in the presence of PPh_3 or $OPPh_3$.	6
2.2	Schematic depicting Gadd's proposed intermediate in the photocatalyic dimerization of olefins.	7
2.3	Reaction scheme depicting the formation of the $Fe(NO)_2(PAr_3)_2$ products.	19
2.4	Infrared spectrum of $Fe(NO)_2(CO)_2$ in CH_2Cl_2.	21
2.5	Infrared spectrum of the reaction mixture during the preparation of $Fe(NO)_2(P(C_6H_4\text{-}p\text{-}F)_3)_2$ in toluene prior to full reflux containing a mixture of the mono and disubstituted products.	22
2.6	Infrared spectrum of the reaction mixture during the preparation of $Fe(NO)_2(P(C_6H_4\text{-}p\text{-}F)_3)_2$ in toluene after several hours of reflux.	23
2.7	300 MHz $^{31}P\{^1H\}$ NMR spectrum of $Fe(NO)_2(P(C_6H_4\text{-}p\text{-}F)_3)_2$ in $CDCl_3$.	26
2.8	Molecular structure of $Fe(NO)_2(P(C_6H_4\text{-}p\text{-}OCH_3)_3)_2$.	29
2.9	Molecular structure of $Fe(NO)_2(P(C_6H_4\text{-}p\text{-}CH_3)_3)_2$ showing the relative orientation of the 2 neighboring molecules.	30
2.10	Molecular structure of $Fe(NO)_2(P(C_6H_4\text{-}p\text{-}F)_3)_2$.	31
2.11	Molecular structure of $Fe(NO)_2(P(C_6H_4\text{-}p\text{-}Cl)_3)_2$.	32

2.12	Molecular structure of $Fe(NO)_2(P(C_6H_4\text{-}p\text{-}CF_3)_3)_2$.	33
2.13	Cyclic voltammogram for a 1 mM solution of $Fe(NO)_2(P(C_6H_4\text{-}p\text{-}F)_3)_2$ in CH_2Cl_2 containing 0.1 M NBu_4PF_6 at a scan rate of 200 mV s^{-1}.	34
2.14	Cyclic voltammogram for a 1 mM solution of $Fe(NO)_2(P(C_6H_4\text{-}p\text{-}CF_3)_3)_2$ in CH_2Cl_2 containing 0.1 M NBu_4PF_6 at a scan rate of 200 mV s^{-1}.	35
2.15	Cyclic voltammogram for a 1 mM solution of $Fe(NO)_2(P(C_6H_4\text{-}p\text{-}CF_3)_3)_2$ in CH_2Cl_2 containing 0.1 M NBu_4PF_6 at a scan rate of 100 mV s^{-1}.	37
2.16	Infrared difference spectrum recorded during the oxidation of $Fe(NO)_2(P(C_6H_4\text{-}p\text{-}F)_3)_2$, in CH_2Cl_2 containing 0.1 M $[NBu_4][PF_6]$ at E_{appl} = 0.17 vs. Fc/Fc^+.	39
2.17	Infrared difference spectrum recorded during the oxidation of $Fe(NO)_2(P(C_6H_4\text{-}p\text{-}CF_3)_3)_2$, in CH_2Cl_2 containing 0.1 M $[NBu_4][PF_6]$ at E_{appl} = 0.57 V vs. Fc/Fc^+.	40
2.18	Infrared difference spectrum recorded during the reduction of $Fe(NO)_2(CO)_2$ in CH_2Cl_2 with 0.1 M $[NBu_4][PF_6]$ at E_{appl} = -2.2 V vs. Fc/Fc^+.	41
2.19	A plot depicting how the acid dissociation constant for substituted PAr_3 is linearly related to the Hammett parameter for the substituents on PAr_3.	45
2.20	Plot depicting the symmetric and antisymmetric ν_{NO}s in toluene, CH_2Cl_2 and acetonitrile versus the Hammett substituent parameter.	46
2.21	Schematic depicting metal-ligand back-bonding.	47
2.22	Plots depicting the symmetric and antisymmetric ν_{NO}s for $Fe(NO)_2(PAr_3)_2$ compounds in (a) toluene, (b) CH_2Cl_2 and (c) Acetonitrile vs. the Hammett substituent parameter.	49

2.23	Plots depicting (a) the symmetric and (b) the antisymmetric ν_{NO} for each $Fe(NO)_2(PAr_3)_2$ as a function of solvent acceptor number.	52
2.24	Plots depicting (a) the symmetric ν_{NO} and (b) the antisymmetric ν_{NO} for each $Fe(NO)_2(PAr_3)_2$ as a function of solvent donor number.	53
2.25	Plot depicting the $\delta(^{31}P)$ chemical shifts for each $Fe(NO)_2(PAr_3)_2$ as a function of the Hammett parameter.	55
2.26	Plot depicting the $\delta(^{31}P)$ chemical shifts for each $Fe(NO)_2(PAr_3)_2$ as a function of the Hammett parameter; an alternative correlation for Figure 2.25.	57
2.27	Plot depicting the $\delta(^{31}P)$ chemical shifts for each $Fe(NO)_2(PAr_3)_2$ as a function of the Brown-Okamoto constant σ_p^+.	58
2.28	Schematic depicting *"attracto"* and *"repulso"* conformations of the $Fe(NO)_2$ group.	59
2.29	Plot depicting $E°'$ for each $Fe(NO)_2(PAr_3)_2$ as a function of the Hammett parameter.	63
2.30	Plot depicting $E°'$ for each $Fe(NO)_2(PAr_3)_2$ as a function of the Brown-Okamoto constant σ_p^+.	64
3.1	Schematic depicting some reactions of nitric oxide with metals and with representative organic fragments.	76
3.2	General equation for an RNO dimer-monomer equilibrium in solution.	77
3.3	^1H NMR spectrum showing peaks for the dimeric and monomeric species at 20 °C in acetonitrile at time 218 s (~3.6 min).	81

3.4	Concentration (M) vs. time (s) traces for the monomer and dimer in acetonitrile at 20°C.	82
3.5	First derivative of the concentration (M) vs. time (s) traces for the monomer and dimer in acetonitrile at 20°C.	84
3.6	A plot of ln K_{eq} versus $1/T$ (Equation 19) for the 2-methyl-2-nitrosopropane dimer-monomer dissociation reaction in acetonitrile.	93
3.7	A plot of ln k versus $1/T$ (Equation 21) for the 2-methyl-2-nitrosopropane dimer-monomer dissociation reaction in acetonitrile.	95
3.8	Free energy reaction coordinate diagram.	97
3.9	A plot of ln (k/T) versus $1/T$ (Equation 23) for the 2-methyl-2-nitrosopropane dimer-monomer dissociation reaction in acetonitrile.	98
3.10	Plot of log K_{eq} (20 °C) versus ε_r.	106
3.11	Plot of log k_1 (20 °C) versus ε_r.	107
3.12	Plot of log K_{eq} (20 °C) versus Z.	110
3.13	Plot of log k_1 (20 °C) versus Z.	111
3.14	Plot of log K_{eq} (20 °C) versus E_T^N.	113
3.15	Plot of log k_1 (20 °C) versus E_T^N.	114
3.16	Plot of log K_{eq} (20 °C) versus DN.	115
3.17	Plot of log k_1 (20 °C) versus DN.	116
3.18	Plot of log k_{-1} (20 °C) versus DN.	118

3.19	Plot of log K_{eq} (20 °C) versus AN.	119
3.20	Plot of log k_1 (20 °C) versus AN.	120
3.21	Plot of log k_{-1} (20 °C) versus AN.	121
3.22	Plot of the experimentally determined log k_1 versus the calculated value.	124
3.23	Plot of log k_{-1} (20 °C) versus the solvent viscosity.	127
3.24	Plot of the experimentally determined log k_{-1} versus the calculated value.	128
3.25	Plot of the experimentally determined log K_{eq} versus the calculated value.	131
3.26	Plot of the entropy of activation versus the enthalpy of activation.	132
3.27	Plot of Gibbs free energy of activation versus the solvent acceptor number.	133

Abstract

This dissertation describes a study of some of the fundamental chemical properties of some dinitrosyl iron phosphine complexes and a study of the dimer-monomer equilibrium of 2-methyl-2-nitrosopropane in various solvents.

Chapter 2 describes the study of some dinitrosyl iron phosphine complexes. Dinitrosyl iron complexes (DNICs) have been invoked as viable entities that contribute towards the biological action of nitric oxide (NO). DNICs derive their basic functionality from the dinitrosyl $Fe(NO)_2$ moiety. Thus, it is important to understand how ancillary ligands bound to the metal affect the fundamental properties of the $Fe(NO)_2$ unit. We have prepared a homologous series of dinitrosyl iron phosphine complexes and characterized them by FTIR and ^{31}P NMR spectroscopy, X-ray crystallography, cyclic voltammetry and fiber-optic infrared spectroelectrochemistry. We then determine and explain the observed trends in the data as a function of phosphine substitution.

Chapter 3 describes the study of a *C*-nitroso compound, namely the dimeric 2-methyl-2-nitrosopropane, in various solvents. Interest in the fundamental properties of *C*-nitroso compounds has been increasing due to the recent recognition of the roles they play in various biological processes (e.g., "shutting down" the activities of various heme enzymes). Our interest in the fundamental chemistry of *C*-nitroso compounds has led us to study the equilibrium established by the dimer 2-methyl-2-nitrosopropane containing a tertiary C-NO group. We have combined a kinetics and equilibrium study into a single project involving a series of solvents over a sufficient temperature range that allows for the calculation of thermodynamic data. The dependence of the rate and equilibrium constants on various solvent parameters is then determined.

Chapter 1. Introduction

Several small molecule gases play crucial roles in the atmosphere and in the urban environment. Species such as ozone and dioxygen have been studied for quite some time, and much is known about their chemistry. Other species such as the diatomic molecule nitric oxide (NO) were for a long time considered to be hazardous gases that were a nuisance to humanity. For example, NO produced from high-temperature combustion devices (from the reaction of nitrogen and oxygen) reacts with urban ozone to produce the brown gaseous derivative that is responsible for the smog in the Los Angeles area.[1] Indeed, much effort in the 20th century was devoted to getting rid of this small NO molecule. Surprisingly, however, in the late 1980s it was discovered that the human body makes NO naturally and that NO was responsible for the maintenance of normal blood pressure in humans. It has now been nearly two decades since *Science* magazine selected NO as the 1992 *Molecule of the Year*.[2-3] Since that time, a tremendous amount of research has gone towards learning more about the role of NO in biological systems, further steering its image away from that of a nasty pollutant and industrial byproduct to that of an essential physiological component. Consistent with its importance, the Nobel prize in Physiology or Medicine was, in 1998, awarded to Robert F. Furchgott, Louis J. Ignarro and Ferid Murad for their individual research contributions that led to the recognition of the role that NO plays in diverse processes in physiology.[4]

At the present time, the roles of NO in biology, in earth science, and in the chemical industry is well established among scientists. However, the public-at-large would probably be surprised to know that a small, seeming inconsequential, molecule has such wide-ranging effects on our daily lives.

It is well known that NO can react with metals, usually via the nitrogen atom, to form what are known as metal nitrosyl (M–NO) compounds. NO can also bridge two metals. Alternatively, two NO molecules can bind a single metal to form what are known as "metal dinitrosyls". NO can also attach to various organic fragments to form a variety of nitroso (termed X-NO) derivatives.[1]

NO is produced in the body by the enzyme "nitric oxide synthase" that catalyzes the oxidation of the amino acid L-arginine to citrulline. Once produced, NO targets metal containing enzymes such as soluble guanyl cyclase and cytochrome P450. NO also binds to some essential protein sites altering their normal function.[3]

Fundamental research in the area of NO chemistry has lead to numerous discoveries including the roles that NO plays in the immune defense system, blood pressure regulation, and in the nervous system.[3]

My Ph.D. research involved two important aspects of NO chemistry that had not been studied previously. They include: (i) a study of some of the fundamental chemical properties of the iron-NO group in dinitrosyl derivatives, and (ii) an equilibrium and kinetics study of an organic nitroso compound that models the chemical and physical behavior of nitroso species as a function of its immediate solvent environment. Both projects were undertaken with the goal of taking graduate-level research projects and placing them in an environment conducive for undergraduate student learning. At the

beginning of my Ph.D. program, I was very interested in undergraduate education and research. Thus, I sought to develop strong chemistry-based thesis projects that could be further developed into undergraduate capstone activities or used as starting points for independent undergraduate research projects.

It is becoming more recognized that excellent research and teaching go hand-in-hand, and that they are not mutually exclusive activities. In fact, there are many efforts underway internationally to encourage and recognize synergistic relationships between research and teaching. In their report, the Boyer commission (sponsored by Carnegie Foundation for the Advancement of Teaching) wrote in part

> *"The university's essential and irreplaceable function has always been the exploration of knowledge. This report insists that the exploration must go on through what has been considered the "teaching" function as well as the traditional "research" function. The reward structures in the modern research university need to reflect the synergy of teaching and research…"*

My thesis will lay out two different research projects that have the potential to be further developed into undergraduate research-teaching experiences. In the next Chapter, I will describe the preparation and chemical properties of a series of new dinitrosyl iron diphosphine complexes. In Chapter 3, I will describe the dimerization/monomerization behavior of a dimeric nitrosoalkane. Both of these projects cover a number of fundamental concepts commonly taught in undergraduate courses and would make an excellent undergraduate teaching laboratory experience.

References

1. Richter-Addo, G. B.; Legzdins, P., *Metal Nitrosyls*. Oxford University Press: New York, 1992.

2. Koshland, D. E., Jr., The Molecule of the Year. *Science* **1992,** *258*, 1861.

3. Culotta, E.; Koshland, D. E., Jr., NO News Is Good News. *Science* **1992,** *258*, 1862-1865.

4. Williams, N., NOBEL PRIZES:NO News Is Good News--But Only for Three Americans. *Science* **1998,** *282* (5389), 610-611.

Chapter 2. Fiber-optic Infrared Reflectance Spectroelectrochemical Studies of Some Dinitrosyl Iron Diphosphine Complexes, $Fe(NO)_2L_2$ ($L = P(C_6H_4X)_3$)

2.1. Introduction

Iron is a major target for NO in biological systems and in the environment. As mentioned in the Introduction chapter, NO usually binds to Fe via the N atom to give an FeNO moiety. Here, the Fe–N–O link may be linear or bent. NO can also interact with more than one metal center to give μ-NO bridged species. Conversely, more than one NO molecule can react with Fe to generate $Fe(NO)_x$ products.

The dinitrosyl $Fe(NO)_2$ moiety has been invoked as a biologically relevant entity by several researchers, notably by Vanin.[1-8] Exogenous and endogenous NO, upon exposure to and contact with Fe-containing biomolecules, generates a species exhibiting a strong EPR $g = 2.03$ signal attributed to an "$Fe(NO)_2$"-containing compound.[4] The exact identity of these species remains elusive due to the fact that other ligands coordinate to the $Fe(NO)_2$ unit to give in reality $Fe(NO)_2(L)_x$ compounds. These latter species are collectively referred to as "dinitrosyl iron compounds" (DNICs). DNICs, although mostly discussed in the literature in the realm of biology, also have significance as potential industrial catalysts. Their syntheses and characterization, to a large extent, preceded their discovery in biology.

Synthetic DNICs display a variety of properties including the ability to transfer oxygen atoms from molecular oxygen to phosphines or alkenes.[9-18] For example, Postel and co-workers demonstrated that dinitrosyl compounds such as $[Fe(NO)_2X]_2$ (X = Cl, I) react with oxygen in the presence of PPh_3 or $OPPh_3$ to produce nitrato complexes such as

$Fe(NO_3)_2X(OPPh_3)_2$.[9-13] These latter nitrato complexes were shown to transfer oxygen atoms to phosphines or cyclohexene and regenerate the nitrosyl moiety. The scheme using PPh_3 or $OPPh_3$ is shown in Figure 2.1.[12]

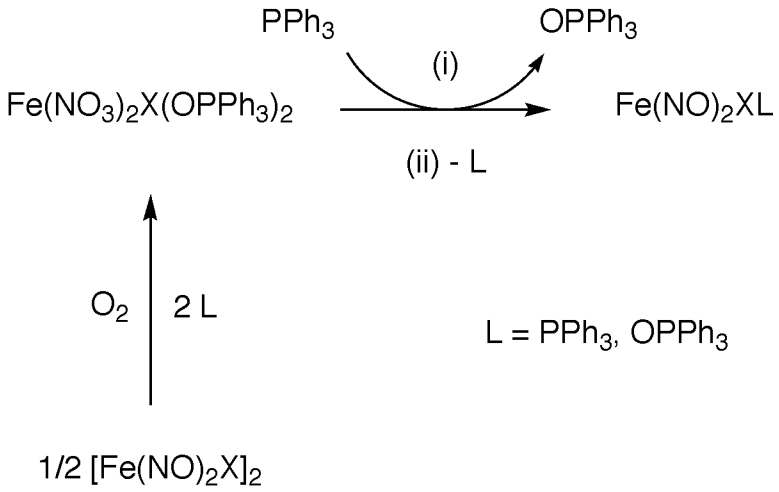


Figure 2.1. Reaction scheme (unbalanced) depicting the oxidation of bis(nitrosyl) iron dimers by molecular oxygen in the presence of PPh_3 or $OPPh_3$. The generated $Fe(NO)_2XL$ compound can be recycled as an additional starting material; thus making the O atom transfer process catalytic.

In 1965, Maxfield (Bartlesville, OK) reported in a patent the use of dinitrosyl iron halides as effective catalysts for the dimerization of diolefins.[18] Others later demonstrated that $Fe(NO)_2$-containing compounds could be used for the cyclodimerization of diolefins.[16] Candlin reported the dimerization of butadiene and isoprene by $Fe(NO)_2(CO)_2$, and Gadd *et al*. proposed that the photocatalytic dimerization might occur via $Fe(NO)_2(\eta^2\text{-}C_4H_8)(\eta^4\text{-}C_4H_8)$ as an intermediate (Figure 2.2).[14-15] In

1994, Li et al. supported this proposal reporting $Fe(NO)_2PPh_3(\eta^2$-TCNE) as the first stable compound containing an olefin π-bonded to an iron dinitrosyl group.[19]

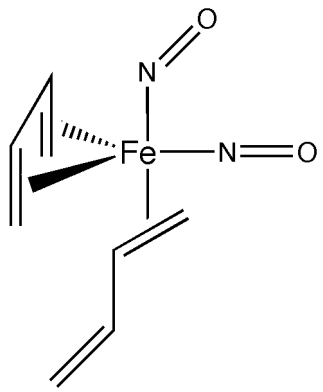


Figure 2.2. Schematic depicting Gadd's proposed intermediate in the photocatalyic dimerization of olefins.

Returning to the biological significance of DNICs, it was originally thought that DNICs formed by reaction of NO with the active center of iron sulfur proteins.[20-22] Indeed, Ricci and co-workers have reported the crystal structure of a stable complex of human glutathione transferase P1-1 containing a post-translationally modified dinitrosyliron glutathionyl moiety.[23] It is now generally accepted, however, that the iron in biological $Fe(NO)_2$ DNICs comes predominately from "freely chelatable iron storage units" and not from FeS proteins.[6, 24-25] For example, Lancaster et al. recently published work describing the direct reaction of NO with the intercellular labile iron and found that NO rapidly and quantitatively reacts with the iron to form stable DNICs detectable by EPR.[24]

All DNICs derive their basic functionality from the dinitrosyl $Fe(NO)_2$ moiety. Given their occurrence in biological systems, it is important that we have a better understanding of their fundamental properties. There is a need to study the inorganic chemistry of the $Fe(NO)_2$ compounds as this will assist with determining the kind of chemistry available to the $Fe(NO)_2$ moiety. Understanding how ancillary ligands bound to the metal affect the fundamental properties of the $Fe(NO)_2$ unit will provide important insight which may be exploited in future reaction studies.

It is known that the carbonyl ligands of $Fe(NO)_2(CO)_2$ can be replaced with sigma donor ligands (L, L') to yield dinitrosyl complexes of the form $Fe(NO)_2L_2$ or $Fe(NO)_2L'L$.[26] Our objective has been to determine how the spectroscopic and electrochemical properties of the $Fe(NO)_2$ group are affected by small changes on the periphery of some dinitrosyliron diphosphine complexes (i.e. $Fe(NO)_2L_2$ with L = $P(C_6H_4X)_3$). To that end, we have prepared and characterized a homologous series of dinitrosyl iron diphosphine complexes by FTIR and ^{31}P NMR spectroscopy, X-ray crystallography, cyclic voltammetry and fiber-optic infrared spectroelectrochemistry.

2.2. Experimental

2.2.1 General

All reactions were performed under an atmosphere of pre-purified nitrogen using standard Schlenk glassware and/or in a Labmaster 100 inert atmosphere glove box (Innovative Technology, Inc. Newburyport, MA). Unless otherwise indicated, all experiments were carried out at ambient room temperature.

2.2.2 Chemicals

Solvents were distilled under nitrogen from appropriate drying agents (CaH_2 or Na) or collected under nitrogen from a Pure Solv 400-5-MD Solvent Purification System (Innovative Technology). $Fe(NO)_2(CO)_2$ was prepared using a published method developed by Hieber and Beutner as described by King.[27] Tris(*p*-methoxyphenyl)phosphine (98%), tri-*p*-tolylphosphine (98%), tri-*m*-tolylphosphine (98%), tri(*p*-chlorophenyl)phosphine (99%), and tris(*p*-fluorophenyl)phosphine (99%), were purchased from Strem Chemical Company (Newburyport, MA). Iron pentacarbonyl, triphenylphosphine, (99%), tris(*p*-trifluoromethylphenyl)phosphine (97%) and tetrabutylammonium hexafluorophosphate (98%) were purchased from Sigma-Aldrich Chemical Company (Milwaukee, WI). Chloroform-*d* (99.8%) was purchased from Cambridge Isotope Laboratories (Andover, MA) in single-use ampoules and used as received or drawn from a stock reagent bottle and subjected to at least three freeze-pump-thaw cycles and stored over Grade 514 Type 4A molecular sieves.

2.2.3 Instrumentation

Infrared spectra were recorded using a Bio-Rad FTS 155 FT-IR spectrometer. $^{31}P\{^1H\}$ NMR spectra were obtained using a Varian Mercury-VX 300 MHz spectrometer equipped with a four-nuclei autoswitchable pulsed field gradient probe. All chemical shifts (δ, ppm) are reported relative to 85% H_3PO_4 (δ = 0 ppm) as an external reference standard.

Cyclic voltammograms were obtained using a BAS CV-50W Voltammetric Analyzer (Bioanalytical Systems, Inc., West Lafayette, IN) equipped with a three-

electrode cell (3 mm Pt disk working electrode, Pt wire auxiliary electrode and a Ag/AgCl or Ag wire quasi-reference electrode). Solutions used were 1 mM in analyte and 0.1 M in $[NBu_4][PF_6]$ in CH_2Cl_2. Ferrocene ($(C_5H_5)_2Fe$), or decamethylferrocene ($(C_5Me_5)_2Fe$) (-0.55 V vs. Fc/Fc^+) were used as internal reference standards. All potentials (V) are reported relative to the ferrocene-ferrocenium couple (Fc/Fc^+; ~+0.46 V vs. SCE).

Infrared spectroelectrochemical measurements were recorded using a Bruker Vector 22 FT-IR spectrometer equipped with a Remspec mid-IR fiber-optic dip probe and a liquid nitrogen cooled MCT detector (Remspec Corporation, Charlton City, MA). The stainless steel mirror on the liquid transmission head of the fiber-optic dip probe was replaced with a 3 mm Pt disk working electrode and equipped with a custom-made electrochemical cell including a Pt wire auxiliary electrode and a Ag/AgCl or Ag wire quasi-reference electrode as previously described.[28]

2.2.4 Synthesis

Each of the dinitrosyl iron diphosphine complexes was prepared using a method based on slightly modified literature procedures.[29-30] To our knowledge, only **4**, $Fe(NO)_2(PPh_3)_2$, has been previously prepared.[29] At the conclusion of each preparative reaction, the complexes were isolated by solvent removal *in vacuo* and purified by dissolution in CH_2Cl_2 or $CHCl_3$ followed by filtration through Celite®. After ^{31}P NMR spectroscopic analyses of aliquots indicated pure products, small amounts of pentane or hexane were added to the filtrates, and the products were allowed to recrystallize by slow solvent evaporation under nitrogen.

2.2.4.1 $Fe(NO)_2(P(C_6H_4\text{-}p\text{-}OCH_3)_3)_2$ (**1**)

Dark red $Fe(NO)_2(CO)_2$ (20 μL, 0.18 mmol) was added by syringe to a toluene solution (5 mL) of $P(C_6H_4\text{-}p\text{-}OCH_3)_3$ (0.129 g, 0.37 mmol) in a Schlenk tube. The light red solution was stirred, heated and allowed to reflux under nitrogen over a period of 3 h. The solution changed from light red to black/dark brown within the first 20 min. The reaction was monitored by infrared spectroscopy and stopped when the infrared spectrum indicated the absence of characteristic carbonyl stretching frequencies for $Fe(NO)_2(CO)_2$ (ν_{CO} = 2090 cm^{-1} and 2040 cm^{-1}) and for the expected mono-carbonyl species (ν_{CO} = 2002 cm^{-1}). Isolated yield: 27%. IR (toluene, cm^{-1}): ν_{NO} = 1711 s and 1667 s; also 1306 w, 1287 s, 1255 s, 1184 w, 1097 w, 826 w, 798 w. $^{31}P\{^1H\}$ NMR ($CDCl_3$): δ 56.4 (s).

2.2.4.2 $Fe(NO)_2(P(C_6H_4\text{-}p\text{-}CH_3)_3)_2$ (**2**)

Dark red $Fe(NO)_2(CO)_2$ (20 μL, 0.18 mmol) was added by syringe to a colorless toluene solution (5 mL) of $P(C_6H_4\text{-}p\text{-}CH_3)_3$ (0.111 g, 0.36 mmol) in a Schlenk tube. The mixture was stirred and heated to reflux under nitrogen for a period of ~3 h. A color change from light red to black/dark brown was observed within the first 30 min. The reaction was stopped when the infrared spectrum indicated the absence of characteristic carbonyl stretching frequencies for $Fe(NO)_2(CO)_2$ (ν_{CO} = 2090 cm^{-1} and 2040 cm^{-1}) and for the expected mono-carbonyl species (ν_{CO} = 2003 cm^{-1}). Isolated yield: 31%. IR (toluene, cm^{-1}): ν_{NO} = 1714 s and 1670 s; also 1197 w, 1189 w, 1116 w, 1095 w, 806 s. $^{31}P\{^1H\}$ NMR ($CDCl_3$): δ 58.4 (s).

2.2.4.3 $Fe(NO)_2(P(C_6H_4\text{-}m\text{-}CH_3)_3)_2$ (**3**)

$Fe(NO)_2(CO)_2$ (22 μL, 0.20 mmol) was added by syringe to a colorless toluene solution (5 mL) of $P(C_6H_4\text{-}m\text{-}CH_3)_3$ (125 mg, 0.41 mmol) in a Schlenk tube. The mixture was stirred, heated and allowed to reflux under nitrogen for a period of 4.75 h. The solution became much darker within the first 30 min and was black/brown by the end of the reaction time. The reaction was stopped when the infrared spectrum indicated the absence of characteristic carbonyl stretching frequencies for $Fe(NO)_2(CO)_2$ (ν_{CO} = 2090 cm^{-1} and 2040 cm^{-1}) and for the expected mono-carbonyl species (ν_{CO} = 2005 cm^{-1}). Isolated yield: 23%. IR (toluene, cm^{-1}): ν_{NO} = 1715 s and 1671 s; also 779 m, 588 w, 549 w. $^{31}P\{^1H\}$ NMR ($CDCl_3$): δ 60.9 (s).

2.2.4.4 $Fe(NO)_2(PPh_3)_2$ (**4**)

The known $Fe(NO)_2(PPh_3)_2$ was prepared using a modified literature method.[29] A toluene solution (5 mL) of $P(C_6H_5)_3$ (94 mg, 0.36 mmol) was treated with $Fe(NO)_2(CO)_2$ (20 μL, 0.18 mmol) under nitrogen. The mixture was heated and allowed to reflux over a period of ~3 h. The reaction was monitored by infrared spectroscopy and stopped once $Fe(NO)_2(CO)_2$ (ν_{CO} = 2090 cm^{-1} and 2040 cm^{-1}) or the known $Fe(NO)_2(PPh_3)(CO)$ (ν_{CO} = 2005 cm^{-1}) were no longer detected. Isolated yield: 22%. IR (toluene, cm^{-1}): ν_{NO} = 1719 s and 1678 s; also 1203 m, 1119 m, 543 m. $^{31}P\{^1H\}$ NMR ($CDCl_3$): δ 60.9 (s).

2.2.4.5 $Fe(NO)_2(P(C_6H_4\text{-}p\text{-}F)_3)_2$ (**5**)

A light yellow toluene solution (5 mL) of $P(C_6H_4\text{-}p\text{-}F)_3$ (127 mg, 0.40 mmol) was charged with $Fe(NO)_2(CO)_2$ (21 μL, 0.19 mmol). The light red/orange solution was

heated and stirred under nitrogen for 3.25 h after which time the infrared spectrum was consistent with the presence of the product and no trace of $Fe(NO)_2(CO)_2$ (ν_{CO} = 2090 cm^{-1} and 2040 cm^{-1}) or the mono-carbonyl species (ν_{CO} = 2009 cm^{-1}) was observed. Isolated yield: 23%. IR (toluene, cm^{-1}): ν_{NO} = 1720 s and 1682 s; also 1589 w, 1300 w, 1234 s, 1161 m, 1094 w, 1013 w, 828 s. $^{31}P\{^1H\}$ NMR ($CDCl_3$): δ 59.3 (s).

2.2.4.6 $Fe(NO)_2(P(C_6H_4\text{-}p\text{-}Cl)_3)_2$ (**6**)

A colorless toluene solution (4 mL) of $P(C_6H_4\text{-}p\text{-}Cl)_3$ (126 mg, 0.35 mmol) was charged with $Fe(NO)_2(CO)_2$ (20 μL, 0.18 mmol). The light red solution was heated and stirred under nitrogen. After 20 min the color of the solution had changed to black/brown. The reaction was allowed to proceed for 3.5 h until the infrared spectrum was consistent with the presence of the dinitrosyl product and the absence of $Fe(NO)_2(CO)_2$ (ν_{CO} = 2090 cm^{-1} and 2040 cm^{-1}) and the mono-carbonyl species (ν_{CO} = 2010 cm^{-1}). Isolated yield: 33%. IR (toluene, cm^{-1}): ν_{NO} = 1722 s and 1682 s; also 1099 w, 1012 m 818 m. $^{31}P\{^1H\}$ NMR ($CDCl_3$): δ 60.9 (s).

2.2.4.7 $Fe(NO)_2(P(C_6H_4\text{-}p\text{-}CF_3)_3)_2$ (**7**)

A colorless toluene solution (7 mL) of $P(C_6H_4\text{-}p\text{-}CF_3)_3$ (165 mg, 0.35 mmol) was charged with $Fe(NO)_2(CO)_2$ (22 μL, 0.20 mmol). The red solution was heated to reflux and turned black within 60 min. The reaction was monitored with infrared spectroscopy and stopped once no trace of the mono-nitrosyl species (ν_{CO} = 2014 cm^{-1}) was detected and the spectrum was consistent with the formation of the dinitrosyl product. Isolated

yield: 33%. IR (toluene, cm^{-1}): ν_{NO} = 1728 m and 1687 s; also 1397 w, 1321 m, 1281 w, 1185 w, 1169 m, 1129 m, 1062 w, 1015 w, 832 m. $^{31}P\{^{1}H\}$ NMR ($CDCl_3$): δ 63.8 (s).

2.2.5 X-ray Crystallography

Suitable crystals for the structural analyses of compounds **1-2** and **5-7** were grown by slow evaporation of solvent under nitrogen at ambient room temperature. X-ray diffraction studies were carried out by Dr. Douglas R. Powell of this department. All samples were mounted on the end of a plastic loop using an inert oil (Paratone N). The samples were cooled to 100(2) K and maintained at this temperature throughout the duration of the experiment. Intensity data for each compound were collected using a diffractometer equipped with a Bruker APEX ccd area detector and graphite-monochromated Mo Kα radiation (λ = 0.71073 Å). The structures were solved by direct methods using the SHELXTL software package (Version 6.10) and refined by full-matrix least-squares methods on F^2. All non-hydrogen atoms were refined anisotropically and all hydrogen atoms were included using idealized parameters. Crystallographic collection and refinement parameters for $Fe(NO)_2(PAr_3)_2$ are given in Table 2.1. The molecular structures for compounds **1-2** and **5-7** are shown in Figures 2.8 – 2.12 in the results section.

2.2.5.1 $Fe(NO)_2(P(C_6H_4\text{-}p\text{-}OCH_3)_3)_2$ (**1**)

A red plate-shaped crystal of dimensions 0.50 x 0.31 x 0.08 mm was selected for structural analysis. Cell parameters were determined from a non-linear least squares fit of 6550 peaks in the range $2.34 < \theta < 27.91°$. A total of 29988 reflections were measured

in the range $2.02 < \theta < 26.00°$ using ω oscillation frames. The data were corrected for absorption by a semi-empirical method giving minimum and maximum transmission factors of 0.774 and 0.962. The data were merged to form a set of 7618 independent data with R(int) = 0.0353 and a coverage of 99.6 %. The monoclinic space group $P2_1/c$ was determined by systematic absences and statistical tests and verified by subsequent refinement.

The molecular structure for **1** is shown in Figure 2.8. One of the *p*-methoxyphenyl groups was disordered. The occupancies of the disordered groups refined to 0.521(3) and 0.479(3). Restraints on the positional parameters of the disordered atoms were required. The displacement ellipsoids are drawn at the 50% probability level.

2.2.5.2 $Fe(NO)_2(P(C_6H_4\text{-}p\text{-}CH_3)_3)_2$ (**2**)

A red prism-shaped crystal of dimensions 0.34 x 0.29 x 0.29 mm was selected for structural analysis. Cell parameters were determined from a non-linear least squares fit of 8062 peaks in the range $2.32 < \theta < 28.26°$. A total of 39881 reflections were measured in the range $1.88 < \theta < 26.00°$ using ω oscillation frames. The data were corrected for absorption by a semi-empirical method giving minimum and maximum transmission factors of 0.840 and 0.866. The data were merged to form a set of 14767 independent data with R(int) = 0.0252 and a coverage of 99.6 %. The triclinic space group $P\bar{1}$ was determined by statistical tests and verified by subsequent refinement.

The molecular structure for **2** is shown in Figure 2.9. There are two molecules per asymmetric unit of the cell. The displacement ellipsoids are drawn at the 50% probability level.

2.2.5.3 $Fe(NO)_2(P(C_6H_4\text{-}p\text{-}F)_3)_2$ (**5**)

A red prism-shaped crystal of dimensions 0.44 x 0.22 x 0.04 mm was selected for structural analysis. Cell parameters were determined from a non-linear least squares fit of 5630 peaks in the range $2.41 < \theta < 25.70°$. A total of 22634 reflections were measured in the range $1.96 < \theta < 25.00°$ using ω oscillation frames. The data were corrected for absorption by a semi-empirical method giving minimum and maximum transmission factors of 0.721 and 0.972. The data were merged to form a set of 6325 independent data with R(int) = 0.0562 and a coverage of 98.3 %. The monoclinic space group $P2_1/c$ was determined by systematic absences and statistical tests and verified by subsequent refinement.

The molecular structure for **5** is shown in Figure 2.10. The structure included one metal complex molecule and one chloroform solvent molecule. (not shown) The displacement ellipsoids are drawn at the 50% probability level.

2.2.5.4 $Fe(NO)_2(P(C_6H_4\text{-}p\text{-}Cl)_3)_2$ (**6**)

A red plate-shaped crystal of dimensions 0.38 x 0.19 x 0.04 mm was selected for structural analysis. Cell parameters were determined from a non-linear least squares fit of 8898 peaks in the range $2.97 < \theta < 26.84°$. A total of 24943 data were measured in the range $2.97 < \theta < 26.00°$ using ω oscillation frames. The data were corrected for absorption by a semi-empirical method giving minimum and maximum transmission factors of 0.702 and 0.966. The data were merged to form a set of 7073 independent data with R(int) = 0.0233 and a coverage of 99.0 %. The monoclinic space group $P2_1/n$ was

determined by systematic absences and statistical tests and verified by subsequent refinement.

The molecular structure for **6** is shown in Figure 2.11. The displacement ellipsoids are drawn at the 50% probability level.

2.2.5.5 $Fe(NO)_2(P(C_6H_4\text{-}p\text{-}CF_3)_3)_2$ (**7**)

A red prism-shaped crystal of dimensions 0.33 x 0.25 x 0.15 mm was selected for structural analysis. Cell parameters were determined from a non-linear least squares fit of 9530 peaks in the range $2.29 < \theta < 28.26°$. A total of 22582 reflections were measured in the range $1.61 < \theta < 26.00°$ using ω oscillation frames. The data were corrected for absorption by a semi-empirical method giving minimum and maximum transmission factors of 0.843 and 0.928. The data were merged to form a set of 8855 independent data with R(int) = 0.0183 and a coverage of 99.1 %. The triclinic space group $P\bar{1}$ was determined by statistical tests and verified by subsequent refinement.

The molecular structure for **7** is shown in Figure 2.12. The structure included one *n*-pentane solvent molecule. (not shown) The *n*-pentane was best modeled using the Squeeze program.[31] The displacement ellipsoids are drawn at the 50% probability level.

Table 2.1. Crystallographic collection and refinement parameters for the $Fe(NO)_2(PAr_3)_2$ products

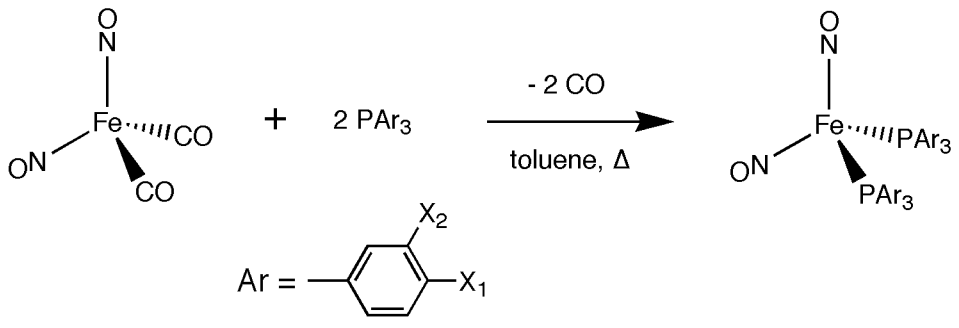
Complex	**1**	**2**	**5 ($CHCl_3$)**	**6**	**7 (C_5H_{12})**
Empirical formula	$C_{42}H_{42}FeN_2O_8P_2$	$C_{42}H_{42}FeN_2O_2P_2$	$C_{37}H_{25}Cl_3F_6FeN_2O_2P_2$	$C_{36}H_{24}Cl_6FeN_2O_2P_2$	$C_{47}H_{36}F_{18}FeN_2O_2P_2$
Formula weight	820.57	724.57	867.73	847.06	1120.57
Crystal system	Monoclinic	Triclinic	Monoclinic	Monoclinic	Triclinic
Space group	$P2_1/c$	$P\bar{1}$	$P2_1/c$	$P2_1/n$	$P\bar{1}$
Unit cell dimensions					
a (Å)	14.467(4)	10.240(2)	13.994(5)	10.340(3)	10.933(2)
b (Å)	10.936(4)	19.409(4)	15.746(6)	35.025(10)	13.024(2)
c (Å)	24.848(8)	21.040(4)	16.716(6)	10.589(3)	16.851(3)
α (°)	90	114.508(5)	90	90	103.280(5)
β (°)	98.498(8)	93.158(6)	97.651(8)	108.399(8)	101.957(5)
γ (°)	90	94.732(6)	90	90	92.653(6)
Volume (Å^3)	3888(2)	3773.5(13)	3651(2)	3638.9(18)	2273.5(7)
Z, Z'	4, 1	4, 2	4, 1	4, 1	2, 1
Density (calculated) Mg/m^3	1.402	1.275	1.579	1.546	1.637
Wavelength (Å)	0.71073	0.71073	0.71073	0.71073	0.71073
Temperature (K)	100(2)	100(2)	100(2)	100(2)	100(2)
F(000)	1712	1520	1752	1712	1132
Absorption coefficient (mm^{-1})	0.527	0.522	0.789	0.980	0.519
Max. and min. transmission	0.962 and 0.774	0.866 and 0.840	0.972 and 0.721	0.966 and 0.702	0.928 and 0.843
Theta range for data collection (°)	2.02 to 26.00	1.88 to 26.00	1.96 to 25.00	2.97 to 26.00	1.61 to 26.00
Reflections collected	29988	39881	22634	24943	22582
Independent reflections	7618 [R(int) = 0.0353]	14767 [R(int) = 0.0252]	6325 [R(int) = 0.0562]	7073 [R(int) = 0.0233]	8855 [R(int) = 0.0183]
Data / restraints / parameters	7618 / 141 / 569	14767 / 0 / 883	6325 / 0 / 478	7073 / 0 / 442	8855 / 0 / 604
wR(F^2 all data) [a]	$wR2$ = 0.1136	$wR2$ = 0.0950	$wR2$ = 0.1148	$wR2$ = 0.0715	$wR2$ = 0.1031
R(F obsd data) [b]	$R1$ = 0.0420	$R1$ = 0.0347	$R1$ = 0.0419	$R1$ = 0.0275	$R1$ = 0.0380
Goodness-of-fit on F^2	1.038	1.012	1.019	1.000	1.004
Observed data [I > 2σ(I)]	6330	12772	5006	6527	8196
Largest and mean shift / s.u.	0.000 and 0.000	0.002 and 0.000	0.001 and 0.000	0.001 and 0.000	0.001 and 0.000
Largest diff. peak and hole (e/Å^3)	0.494 and -0.348	0.473 and -0.256	1.238 and -0.460	0.390 and -0.206	1.116 and -0.434

[a] $wR2 = \{ \Sigma [w(F_o^2 - F_c^2)^2] / \Sigma [w(F_o^2)^2] \}^{1/2}$ [b] $R1 = \Sigma ||F_o| - |F_c|| / \Sigma |F_o|$

2.3. Results

2.3.1 Synthesis

All of the compounds in this study were readily prepared using a modified literature procedure as depicted in Figure 2.3.[29-30] $Fe(NO)_2(CO)_2$, the starting compound, was prepared using a published two step synthesis involving the reaction of $Fe(CO)_5$ with $NaNO_2$ and stored at -20 °C under nitrogen. $Fe(NO)_2(CO)_2$ was then reacted with the desired phosphine in toluene under nitrogen to obtain the desired product.



	1	2	3	4	5	6	7
X_1	OCH_3	CH_3	H	H	F	Cl	CF_3
X_2	H	H	CH_3	H	H	H	H

Figure 2.3. Reaction scheme depicting the formation of the $Fe(NO)_2(PAr_3)_2$ products.

The isolated yields and colors for each compound are provided in Table 2.2. Each reported yield and color refers to the isolated product after it had been purified and dried for several days under nitrogen. The isolated wet products were in general the same color as the dried product, but appeared darker in all cases. All of the compounds in this work

were found to be stable under nitrogen in the solid state for more than twelve months as determined by infrared spectroscopy and/or cyclic voltammetry.

Table 2.2. Colors and isolated yields of the $Fe(NO)_2(PAr_3)_2$ products

Complex	Substituent	Color	Isolated Yield
1	*p*-OCH_3	dark brown	27%
2	*p*-CH_3	brown	31%
3	*m*-CH_3	brown	23%
4	*p*-H	black	22%
5	*p*-F	black	23%
6	*p*-Cl	brown	33%
7	*p*-CF_3	lt. reddish brown	33%

2.3.2 Infrared Spectroscopy

The progress of the reactions to prepare the $Fe(NO)_2(PAr_3)_2$ compounds were easily monitored by infrared spectroscopy. The solution infrared spectrum of the starting compound, $Fe(NO)_2(CO)_2$, shown in Figure 2.4, exhibits two nitrosyl and two carbonyl signals which correspond to the symmetric and antisymmetric stretches of the dinitrosyl and dicarbonyl moieties.[32] The carbonyl stretching vibrations (ν_{CO} = 2087 cm^{-1} and 2036

cm^{-1}) appear at higher energy than the nitrosyl stretches (ν_{NO} = 1807 cm^{-1} and 1760 cm^{-1}) and the symmetric stretch of each pair appears at higher energy than the antisymmetric stretch.

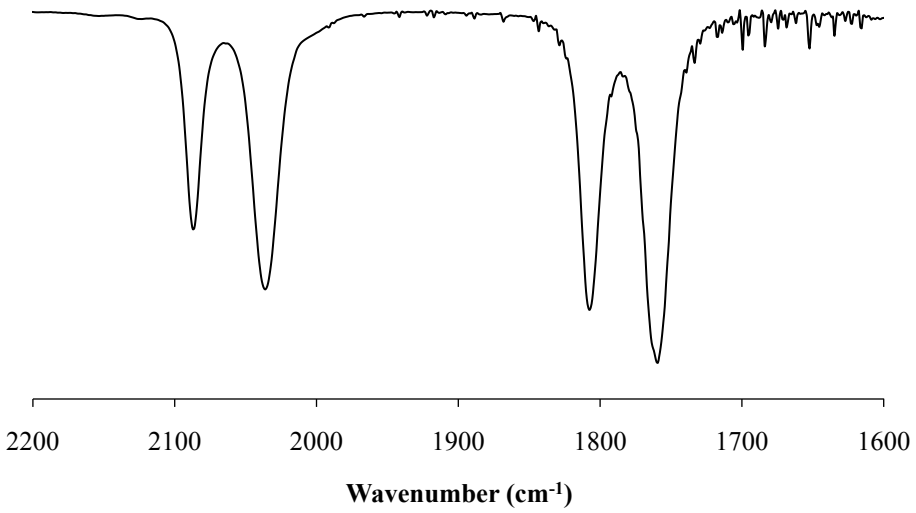


Figure 2.4. Infrared spectrum of $Fe(NO)_2(CO)_2$ in CH_2Cl_2; ν_{CO} (sym) = 2087 cm^{-1} ν_{CO} (asym) = 2036 cm^{-1}; ν_{NO} (sym) = 1807 cm^{-1}, ν_{NO} (asym) 1760 cm^{-1}.

Addition of the desired phosphine to a stirred toluene solution of $Fe(NO)_2(CO)_2$ at room temperature under nitrogen resulted in the replacement of at least one carbonyl group as indicated by the disappearance of the associated infrared bands of the starting compound. For example, the infrared spectrum of the reaction mixture containing $Fe(NO)_2(CO)_2$ and $P(C_6H_4$-*p*-$F)_3$ before heating to full reflux is shown in Figure 2.5. The spectrum indicates that a mixture of the mono and disubstituted products forms prior to reflux. In addition to the bands assigned to the dinitrosyl group of the $Fe(NO)_2(P(C_6H_4$-*p*-$F)_3)_2$ product at 1720 cm^{-1} and 1682 cm^{-1}, the band at 2009 cm^{-1} is assigned to the

carbonyl group of $Fe(NO)_2(P(C_6H_4\text{-}p\text{-}F)_3)(CO)$, (only a single ν_{NO} is expected for this compound) and the bands at 1763 cm^{-1} and 1720 cm^{-1} are assigned to the dinitrosyl group of $Fe(NO)_2(P(C_6H_4\text{-}p\text{-}F)_3)(CO)$. All the bands are shifted to lower frequencies than those present in $Fe(NO)_2(CO)_2$.

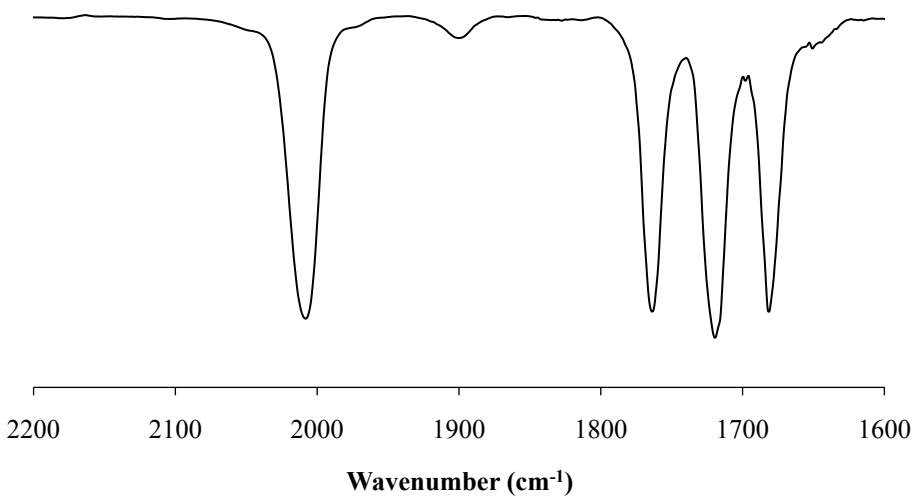


Figure 2.5. Infrared spectrum of the reaction mixture during the preparation of $Fe(NO)_2(P(C_6H_4\text{-}p\text{-}F)_3)_2$ in toluene prior to full reflux containing a mixture of the mono and disubstituted products. $Fe(NO)_2(P(C_6H_4\text{-}p\text{-}F)_3)(CO)$ (ν_{CO} = 2009 cm^{-1}, ν_{NO} = 1763 cm^{-1} and 1720 cm^{-1}) and $Fe(NO)_2(P(C_6H_4\text{-}p\text{-}F)_3)_2$ (ν_{NO} = 1720 cm^{-1} and 1682 cm^{-1}).

The remaining carbonyl group in $Fe(NO)_2(P(C_6H_4\text{-}p\text{-}F)_3)(CO)$ was completely replaced upon the application of heat. The infrared spectrum for the product, $Fe(NO)_2(P(C_6H_4\text{-}p\text{-}F)_3)_2$, which lacks the peak for the carbonyl present in $Fe(NO)_2(P(C_6H_4\text{-}p\text{-}F)_3)(CO)$, is shown in Figure 2.6.

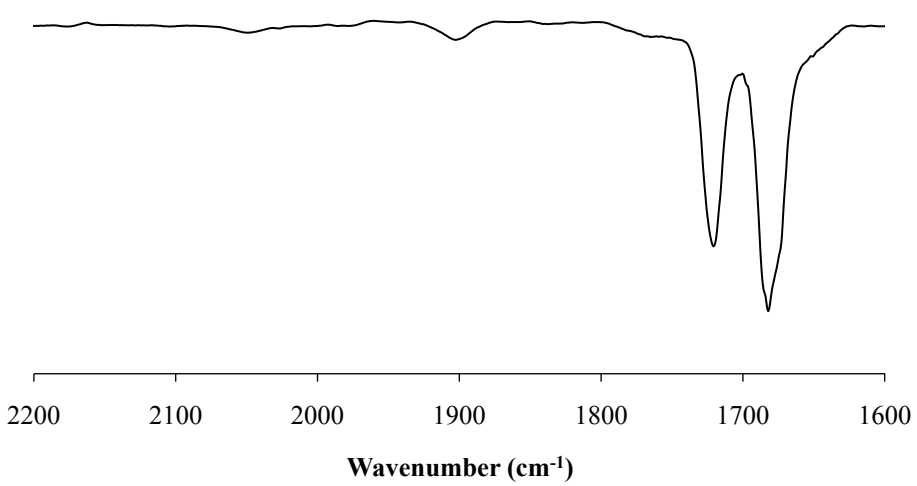


Figure 2.6. Infrared spectrum of the reaction mixture during the preparation of $Fe(NO)_2(P(C_6H_4\text{-}p\text{-}F)_3)_2$ in toluene after several hours of reflux; ν_{NO} = 1720 cm^{-1} and 1682 cm^{-1}.

As with the replacement of one carbonyl from $Fe(NO)_2(CO)_2$, replacement of the carbonyl from $Fe(NO)_2(P(C_6H_4\text{-}p\text{-}F)_3)(CO)$ was accompanied with a decrease in the infrared stretching frequencies for the dinitrosyl group. The dinitrosyl stretching frequencies, ν_{NO}s, in $Fe(NO)_2(P(C_6H_4\text{-}p\text{-}F)_3)_2$ are lower relative to the ν_{NO}s present in both $Fe(NO)_2(CO)_2$ and $Fe(NO)_2(P(C_6H_4\text{-}p\text{-}F)_3)(CO)$. The IR spectral shifts for the reactions between $Fe(NO)_2(CO)_2$ and the other phosphines were similar. At room temperature and prior to full reflux, mixtures of the mono and disubstituted products were evident in the infrared spectra. In all cases, it was necessary to carry out the reaction at about 80°C to affect complete replacement of the second carbonyl. This observation is consistent with other previous studies on dinitrosyl iron complexes.[19, 29]

The infrared data for each complex in three different solvents are summarized in Table 2.3. The ν_{NO}s for compounds containing electron-donating substituents were lower than those for compounds containing electron-withdrawing substituents. A solvent effect was observed on the ν_{NO}s. In general, the ν_{NO}s obtained in CH_2Cl_2 were between those determined in toluene and in acetonitrile. These results will be discussed later.

Table 2.3. Infrared data for the $Fe(NO)_2(PAr_3)_2$ products †

Complex	Substituent	σ	ν_{NO} (cm^{-1})		
			CH_3CN	CH_2Cl_2	$C_6H_5CH_3$
1	*p*-OCH_3	-0.27	1703 1660	1704 1659	1711 1667
2	*p*-CH_3	-0.17	1708 1665	1708 1663	1714 1670
3	*m*-CH_3	-0.07	1710 1667	1711 1664	1715 1671
4	*p*-H	0.00	1712 1670	1715 1670	1719 1678
5	*p*-F	0.06	1715 1673	1719 1674	1720 1682
6	*p*-Cl	0.23	1720 1677	1723 1678	1722 1682
7	*p*-CF_3	0.54	1728 1686	1730 1685	1728 1687

† σ = the Hammett σ_p or σ_m substituent parameter

2.3.3 ^{31}P NMR Spectroscopy

Each of the dinitrosyl compounds in this study was characterized using ^{31}P NMR spectroscopy. Proton decoupled spectra were obtained on a 300 MHz spectrometer at room temperature in $CDCl_3$. The chemical shifts $\delta(^{31}P)$ for each compound along with the chemical shifts $\delta(^{31}P)$ for the corresponding free ligands are shown in Table 2.4. The spectrum for **5**, $Fe(NO)_2(P(C_6H_4\text{-}p\text{-}F)_3)_2$, is shown in Figure 2.7 as a representative example. Each compound exhibited a single resonance consistent with two chemically equivalent phosphorus atoms in the range 57-64 ppm vs. 85% phosphoric acid as an external reference standard.

Table 2.4. $^{31}P\{^1H\}$ NMR data for the $Fe(NO)_2(PAr_3)_2$ products †

Complex	Substituent	σ	δ (ppm)		Δδ
			free ligand	complex	
1	*p*-OCH_3	-0.27	-9.6	56.4	66.0
2	*p*-CH_3	-0.17	-7.4	58.4	65.8
3	*m*-CH_3	-0.07	-4.7	60.9	65.6
4	*p*-H	0	-4.9	60.9	65.8
5	*p*-F	0.06	-8.6	59.3	67.9
6	*p*-Cl	0.23	-8.0	60.9	68.9
7	*p*-CF_3	0.54	-5.5	63.8	69.3

† Chemical shifts, δ (ppm), are referenced to 85% H_3PO_4 (δ = 0 ppm)

The resonances for the corresponding free phosphine ligands occur in the range -5 to -11 ppm vs. 85% phosphoric acid. Upon complexation, there was a coordination shift of about 70 ppm downfield. Similar coordination shifts have been observed in other dinitrosyl phosphine complexes.[26, 33-34]

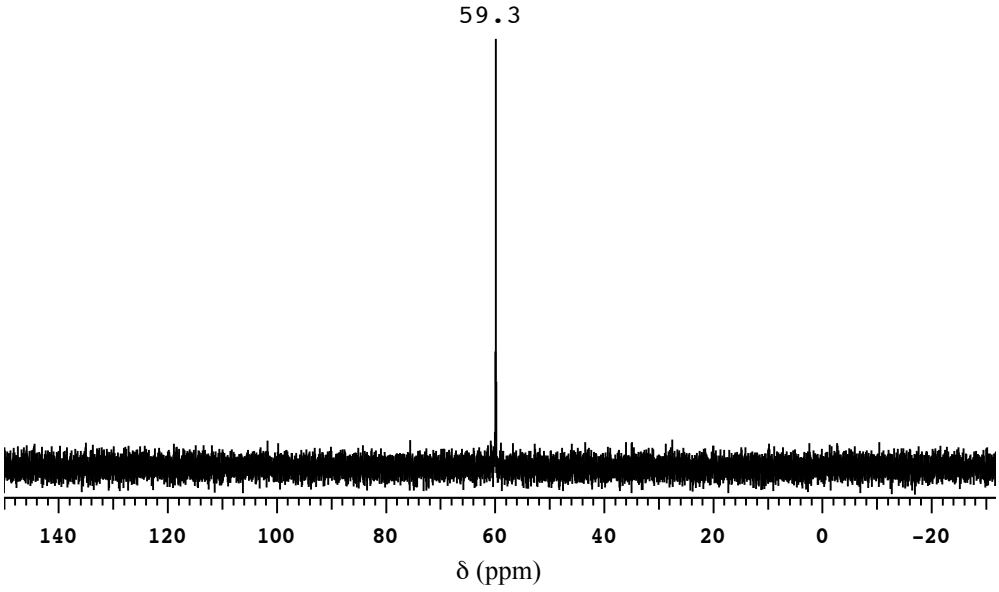


Figure 2.7. 300 MHz $^{31}P\{^{1}H\}$ NMR spectrum of, **5**, $Fe(NO)_2(P(C_6H_4\text{-}p\text{-}F)_3)_2$ in $CDCl_3$. 85% H_3PO_4 was used as an external reference ($\delta = 0$ ppm).

It is clear that the substituents on the P atom affect the ^{31}P chemical shift value. In general, the compounds with electron-withdrawing substituents tend to have higher chemical shifts (δ) appearing further up field from the parent compound (*p*-H) while, in contrast, compounds with electron-donating substituents tend to have lower chemical shifts appearing farther downfield from the parent compound. There seems to be some inconsistencies in this trend. This is a point that will be addressed later in the discussion section.

2.3.4 X-ray crystallography

Despite the intense research efforts by many research groups into the chemistry and relevance of DNICs, it is surprising that very little structural data was available prior to my work on the $Fe(NO)_2(PAr_3)_2$ compounds. Suitable crystals for X-ray diffraction studies were grown by slow evaporation of solvent under nitrogen at ambient room temperature. Molecular structures for compounds **1-2** and **5-7** are shown in Figures 2.8 – 2.12. Selected bond angles (°) and distances (Å) for $Fe(NO)_2(PAr_3)_2$ are presented in Table 2.5 and in Table 2.6 respectively.

Table 2.5. Selected bond angles (°) for the $Fe(NO)_2(PAr_3)_2$ products

Complex	Substituent	∠P-Fe-P	∠N-Fe-N	∠O••Fe••O	∠Fe-N-O
1	*p*-OCH_3	105.97(3)	128.49(11)	127.96	177.65(19) 177.5(2)
2	*p*-CH_3	106.00(2)	129.89(7)	130.31	179.31(16) 175.05(15)
		105.57(2)	124.29(8)	121.67	179.10(16) 173.84(15)
***4**	*p*-H	111.9(1)	123.8(4)	122.47	178.2(7) 178.2(7)
5	*p*-F	108.27(4)	127.02(11)	125.62	178.1(2) 177.0(2)
6	*p*-Cl	106.80(3)	127.78(7)	127.15	178.76(15) 177.67(14)
7	*p*-CF_3	105.25(2)	122.20(9)	118.46	175.96(18) 173.50(17)

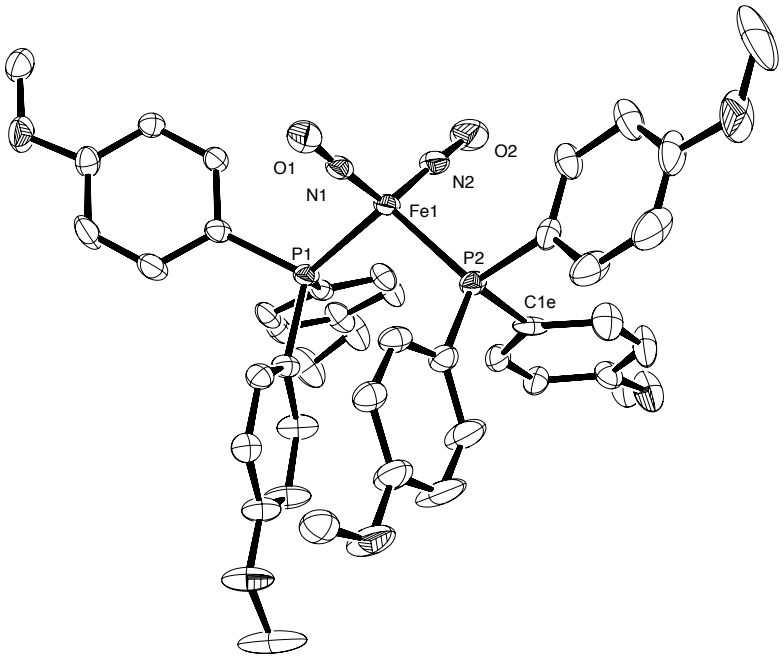
* The data for this compound was taken from the literature.[35]

Table 2.6. Selected bond distances (Å) for the $Fe(NO)_2(PAr_3)_2$ products

Complex	Substituent	C-P	P-Fe	Fe-N	N-O
1	*p*-OCH_3	1.830(3)	2.254(1) 2.247(1)	1.655(2) 1.654(2)	1.200(3) 1.184(3)
2	*p*-CH_3	1.829(2)	2.260(1) 2.240(1)	1.655(2) 1.659(2)	1.191(2) 1.195(2)
		1.825(2)	2.257(1) 2.245(1)	1.651(2) 1.652(2)	1.190(2) 1.187(2)
***4**	*p*-H	1.833(7)	2.267(2)	1.650(7)	1.190(10) 1.190(10)
5	*p*-F	1.830(3)	2.242(1) 2.247(1)	1.657(2) 1.653(2)	1.191(3) 1.197(3)
6	*p*-Cl	1.829(2)	2.241(1) 2.231(1)	1.659(2) 1.658(2)	1.188(2) 1.186(2)
7	*p*-CF_3	1.835(2)	2.248(1) 2.250(1)	1.655(2) 1.657(2)	1.184(2) 1.185(2)

* The data for this compound was taken from the literature.[35]

A



B

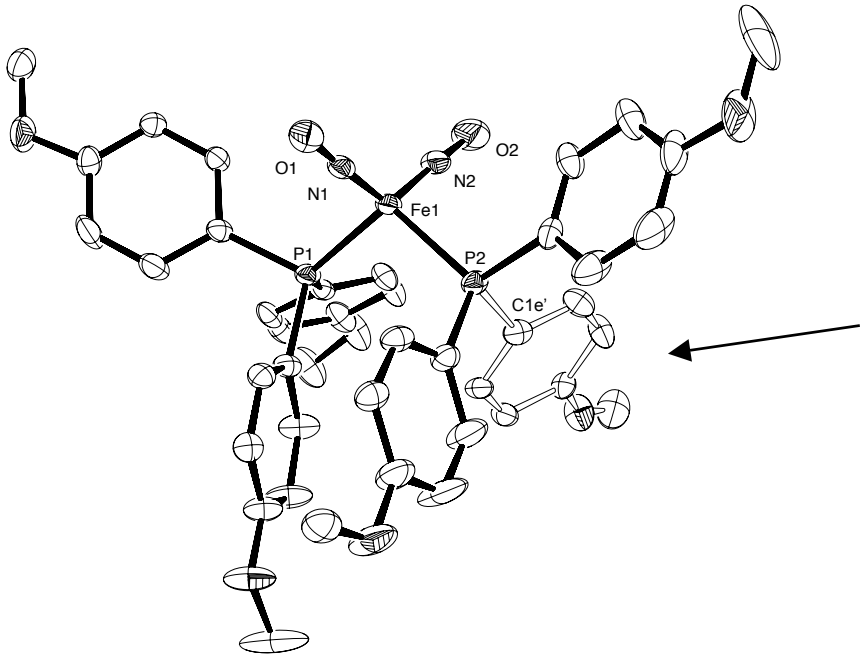


Figure 2.8. Molecular structure of **1**, $Fe(NO)_2(P(C_6H_4\text{-}p\text{-}OCH_3)_3)_2$. Hydrogen atoms have been omitted for clarity. The bottom figure depicts the disorder of one of the phenyl rings (indicated by the arrow) of one of the phosphine ligands. The displacement ellipsoids are drawn at the 50% probability level.

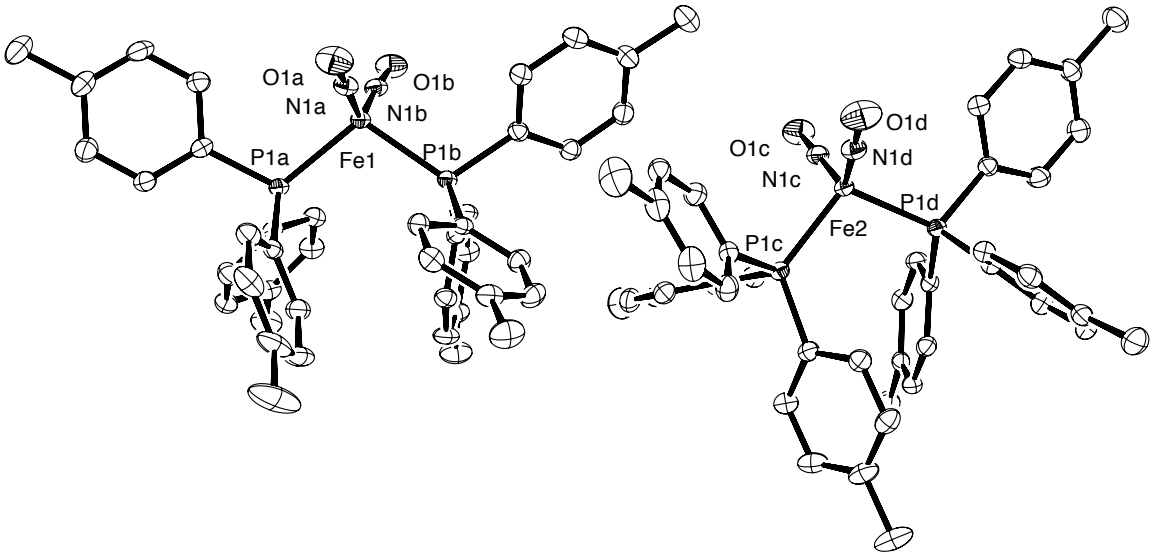


Figure 2.9. Molecular structure of **2**, $Fe(NO)_2(P(C_6H_4\text{-}p\text{-}CH_3)_3)_2$ showing the relative orientation of the 2 neighboring molecules. There are two distinct molecules per asymmetric unit of the cell. Hydrogen atoms have been omitted for clarity. The displacement ellipsoids are drawn at the 50% probability level.

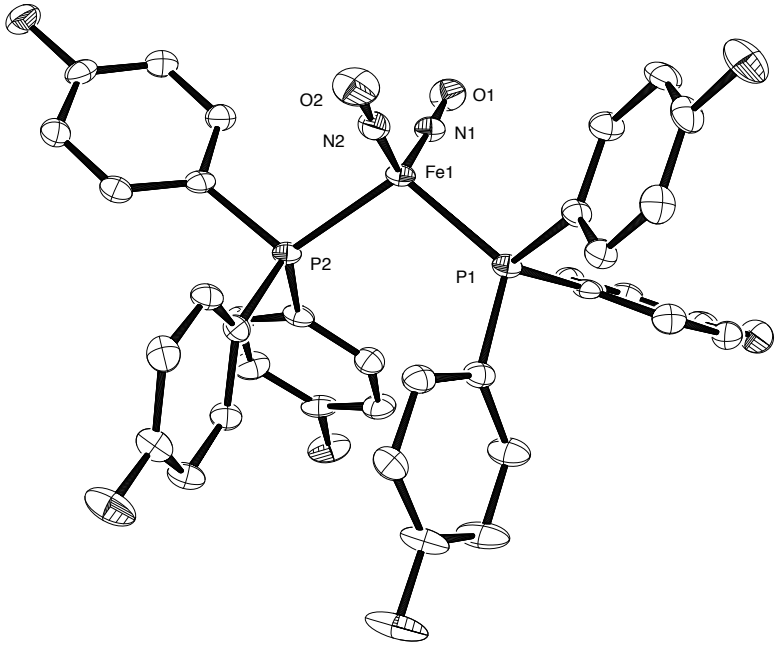


Figure 2.10. Molecular structure of **5**, $Fe(NO)_2(P(C_6H_4\text{-}p\text{-}F)_3)_2$. Hydrogen atoms have been omitted for clarity. The displacement ellipsoids are drawn at the 50% probability level.

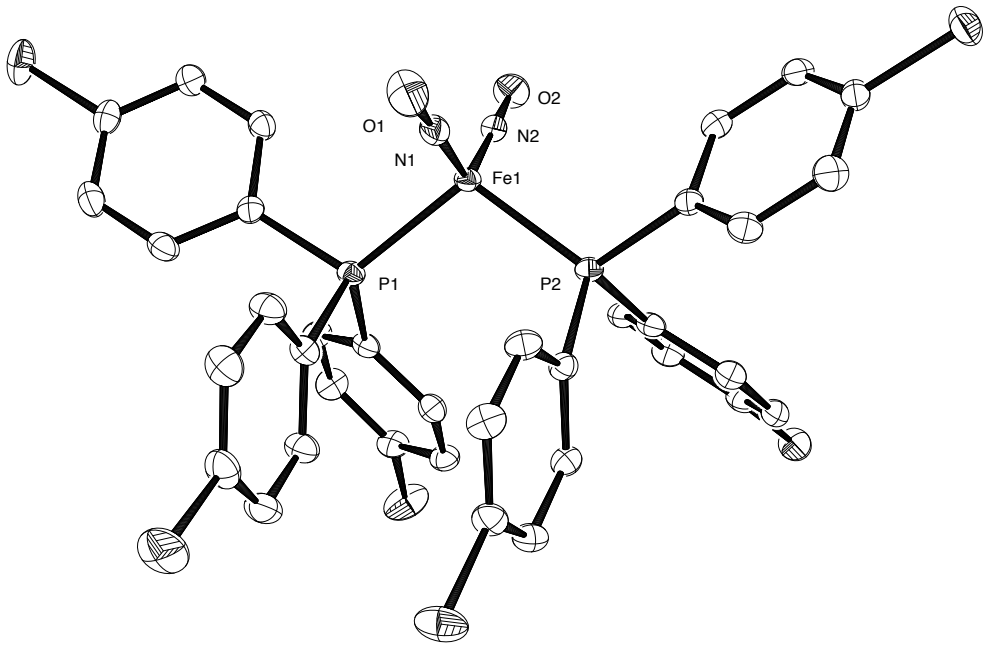


Figure 2.11. Molecular structure of **6**, $Fe(NO)_2(P(C_6H_4\text{-}p\text{-}Cl)_3)_2$. Hydrogen atoms have been omitted for clarity. The displacement ellipsoids are drawn at the 50% probability level.

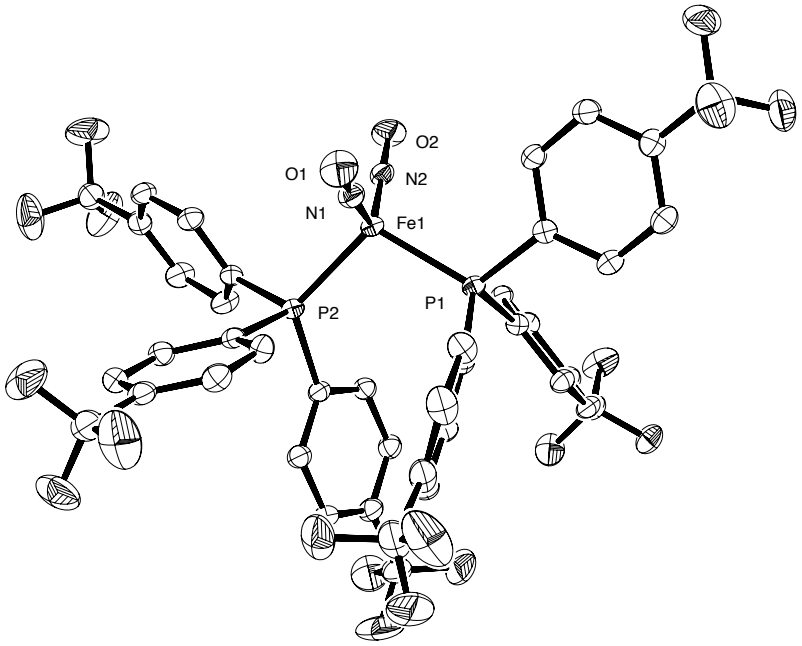


Figure 2.12. Molecular structure of **7**, $Fe(NO)_2(P(C_6H_4\text{-}p\text{-}CF_3)_3)_2$. Hydrogen atoms have been omitted for clarity. The displacement ellipsoids are drawn at the 50% probability level.

2.3.5 Electrochemistry

The redox behavior of compounds **1-7** were examined in CH_2Cl_2 using cyclic voltammetry. Each compound undergoes a 1-electron oxidation process within the solvent potential range examined under the experimental conditions described in Section 2.2.3. No reduction processes were observed. A representative cyclic voltammogram for **5**, $Fe(NO)_2(P(C_6H_4\text{-}p\text{-}F)_3)_2$, is shown in Figure 2.13.

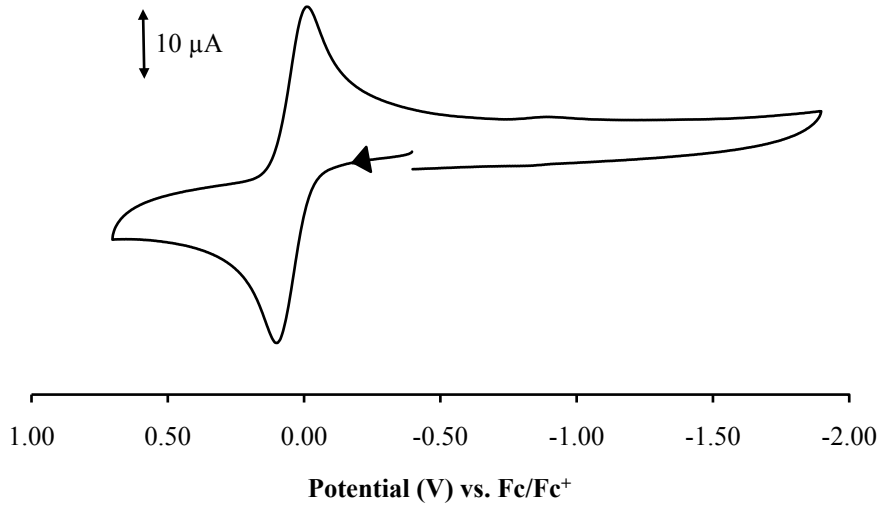


Figure 2.13. Cyclic voltammogram for a 1 mM solution of $Fe(NO)_2(P(C_6H_4\text{-}p\text{-}F)_3)_2$ in CH_2Cl_2 containing 0.1 M NBu_4PF_6 at a scan rate of 200 mV s^{-1}.

The cyclic voltammograms for compounds **1–3** (*p*-OCH_3, *p*-CH_3, and *m*-CH_3) and **5–6** (*p*-F and *p*-Cl) were similar to that of **4** (*p*-H) except that the formal electrode potential, $E°' = [(E_{pa} + E_{pc})/2]$, was shifted more negative for **1–3** and more positive for **5–6** relative to that of **4**. The E_{pa} for **7**, $Fe(NO)_2(P(C_6H_4\text{-}p\text{-}CF_3)_3)_2$, was the most positive

of the seven compounds studied and its cyclic voltammogram was significantly different from those of the other six compounds. A representative cyclic voltammogram for **7** is shown in Figure 2.14.

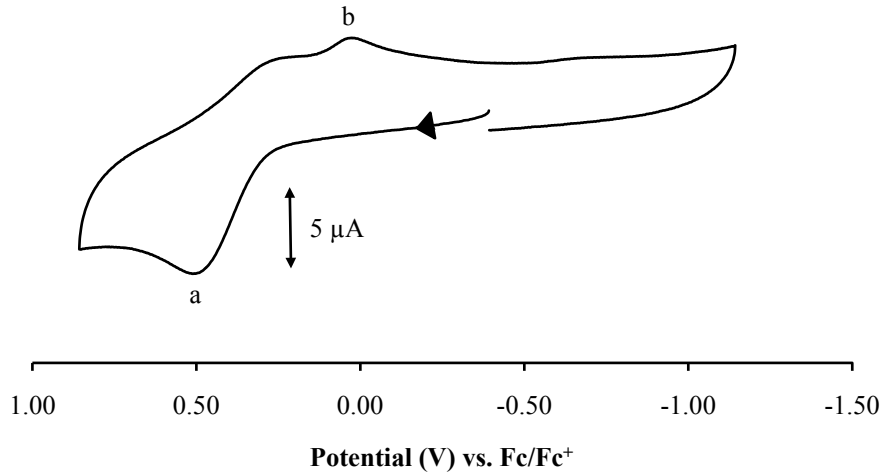


Figure 2.14. Cyclic voltammogram for a 1 mM solution of $Fe(NO)_2(P(C_6H_4\text{-}p\text{-}CF_3)_3)_2$ in CH_2Cl_2 containing 0.1 M NBu_4PF_6 at a scan rate of 200 mV s^{-1}.

The electrochemical data for each compound is summarized in Table 2.7. Compounds containing electron-donating substituents had lower formal electrode potentials, $E°'$, while those with electron-withdrawing substituents had higher formal electrode potentials. The cyclic voltammetry results obtained for **1** and **7** will now be described as representative examples and compared to the other compounds.

Table 2.7. Formal electrode potentials (V vs. Fc/Fc^+) and related electrochemical data for the $Fe(NO)_2(PAr_3)_2$ products in CH_2Cl_2 (scan rate = 0.1 V s^{-1}) †

Complex	Substituent	σ	E_{pa}	E_{pc}	ΔE_p	$E°'$	i_{pc}/i_{pa}	$\Delta E_{p(ref)}$
1	*p*-OCH_3	-0.27	-0.15	-0.27	0.12	-0.21	1.0	0.09
2	*p*-CH_3	-0.17	-0.12	-0.26	0.14	-0.19	0.97	0.11
3	*m*-CH_3	-0.07	-0.11	-0.21	0.10	-0.16	0.89	0.08
4	*p*-H	0.00	-0.08	-0.17	0.09	-0.13	1.00	0.08
5	*p*-F	0.06	0.10	0.00	0.10	0.05	1.00	0.09
6	*p*-Cl	0.23	0.14	0.06	0.08	0.10	1.00	0.06
7	*p*-CF_3	0.54	0.51	--	--	--	--	0.06

† All potentials are referenced to the ferrocene-ferrocenium couple, Fc/Fc^+. σ = the Hammett substituent parameter; E_{pa} and E_{pc} = the anodic and cathodic peak potentials respectively. $E°'$ = the formal electrode potential = $(E_{pa} + E_{pc})/2$; $\Delta E_p = | E_{pa} - E_{pc} |$, $\Delta E_{p(ref)} = \Delta E_p$ of the internal reference standard; i_{pc}/i_{pa} = the ratio of peak currents = $(i_{pc})_0/i_{pa} + (0.485(i_{sp})_0)/i_{pa} + 0.086$.

The cyclic voltammogram of **1**, $Fe(NO)_2(P(C_6H_4$-*p*-$OCH_3)_3)_2$, in CH_2Cl_2 exhibits a reversible one-electron oxidation at $E°'$ = -0.21 V vs. Fc/Fc^+ under the experimental conditions employed throughout this study. At a scan rate, ν, of 0.10 V s^{-1}, the separation in peak potentials, ΔE_p, averages 120 mV. The anodic to cathodic peak current ratio, i_{pa}/i_{pc}, is 1.0. The i_{pa}/i_{pc} value is constant from a scan rate of 0.05 V s^{-1} to 1.2 V s^{-1}. The i_{pa} value varies linearly with $\nu^{1/2}$ over the entire scan rate range employed. The separation in peak potentials, ΔE_p, increases slightly with increasing scan rate, being in one determination 98 mV at 0.10 V s^{-1} and 134 mV at 0.50 V s^{-1}. Under the same conditions, the internal reference standard, ferrocene, has a peak separation of 76 mV at

0.10 V s^{-1} and 97 mV at 0.50 V s^{-1}. Lastly, in the case of $Fe(NO)_2(P(C_6H_4\text{-}p\text{-}OCH_3)_3)_2$, if the scan is extended to the solvent limit, there is some evidence for a second oxidation, however, this wave cannot be fully determined using our solvent system.

As mentioned previously the cyclic voltammogram of compound **7** is significantly different from the other six compounds. The cyclic voltammogram of **7**, $Fe(NO)_2(P(C_6H_4\text{-}p\text{-}CF_3)_3)_2$, in CH_2Cl_2 exhibits a chemically irreversible oxidation. At a scan rate of 0.20 V s^{-1} the anodic peak potential occurs at E_{pa} = 0.51 V vs. Fc/Fc^+. (point a on Figure 2.14) A small cathodic peak occurs at E_{pc} = -0.04 V vs. Fc/Fc^+. This peak (point b on Figure 2.14) appears larger if the scan is taken farther in the anodic direction (i.e. closer to the solvent limit). A cyclic voltammogram showing only the anodic peak is shown in Figure 2.15. The i_{pa} value varies linearly with $\nu^{1/2}$ over the entire scan rate range employed. Under the same conditions, the internal reference standard, $(Cp^*)_2Fe$, has a peak separation of 66 mV at 0.05 V s^{-1} and 83 mV at 0.50 V s^{-1}.

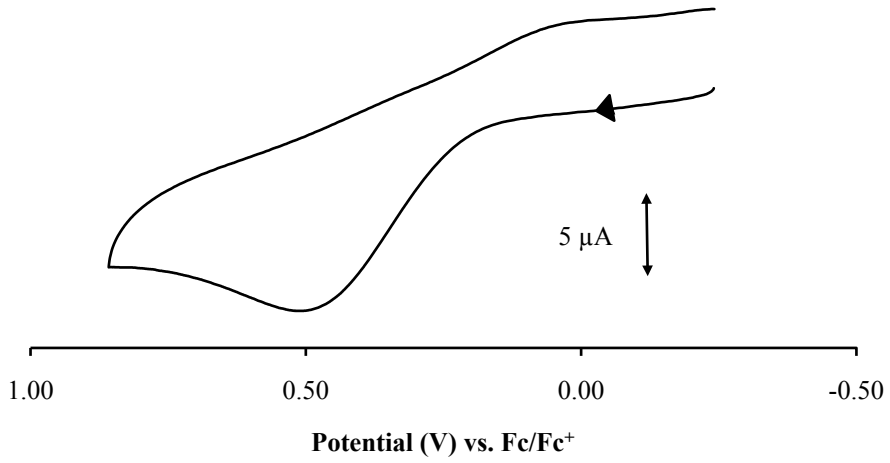


Figure 2.15. Cyclic voltammogram for a 1 mM solution of $Fe(NO)_2(P(C_6H_4\text{-}p\text{-}CF_3)_3)_2$ in CH_2Cl_2 containing 0.1 M NBu_4PF_6 at a scan rate of 100 mV s^{-1}.

2.3.6 Infrared Spectroelectrochemistry

The infrared spectroelectrochemistry of each compound (**1-7**) was examined at room temperature in CH_2Cl_2 under the conditions described in Section 2.2.3. The applied potential, E_{appl}, and the data obtained are summarized in Table 2.8. Each of the electrogenerated compounds exhibited symmetric and antisymmetric nitrosyl stretching frequencies that were ~100 cm^{-1} higher than the ν_{NO}s observed in the neutral compounds. The ν_{NO}s for compounds containing electron-donating substituents were lower than those for compounds containing electron-withdrawing substituents.

Table 2.8. Infrared spectroelectrochemical data obtained for the $Fe(NO)_2(PAr_3)_2$ products in CH_2Cl_2 †

Complex	Substituent	σ	E_{appl}	ν_{NO} (cm^{-1})		
				Neutral	Oxidized	$\Delta\nu_{NO}$
1	*p*-OCH_3	-0.27	-0.05	1704 1659	1805 1758	101 99
2	*p*-CH_3	-0.17	-0.06	1708 1663	1810 1763	102 100
3	*m*-CH_3	-0.07	0.01	1711 1664	1812 1764	101 100
4	*p*-H	0.00	0.04	1715 1670	1816 1767	101 97
5	*p*-F	0.06	0.17	1719 1674	1820 1770	101 96
6	*p*-Cl	0.23	0.26	1723 1678	1823 1772	100 94
7	*p*-CF_3	0.54	0.62	1730 1685	1827 1759,1778	97 74

† E_{appl} is the applied potential (V) relative to the ferrocene-ferrocenium couple, Fc/Fc^+. E_{appl} was typically set at 0.05 V – 0.12 V more positive than E_{pa}. $\Delta\nu_{NO}$ is the difference between ν_{NO} for the singly oxidized compound and the corresponding ν_{NO} for the neutral compound.

A representative infrared difference spectrum recorded during controlled potential oxidation of $Fe(NO)_2(P(C_6H_4\text{-}p\text{-}F)_3)_2$ is shown in Figure 2.16. The ν_{NO}s for the neutral starting compound are shown as disappearing at 1674 cm^{-1} and 1719 cm^{-1}. The ν_{NO}s for the oxidized species appear at 1770 cm^{-1} and 1820 cm^{-1} which suggests the formation of a cationic $Fe(NO)_2$ containing species such as $[Fe(NO)_2(P(C_6H_4\text{-}p\text{-}F)_2]^+$.

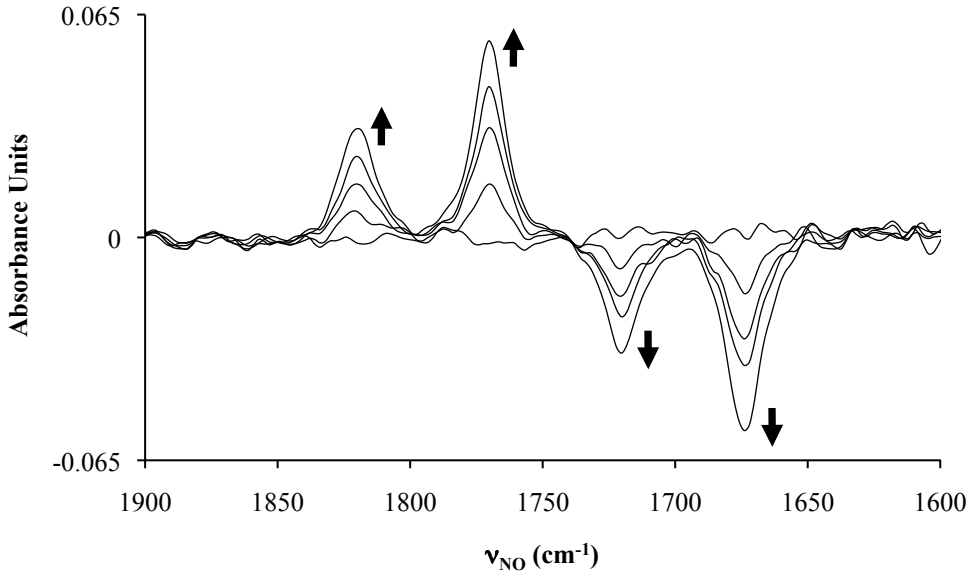


Figure 2.16. Infrared difference spectrum recorded during the oxidation of **5**, $Fe(NO)_2(P(C_6H_4\text{-}p\text{-}F)_3)_2$, in CH_2Cl_2 containing 0.1 M $[NBu_4][PF_6]$ at E_{appl} = 0.17 V vs. Fc/Fc^+. ν_{NO}s for the neutral compound are shown growing downward at 1674 cm^{-1} and 1719 cm^{-1} while ν_{NO}s for the oxidized species appear growing upward at 1770 cm^{-1} and 1820 cm^{-1}.

The difference spectra for the other compounds studied were all similar to that of **5,** $Fe(NO)_2(P(C_6H_4\text{-}p\text{-}F)_3)_2$, except for the spectrum recorded during the oxidation of $Fe(NO)_2(P(C_6H_4\text{-}p\text{-}CF_3)_3)_2$ which is depicted in Figure 2.17.

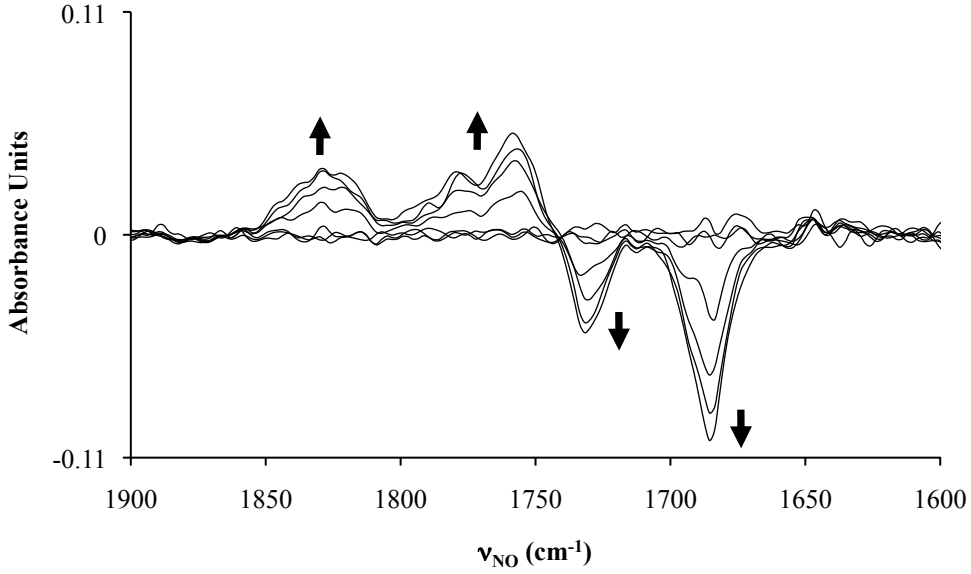


Figure 2.17. Infrared difference spectrum recorded during the oxidation of **7**, $Fe(NO)_2(P(C_6H_4\text{-}p\text{-}CF_3)_3)_2$, in CH_2Cl_2 containing 0.1 M $[NBu_4][PF_6]$ at E_{appl} = 0.57 V vs. Fc/Fc^+. ν_{NO}s for the neutral compound are shown growing downward at 1685 cm^{-1} and 1730 cm^{-1} while evidence of the ν_{NO}s for the oxidized species appear growing upward at 1759 cm^{-1}, 1778 cm^{-1} and 1827 cm^{-1}.

The peaks for the oxidized species in the spectrum for $Fe(NO)_2(P(C_6H_4\text{-}p\text{-}CF_3)_3)_2$ are not as clearly defined as those for the other compounds which suggests that the formation of the presumed cationic $Fe(NO)_2$ containing species such as $[Fe(NO)_2(P(C_6H_4\text{-}p\text{-}CF_3)_2]^+$ is short lived.

The starting compound for this work is itself a dinitrosyl compound. Its properties are very different from the diphosphine complexes as a result of it having two carbonyl ligands (π-acids) instead of two phosphine ligands (Lewis bases). Not surprisingly, the oxidation of $Fe(NO)_2(CO)_2$ under our conditions did not produce a useful result. The electrochemical reduction of $Fe(NO)_2(CO)_2$ in *dry* DMF at an HMDE

had been previously reported.[36] We were able to obtain the infrared difference spectrum of $Fe(NO)_2(CO)_2$ in CH_2Cl_2 solution. As shown in Figure 2.18 the four IR bands for the neutral compound grow downward (ν_{CO} = 2087 cm^{-1} and 2036; ν_{NO} = 1807 cm^{-1} and 1760 cm^{-1}) while the bands for the reduced species shown grow upward at lower wavenumbers (ν_{CO} = 1975 cm^{-1} and 1892; ν_{NO} = 1622 cm^{-1} and 1567 cm^{-1}).

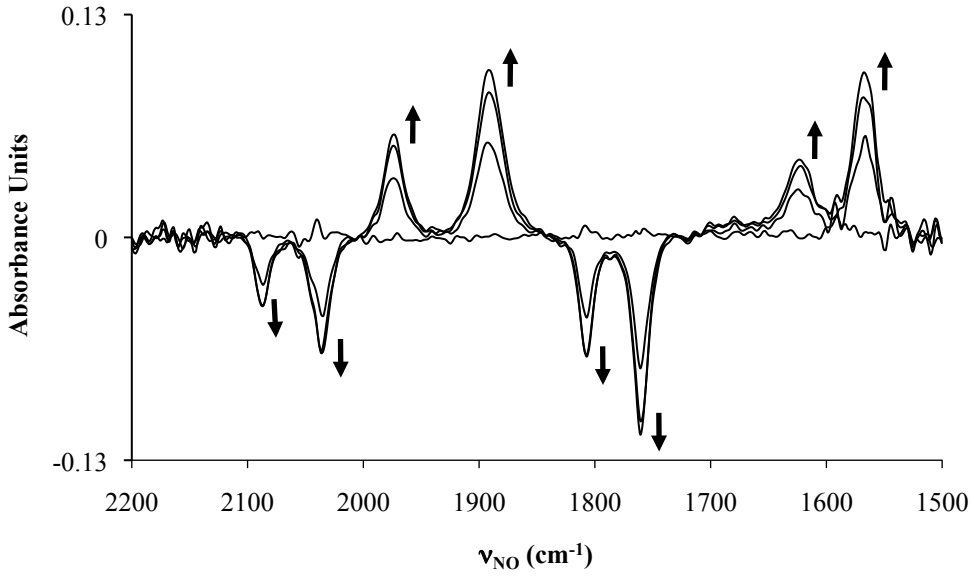


Figure 2.18. Infrared difference spectrum recorded during the reduction of $Fe(NO)_2(CO)_2$ in CH_2Cl_2 with 0.1 M $[NBu_4][PF_6]$ at E_{appl} = -2.2 V vs. Fc/Fc^+. ν_{NO}s for the neutral compound are shown growing downward (ν_{CO} = 2087 cm^{-1} and 2036; ν_{NO} = 1807 cm^{-1} and 1760 cm^{-1}) while ν_{NO}s for the singly reduced compound are shown growing upward at lower wavenumbers. (ν_{CO} = 1975 cm^{-1} and 1892 cm^{-1}; ν_{NO} = 1622 cm^{-1} and 1567 cm^{-1})

2.4. Discussion

2.4.1 Synthesis

The starting compound, $Fe(NO)_2(CO)_2$, is a toxic, air sensitive, deep red liquid. The solid form melts at ~18 °C.[27] Previous preparations of $Fe(NO)_2L_2$ (L = σ donor ligand) type compounds have involved carrying out the reaction directly with $Fe(NO)_2(CO)_2$ in a sealed vessel without solvent or from $[Fe(NO)_2(\mu\text{-}X)]_2$ (X = Cl, Br, I) under reducing conditions.[29-30, 37-38] These types of compounds have also been prepared by a reductive substitution reaction involving $[(RS)_2Fe(NO)_2]$ anions with excess PPh_3 and by reaction of phosphines with $Fe(NO)_2(PR_3)X$ as shown in Equations 1 and 2.[39-40]

$$[(RS)_2Fe(NO)_2]^- \xrightarrow[10\ PPh_3]{\text{(1,1-biphenyl) sodium}} (Ph_3P)_2Fe(NO)_2 + 2RS^- \qquad (1)$$

$$Fe(NO)_2(PAr_3)X + PAr_3 \xrightarrow{Na(Hg)} Fe(NO)_2(PAr_3)_2 + NaX \qquad (2)$$

Bitterwolf recently published a one-pot synthesis of $Fe(NO)_2(PAr_3)_2$ type compounds based on the reductive substitution (Equation 3) of $Na_2[Fe_2(NO)_4(\mu\text{-}S_2O_3)_2]$ in the presence of phosphines and phosphites.[41]

$$[Fe_2(NO)_4(\mu\text{-}S_2O_3)_2]^{2-} + 4PAr_3 \xrightarrow{Zn} 2Fe(NO)_2(PAr_3)_2 + 2S_2O_3^{2-} \qquad (3)$$

The current preparation of $Fe(NO)_2(PAr_3)_2$ type compounds is based on a modified literature procedure involving the reaction of $Fe(NO)_2(CO)_2$ with substituted triarylphosphines in toluene.[29-30] Toluene was selected because it had a boiling point high enough to allow displacement of the second carbonyl ligand under refluxing conditions.

2.4.2 Infrared Spectroscopy

It is known that the substituents on the phenyl rings of triarylphosphines affect their basicities.[42-45] The position of the dinitrosyl stretching frequency measured upon coordination with a phosphine ligand is related to the electron donor capacity or the Lewis basicity of the ligand and to the donor or acceptor capacity of the solvent in which the measurement is taken.[46-49] Several methods have been used to quantify this type of substituent effect. One of the most widely applied and useful is the Hammett substituent constant or Hammett parameter, σ.[50]

Hammett parameters are linear free energy relationships that can be used as a measure of the electronic effects of ligands.[51] They were first determined by Louis Hammett in the 1930s based on his study of benzoic and phenylacetic acid equlibria as a function of substituent groups on the aromatic ring.[52] Hammett parameters can provide an approximate measure of the inductive effects from substituents positioned on the aromatic ring relative to the site of interest. In this case they can be thought of as a relative measure of phosphine ligand basicity. Hammett constants for each substituent used in this work and the corresponding pK_as of the protonated phosphine ligands are given in Table 2.9.[45]

Table 2.9. Hammett parameters (σ) for substituents on substituted PAr_3 and pK_a values for the corresponding acids †

Complex	Substituent	σ	pK_a
1	*p*-OCH_3	-0.27	4.57
2	*p*-CH_3	-0.17	3.84
3	*m*-CH_3	-0.07	3.30
4	*p*-H	0.00	2.73
5	*p*-F	0.06	1.97
6	*p*-Cl	0.23	1.03
7	*p*-CF_3	0.54	-1.55

† The cited pK_a corresponds to the acid dissociation process: $HPAr_3^+ \rightleftharpoons H^+ + PAr_3$
The pK_a data was obtained from the literature.[45, 53] σ is the Hammett σ_p or σ_m parameter.

It was previously reported and it is shown in Figure 2.19 that the Hammett parameter, σ, correlates linearly with the pK_as of the phosphines used in this study.[45] The order of ligand basicity is the same as the order of the Hammett σ_p and σ_m parameters (i.e. Hammett constants for substituents in *para* and *meta* positions). The Hammett parameter for a hydrogen atom substituent is arbitrarily set to zero. Electron donating groups have negative Hammett parameters while electron-withdrawing groups have positive Hammett parameters relative to the unsubstituted parent compound (i.e. *p*-H or *m*-H).

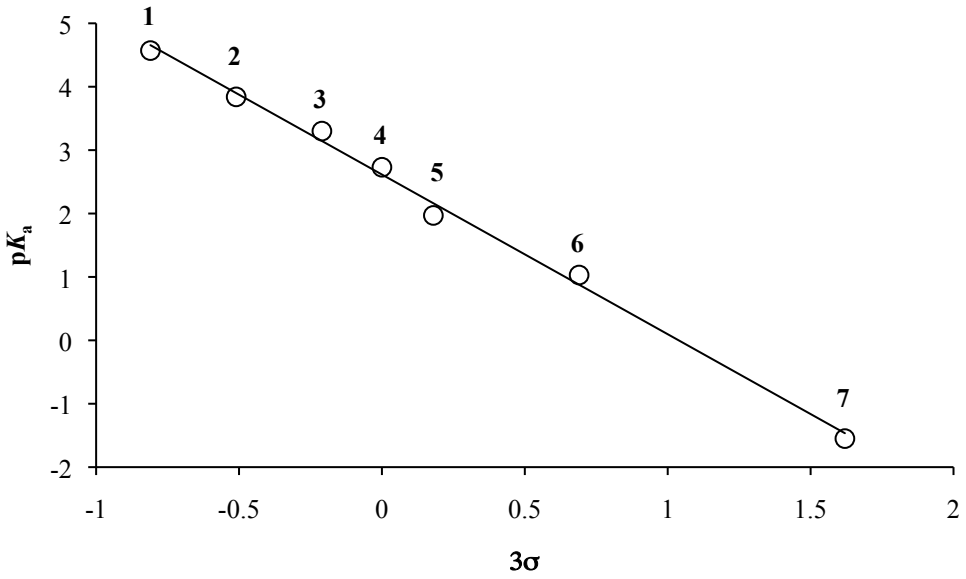


Figure 2.19 A plot depicting how the acid dissociation constant for substituted PAr_3 is linearly related to the Hammett parameter for the substituents on PAr_3. (The data for this plot was obtained from the literature.[45, 53])

We thus set out to determine if a correlation exists between σ and spectroscopic properties of the $Fe(NO)_2(PAr_3)_2$ products. A plot showing the infrared stretching frequencies for each substituted compound in three different solvents (toluene, CH_2Cl_2 and acetonitrile) as a function of Hammett parameter is shown in Figure 2.20. Separate plots of the infrared stretching frequencies for the dinitrosyl groups as a function of Hammett parameter in the same three solvents are shown in Figures 2.22 A - C The IR data is given in Table 2.3 in the results section.

In general, compounds with the more basic phosphines have lower ν_{NO}s while compounds with the less basic phosphines have higher ν_{NO}s. The effect of solvent appears to be greater on the symmetric ν_{NO}s of compounds with electron-donating substituents. The ν_{NO}s of the compound with the most electron-withdrawing substituent,

7, *p*-CF_3, are close together and appear to not be as affected by solvent differences as those with more electron donating substituents. For most of the series, frequencies obtained in the non-polar and non-coordinating solvent toluene were higher than those obtained in CH_2Cl_2 (a polar non-coordinating solvent) or in acetonitrile (a polar coordinating solvent). The ν_{NO}s obtained in CH_2Cl_2 were generally in-between those obtained in toluene and in acetonitrile although they tended to be closer to those obtained in acetonitrile as can be seen in Figure 2.20. The effect of solvent on ν_{NO} appears to be greater on the compounds with the more basic ligands.

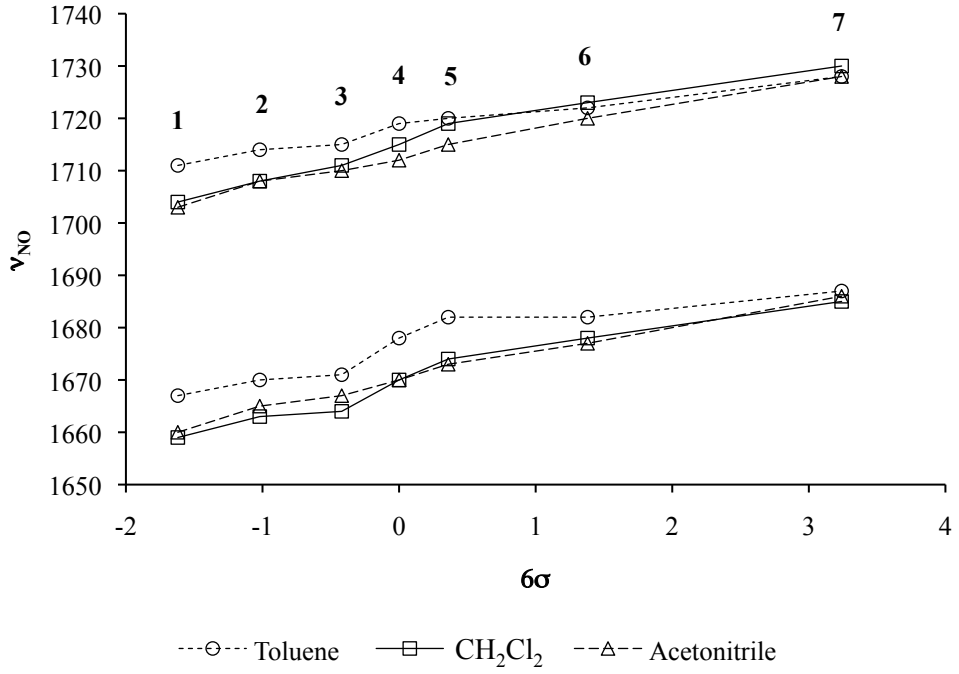


Figure 2.20. Plot depicting the symmetric and antisymmetric ν_{NO}s in toluene, CH_2Cl_2 and acetonitrile versus the Hammett substituent parameter.

In Figures 2.20 and 2.22 A - C it can be observed that electron-withdrawing substituents on the triarylphosphines, PAr_3, shifted the ν_{NO}s to higher frequencies (by 9 – 16 cm^{-1}) relative to the parent compound $Fe(NO)_2(PPh_3)_2$ (i.e. *p*-H). In contrast, electron-donating substituents shifted ν_{NO}s to lower frequencies. (by 8 – 11 cm^{-1}). The largest shifts in ν_{NO} were observed in the polar CH_2Cl_2 and the polar coordinating solvent acetonitrile.

The shifts in ν_{NO} as a function of Hammett parameter can be rationalized on the basis of the ligand basicity and concept of back-bonding (Figure 2.21). The more basic ligands (those with electron-donating substituents) contribute more electron density to the iron center and thus increase back-bonding from the filled *d*-orbitals on the metal to the anti-bonding orbitals on the nitrosyls resulting in a relatively lower ν_{NO}. Conversely, the less basic ligands (those with electron-withdrawing substituents) contribute less electron density to the iron center and, as a result, the metal to ligand back-bonding is less as indicated by relatively higher ν_{NO}s.

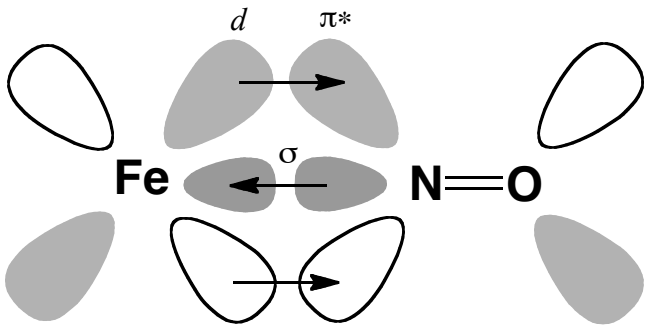


Figure 2.21. Schematic depicting metal-ligand back-bonding. The coordination of the phosphine ligand (not pictured) on the metal increases electron density at the iron center, which in turn produces enhanced back-bonding from the filled *d*-orbital on the metal to the anti-bonding orbital on NO resulting in a lowering of ν_{NO}.

While the plots for toluene and CH_2Cl_2 fit linearly with the Hammett parameter, a slight bending can be detected near the point where the substituents change from electron-withdrawing to electron-donating. It is possible for the data to be fitted to two separate lines at this juncture as shown in Figures 2.22 A and B. This observation tends to support having different modes of interaction between the different solvent types and the two classes of $Fe(NO)_2(PAr_3)_2$ compounds. In addition, the two lines *may* also be explained by the $Fe(NO)_2$ moiety in the two classes adopting two slightly different conformations (or extent of *attracto* distortions) in different solvent types. Toluene and CH_2Cl_2 are both non-coordinating solvents and the plots of ν_{NO} versus σ for both of these solvents possess the two-line feature. Compound **3**, $Fe(NO)_2(P(C_6H_4\text{-}m\text{-}CH_3)_3)_2$ deviates from the lines in CH_2Cl_2 and in toluene more than any of the *para* substituted compounds. In contrast, the plot of ν_{NO} versus σ for acetonitrile is quite linear and cannot be fitted to two separate lines. This suggests that the coordinating solvent interacts in a way not present in toluene or CH_2Cl_2.

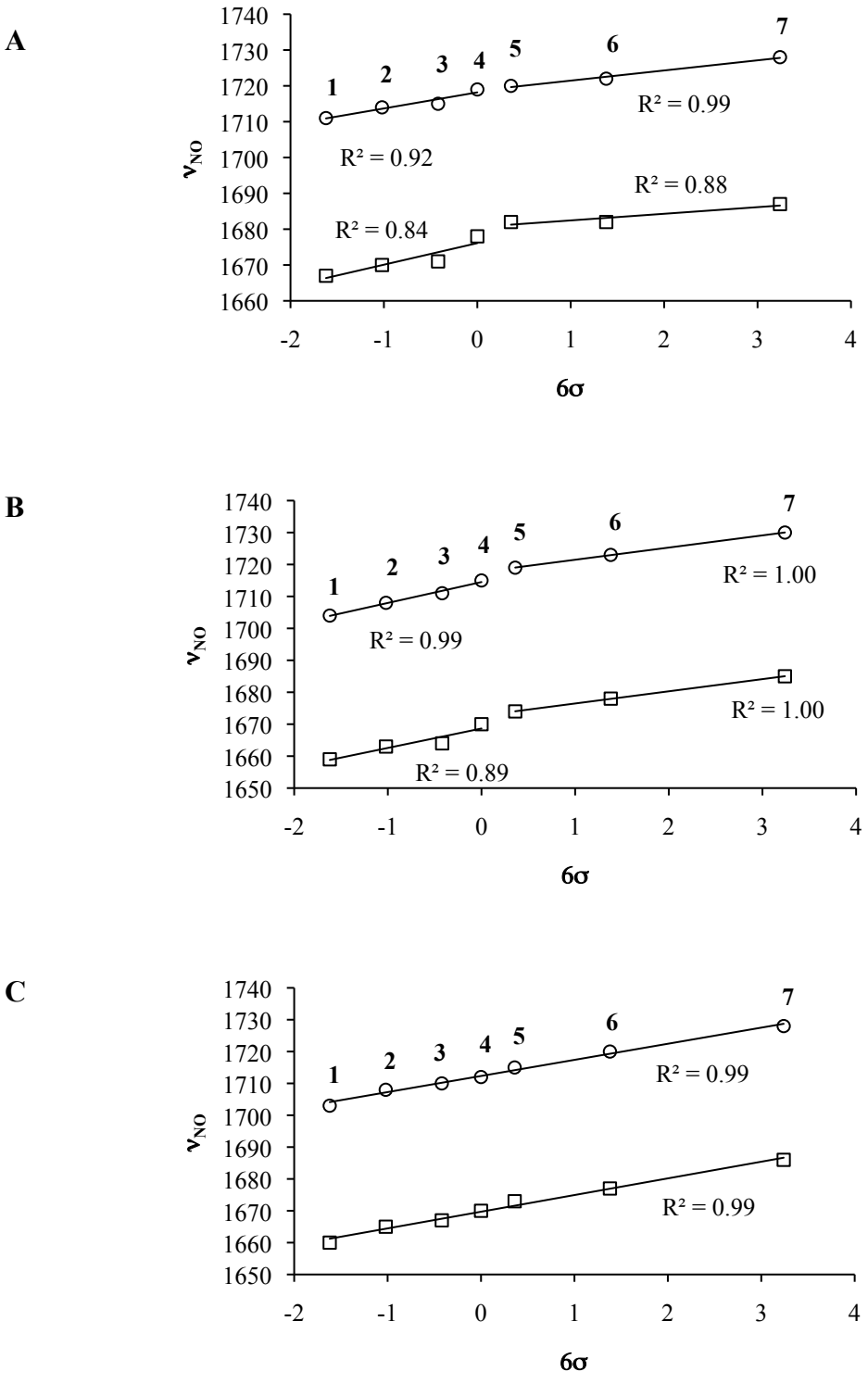


Figure 2.22. Plots depicting the symmetric and antisymmetric ν_{NO}s for $Fe(NO)_2(PAr_3)_2$ compounds in (A) toluene, (B) CH_2Cl_2 and (C) acetonitrile vs. the Hammett substituent parameter.

For instance, if the oxygen atom on the dinitrosyl complexes acts as a donor to the solvent, there should be a relationship between the infrared stretching frequency and the solvent acceptor number (AN).[54-56] The solvent acceptor number is a quantitiative empirical measure of the electrophillic behavior of a solvent. It was developed by Gutmann and co-workers based on ^{31}P chemical shift measurements of triethylphosphine oxide dissolved in the solvent of interest. The ^{31}P resonance of triethylphosphine oxide acts as a highly sensitive probe towards solvent change because the oxygen in the PO bond interacts differently with different solvents.

Similarly, if the solvent behaves as a donor towards the dinitrosyl compounds of interest there should be a relationship between the ν_{NO} and the solvent donor number (DN).[55-57] The donor number is a measure of the basicity or donor ability of a solvent. Also developed by Gutmann, it is defined as the negative enthalpy of reaction of a base with the Lewis acid antimony pentachloride, $SbCl_5$. Higher donor numbers are associated with stronger Lewis bases. The donor and acceptor numbers for the solvents used in this work and for some other representative solvents are provided in Table 2.10.

Plots showing the influence of the solvent acceptor number on ν_{NO} are shown in Figures 2.23 A - B and plots showing the influence of the solvent donor number on ν_{NO} are shown in Figures 2.24 A - B. From these plots it can be seen that both the donor and acceptor properties of the solvents clearly have an effect on ν_{NO}. As the solvent acceptor number increases ν_{NO} generally decreases. This trend is generally consistent throughout the series. Some small exceptions occur upon going from the polar coordinating acetonitrile solvent to the polar non-coordinating CH_2Cl_2.

Table 2.10. Solvent Acceptor and Donor numbers†

Solvent	AN	DN
Cyclohexane	0	0
Ether	3.9	19.2
Toluene	8.2	0.1
CCl_4	8.6	0
Dioxane	10.8	14.8
Acetonitrile	18.9	14.1
Dichloromethane	20.4	1
Chloroform	23.1	4

† The units for both DN and AN are kcal mol^{-1}. The values in this table were taken from references.[54, 56, 58-59]

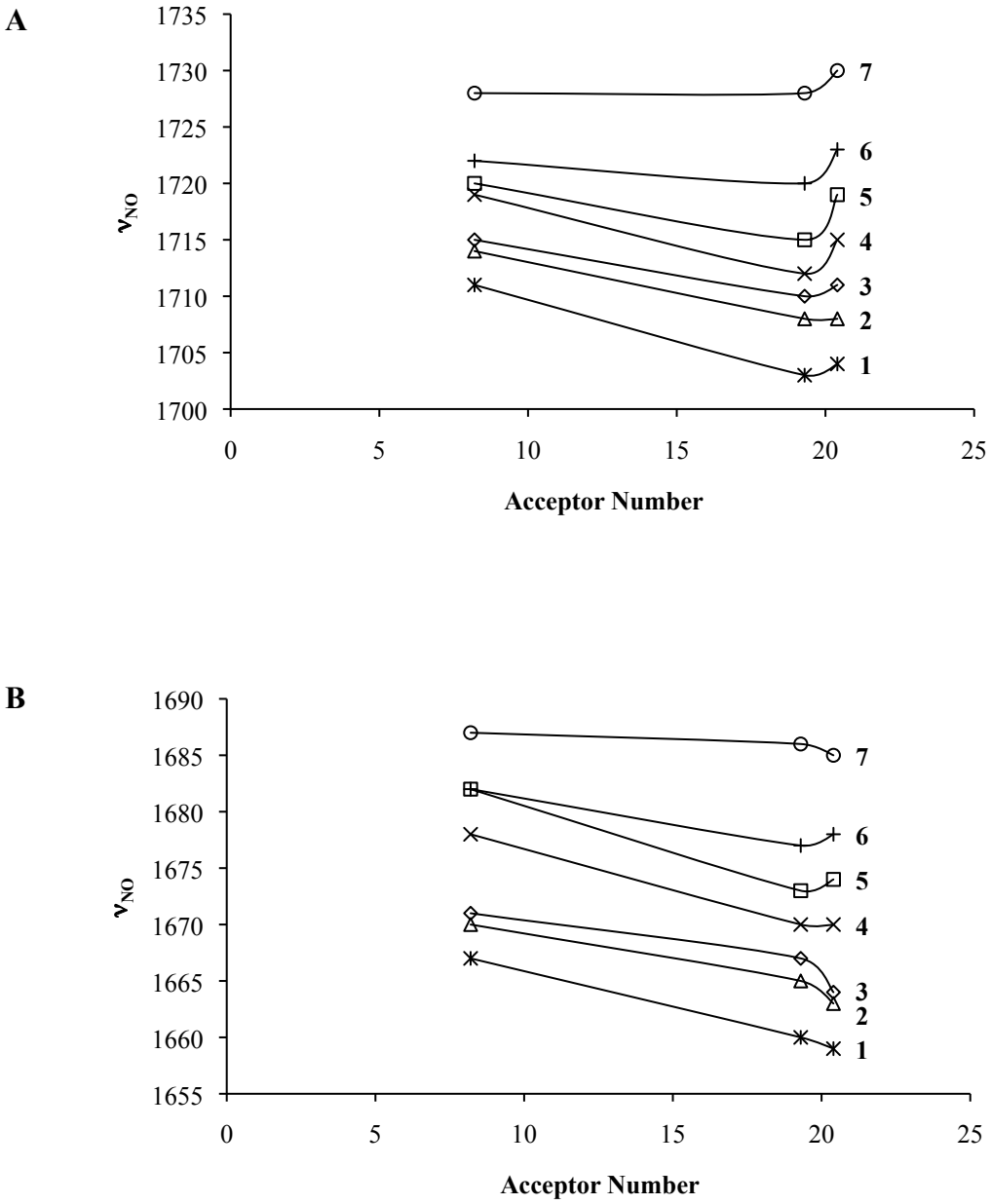


Figure 2.23. Plots depicting (A) the symmetric and (B) the antisymmetric ν_{NO} for each $Fe(NO)_2(PAr_3)_2$ as a function of solvent acceptor number. The solvents are (from left to right) toluene, acetonitrile, and CH_2Cl_2. (AN = 8.2, 18.9 and 20.4 respectively)

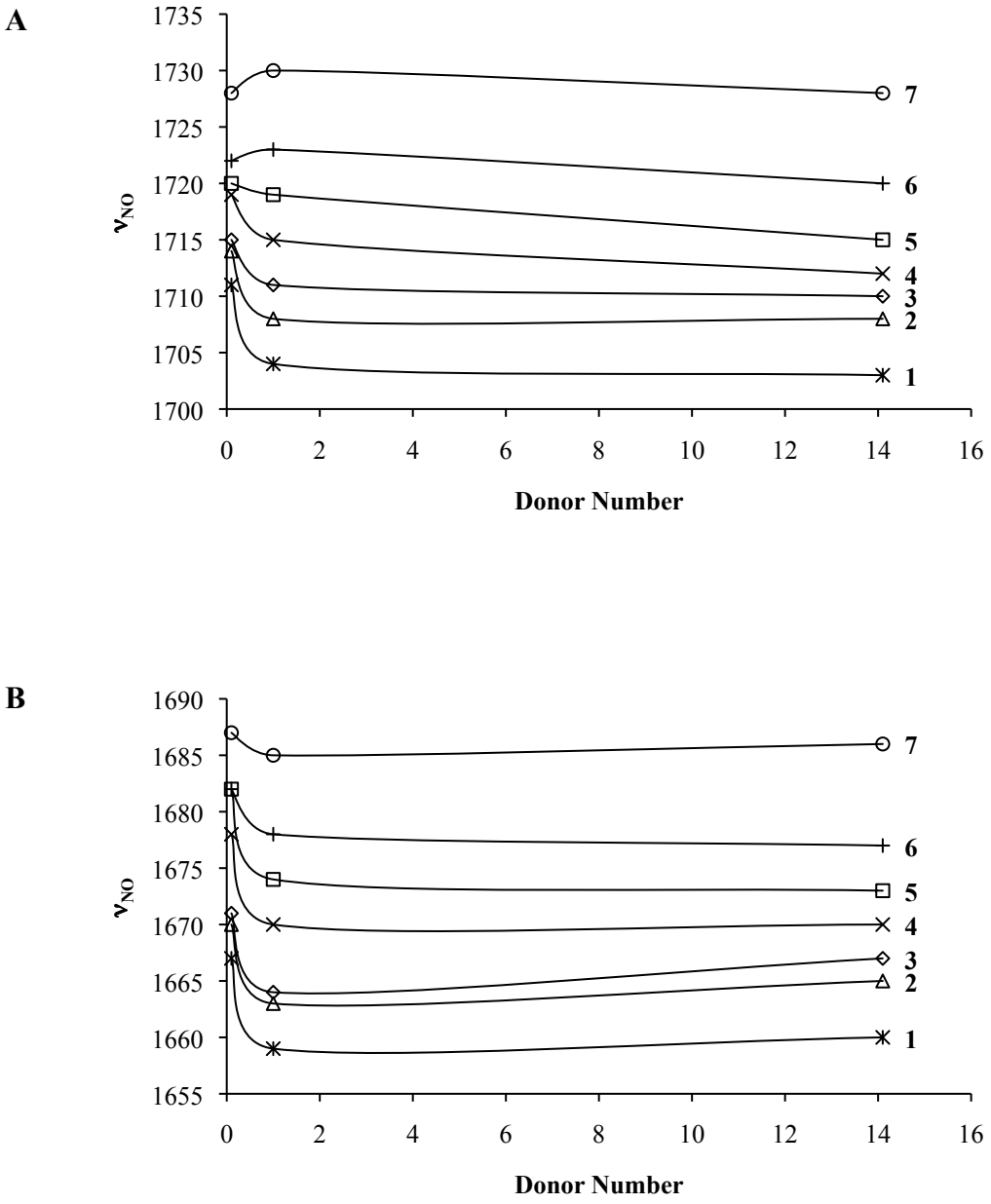


Figure 2.24. Plots depicting (A) the symmetric ν_{NO} and (B) the antisymmetric ν_{NO} for each $Fe(NO)_2(PAr_3)_2$ as a function of solvent donor number. The solvents are (from left to right) toluene, CH_2Cl_2 and acetonitrile. (DN = 0.1, 1.0 and 14.1 respectively)

As shown on the previous page an interesting pattern is also observed when the ν_{NO} data is plotted against the solvent donor number (Figures 2.24 A - B). In general, ν_{NO} decreases with increasing donor number. The effect is much more pronounced upon moving from the less basic phosphines to the more basic phosphines (top-to-bottom in the plots). Two exceptions stand out among the symmetric ν_{NO} data in that the *p*-CF_3 and the *p*-Cl compounds both increase slightly before decreasing.

These solvent acceptor and donor number analyses herein are consistent with the notion that the DNICs studied can behave as both donors toward the solvent and acceptors from the solvent. The results suggest an interaction between the solvent acceptor orbitals and the *basic* dinitrosyl oxygens. Essentially the NO ligands behave as Lewis bases toward the solvent. However, dinitrosyl moieties are rather complex as there is not a single ν_{NO} trend to follow. In general, as the solvent's ability to accept electron density increases (i.e. increasing AN), we observe lower ν_{NO}s. These results also support the notion that the solvent may donate electron density to the DNICs. As the solvent donor number increased, the ν_{NO}s generally decreased, which is an observation consistent with the fact that increased electron density at the metal results in enhanced metal to ligand backdonation of electron density. While the donor number results do not show a large steady decrease in ν_{NO} over the entire range studied, there is a clear initial decrease in ν_{NO} upon going from the non-polar and non-coordinating toluene to the more polar solvents. Both the solvent acceptor and the donor number results nicely support some previous related solvent effects studies involving $Fe(NO)_2(P(C_6H_5)_3)_2$ and some related DNICs.[47-48]

Gutmann described the variation of ν_{NO}s on complexes of the type $Fe(NO)_2(CO)L$ (where L = CO, $P(OC_6H_5)_3$, $As(C_6H_5)_3$, $P(C_6H_5)_3$ and $P(C_6H_{11})_3$) in three different solvents (C_6H_{12}, CCl_4 and $CHCl_3$) and found that the frequency differences of the iron nitrosyl carbonyl derivatives of the type $Fe(NO)_2(CO)L$ were increased by increased solvent acceptor number and in the order of increasing basicity of the ligand.[48] The results of this current work are consistent with his finding even though our set of ligands are more uniform and the changes between each ligand are relatively small (i.e. the *para* or *meta* substituent) and far removed from the coordination center.

2.4.3 ^{31}P NMR spectroscopy

The ^{31}P NMR data as a function of the Hammett parameter σ_p can immediately be fitted to two separate lines as shown in Figure 2.25.

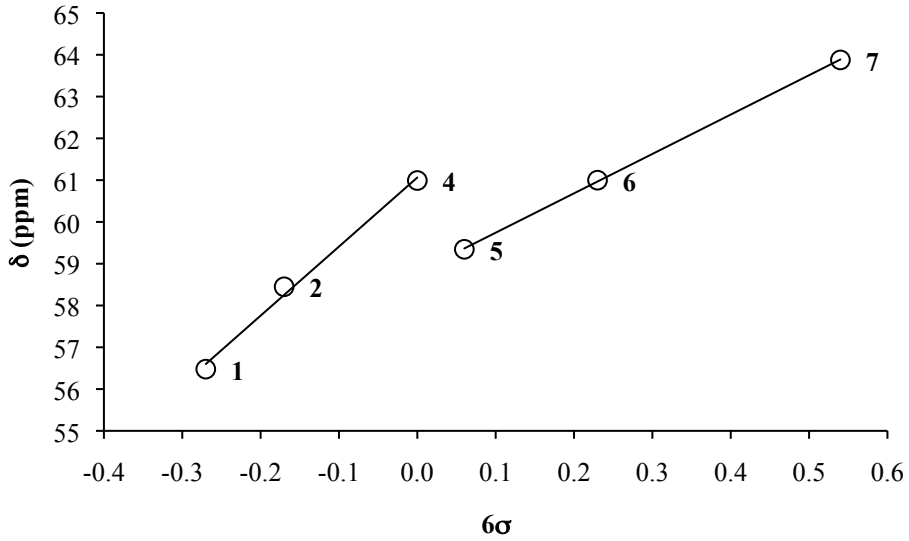


Figure 2.25. Plot depicting the $\delta(^{31}P)$ chemical shifts for each $Fe(NO)_2(PAr_3)_2$ as a function of the Hammett parameter.

The line on the left (compounds **1, 2** and **4**) consists of the chemical shifts of compounds with electron-donating substituents on PAr_3. A second line on the right (compounds **5, 6** and **7**) consists of the chemical shifts of compounds with electron-withdrawing substituents on PAr_3. As mentioned in the previous section on infrared spectroscopy, the Hammett parameter σ_p can be thought of as a measure of ligand basicity. Thus, in general, on going from the more basic phosphines to the less basic phosphines the chemical shift appears further upfield. It is not entirely clear why there is a break in the linear trend in ^{31}P chemical shifts on going from electron-donating substituents to electron-withdrawing substituents. However, the absence of a single linear correlation between the chemical shift and basicity indicates that the inductive effect that controls basicity is not the major influence on the chemical shift in these complexes.

Upon closer inspection of the Hammett plot in Figure 2.25 it can be seen that it is possible to group the ^{31}P NMR data in a different way. Some of the substituents contain lone pairs (*p*-OCH_3, *p*-F, *p*-Cl) and are thus able to participate in a direct resonance interaction with the phosphorus atom. Considering only those substituents capable of direct resonance yields a clear linear correlation (Figure 2.24). Curiously, the *p*-CF_3 substituent also falls on the trend line.

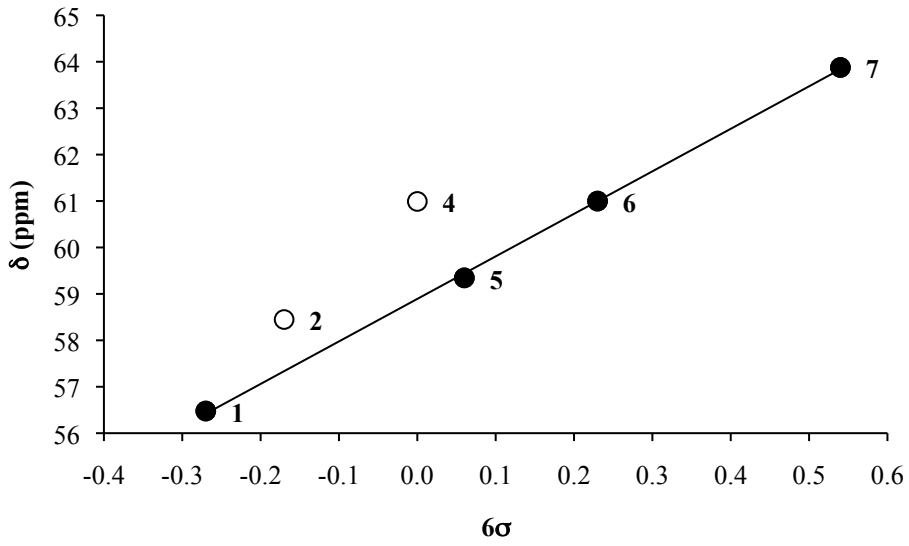


Figure 2.26. Plot depicting the $\delta(^{31}P)$ chemical shifts for each $Fe(NO)_2(PAr_3)_2$ as a function of the Hammett parameter; an alternative correlation for Figure 2.25. The dark filled markers indicate those substituents capable of participating in a direct resonance interaction with the phosphorus atom.

It is known that the Hammett parameter gives poor correlations when resonance interactions are involved. A separate set of linear free energy relationships (LFER) like Hammett parameters are available for use in cases where resonance interactions are possible. A plot of $\delta(^{31}P)$ versus the Brown-Okamoto constant σ_p^+ gives a straight line as shown in Figure 2.27.

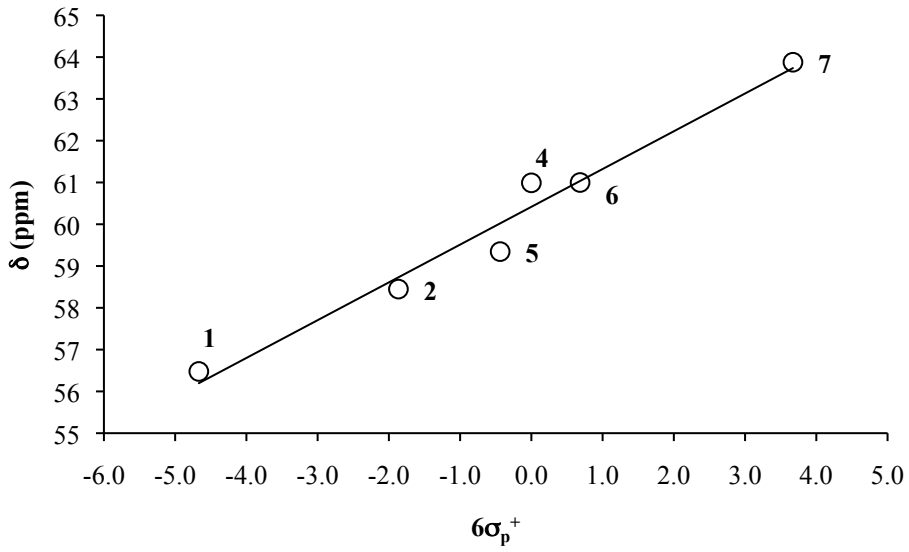


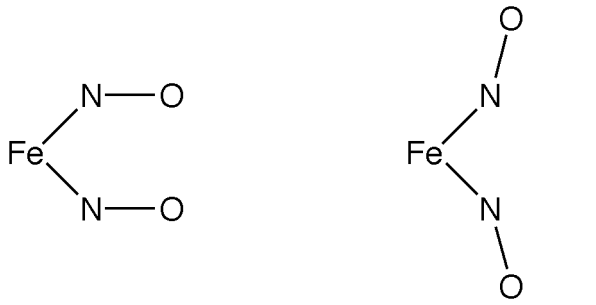
Figure 2.27. Plot depicting the $\delta(^{31}P)$ chemical shifts for each $Fe(NO)_2(PAr_3)_2$ as a function of the Brown-Okamoto constant σ_p^+. The Brown-Okamoto constant is used in cases where substituents are capable of participating in a direct resonance interaction with the phosphorus atom.

It is evident that the ^{31}P NMR chemical shift is affected by small changes on the periphery of the PAr_3 ligands. Based on our data, some combination of ligand basicity and resonance factors play important roles. However, the relative contribution of each factor is not clear.

2.4.4 X-ray Crystallography

As has been discussed in the previous sections, the electron density at the iron atom in $Fe(NO)_2(PAr_3)_2$ compounds is affected by the use of different substituents attached to the aromatic rings of the phosphine ligands. It is reasonable to expect structural differences in the $Fe(NO)_2$ fragment as a consequence of different substituents being attached.

All of the studied compounds possess a distorted tetrahedral geometry around at the iron center. The iron is bound to two nitrosyl groups via the nitrogen atoms and to two phosphine ligands via the phosphorus atom. The N-Fe-N bond angles are in the range 122° – 130° while the P-Fe-P bond angles are in the range 105° - 109°. The Fe-N-O bond angles range between 173° - 180°. As a whole, the $Fe(NO)_2$ unit is in an "*attracto"* conformation where the O••Fe••O < N-Fe-N bond angle (Figure 2.28).



"*attracto*" O••Fe••O < N-Fe-N

"*repulso*" O••Fe••O > N-Fe-N

Figure 2.28. Schematic depicting *"attracto"* and *"repulso"* conformations of the $Fe(NO)_2$ group.[32]

The *"attracto"* conformation tends to be characteristic of first row transition-metal dinitrosyls, which incorporate good pi-accepting ligands.[32] The Fe-N bond lengths of ~1.65 Å are all shorter than 1.688(3) found in $Fe(NO)_2(CO)_2$.[60]

There doesn't appear to be a clear pattern in the X-ray data. This is likely due to the fact that the changes are very small. However, some noteworthy observations can be made by comparing the two extremes (electron-donating substituents vs. electron-withdrawing substituents) relative to the parent $Fe(NO)_2(PPh_3)_2$ compound.

The O••Fe••O bond angle of the parent compound is ~122.47°. Replacement of the hydrogen with the more electron donating methoxy group is accompanied by an increase in the O••Fe••O bond angle of ~5.5° Conversely, replacement of the of the hydrogen with CF_3, a more electron withdrawing group is accompanied by a ~4.0° decrease in the O••Fe••O bond angle. All three of these phosphines have cone angles of ~145° and thus we would expect sterics to be a small factor. Similar results are observed within the M-N-O bond angles. Overall, electron donating substituents promote increased metal-ligand backbonding which is manifest as wider bond angles. The opposite is true for electron withdrawing substituents.

The molecular structures for $Fe(NO)_2(PPh_3)_2$ and $[Fe(NO)_2(PPh_3)_2]PF_6$ were published by Albano and Atkinson respectively.[30, 35] Atkinson noted a number of important differences between the structure of the neutral compound and that of the cation. First, oxidation of $Fe(NO)_2(PPh_3)_2$ was accompanied with a substantial increase (0.095 Å) in the Fe-P bond length from 2.267(2) Å in the neutral compound to 2.362(1) Å in the cation. This is an effect that is consistent with increased Fe-P π back-bonding character in the HOMO of $Fe(NO)_2(PPh_3)_2$. The N-O bond was observed to have

shortened (Δ -0.03 Å) from 1.190(10) Å in the neutral compound to 1.160(6) Å in the cation while the Fe-N bond was lengthened (Δ +0.011 Å) from 1.650(7) Å in the neutral compound to 1.661(4) Å in the cation. The effects on these two bonds was consistent with π back-bonding to the nitrosyl π* orbitals, but was relatively small. Nevertheless, Atkinson reported a higher nitrosyl IR stretching frequency for the cation [$\Delta\nu_{NO}$ = ~100 cm^{-1}] which is consistent with a 1-electron metal centered oxidation. The geometry around the iron center of $(Ar_3P)_2Fe(NO)_2$ changed markedly upon oxidation. The interphosphine angle, P-Fe-P, increased by 11.2° and the internitrosyl angle decreased by 10.3°. Finally, the nitrosyl ligands in the cation bent inward toward each other in an *"attracto"* confirmation [Δ(∠ Fe-N-O) = 12.0°].

All of the observations reported by Atkinson were consequences of the single electron oxidation of $Fe(NO)_2(PPh_3)_2$ which is the extreme case of perturbing electron density at the metal center. It might be expected that some intermediate effects would be observed, as described in my work using ligands to "fine tune" the density to a lesser extent. The results of electrochemical oxidation of our compounds are discussed in the next section.

2.4.5 Electrochemistry

The cyclic voltammogram for compound **4,** $Fe(NO)_2(P(C_6H_6)_3)_2$, was previously reported by Atkinson to have a single diffusion controlled fully reversible oxidation in CH_2Cl_2 at $E°'$ = 0.37 V vs. SCE (-0.10 vs. Fc/Fc^+). No reductions were observed in the potential range 0.00 to -1.80 V vs. SCE. The present determination for **4** agrees within 30 mV of Atkinson's result. Except for the compound **7**, $Fe(NO)_2(P(C_6H_4\text{-}p\text{-}CF_3)_3)_2$, each of the other compounds analyzed exhibited a single reversible oxidation within the potential range examined. The electrochemical data for each compound is summarized in Table 2.7.

Changing the bascitiy of the ligands attached to the iron metal center can be expected to affect the formal redox potential of the compound. Compounds with more electron density available at the metal center should be easier to oxidize relative to the parent compound whereas those compounds with less electron density available should be more difficult to oxidize than the parent. It was observed that compounds with the most basic phosphine ligands were the easiest to oxidize as indicated by their lower $E°'$ values. Changing to more electron withdrawing substituents caused a noticeable increase in $E°'$ from -0.21 V vs. Fc/Fc^+ in **1** to 0.10 V in **6**, a difference of 0.31 V. The largest single $\Delta E°'$ ($\Delta E°' = E_x - E_{parent}$) occurred upon changing from *p*-H to *p*-F ($\Delta E°'$ = 0.18 V). All of the other differences were < 0.05 V. E_{pa} for **7**, $Fe(NO)_2(P(C_6H_4\text{-}p\text{-}CF_3)_3)_2$, was much more positive than that of any of the other compounds occurring at 0.51 V vs. Fc/Fc^+ which is 0.37 V more positive than E_{pa} in **6**, $Fe(NO)_2(P(C_6H_4\text{-}p\text{-}Cl)_3)_2$.

A Hammett plot of *E*°' versus 6σ can be fitted to two lines which look very similar to the two line plot obtained from the ^{31}P NMR data analysis. However, in this case, the compounds clearly fall into two separate groups. (i.e. electron withdrawing and electron donating)

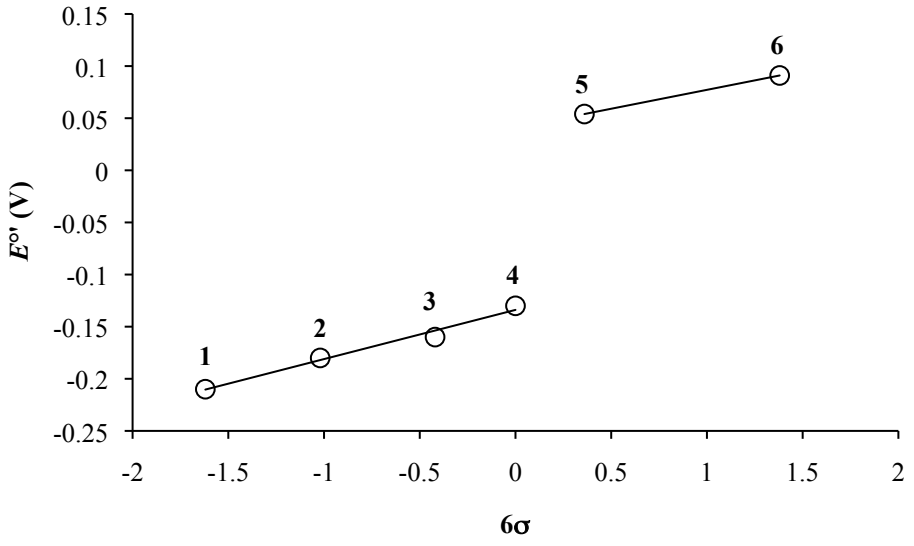


Figure 2.29. Plot depicting *E*°' for each $Fe(NO)_2(PAr_3)_2$ as a function of the Hammett parameter.

Attempting to fit the data to a single trend line gives a slope of 0.11 with r^2 = 0.82. Better fits result if two separate lines are used for the two groups. The slopes of the lines obtained are similar. The line obtained from the electron donating groups has a slope 0.047 with r^2=0.98 while the line obtained for electron withdrawing groups had a slope of slope = 0.036 with r^2 = 1 since there are only two compounds. Comparing only the *para* substituted compounds and leaving out the one *meta* substituted compound

improves the fit for the electron donating groups and gives a slope = 0.049 with r^2=0.999. Parallel lines similar to those described here and involving the same substituents on phenyl rings have been reported for a Hammett plot of the relative reactivities of *para*-substituted phenylacetyenes.[61]

Hammett plots are known to give poor correlations when resonance factors are involved. Therefore an attempt was made to obtain a correlation between *E*°' and Brown-Okamoto constants as was done with the ^{31}P NMR data in Section 2.4.3. No single linear correlation was found as shown in Figure 2.30. The same two separate groups are present which seems to suggest that resonance is not a major factor separating the two groups.

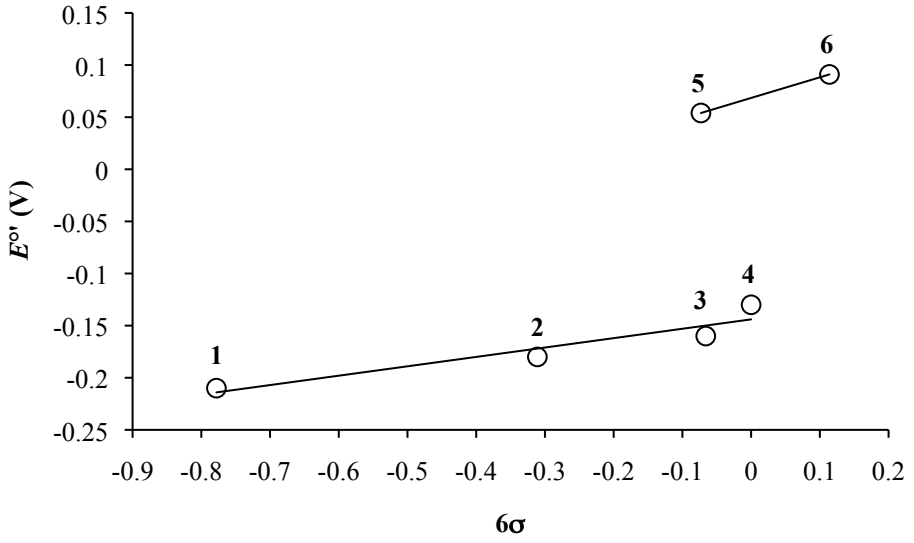


Figure 2.30. Plot depicting *E*°' for each $Fe(NO)_2(PAr_3)_2$ as a function of the Brown-Okamoto constant σ_p^+.

2.4.6 Infrared Spectroelectrochemistry

All of the studied compounds are easily oxidized to what are presumably $[Fe(NO)_2]^+$ containing species. The formation of each electrogenerated product is indicated by the appearance of two infrared bands shifted to higher wave numbers relative to the neutral compound. Simultaneously, the two infrared bands at lower wavenumbers which are associated with the neutral compound disappear. $\Delta\nu_{NO}$ for each oxidation is approximately 100 cm^{-1} which is an indication that the oxidations are metal centered.

The difference spectra for all compounds studied are similar except for the spectrum for **7**, $Fe(NO)_2(P(C_6H_4\text{-}p\text{-}CF_3)_3)_2$. The IR bands for $\mathbf{7}^+$ are not clearly defined and do not appear as symmetrical as those of the other compounds. This observation suggests that $\mathbf{7}^+$ is short lived (perhaps releasing NO) compared to the other products on the time scale of the experiment.

The relative order of the ν_{NO}s for product species is the same as that of the neutral compounds previously described. While as previously stated $\Delta\nu_{NO}$ for each compound is approximately 100 cm^{-1}, the antisymmetric stretches for the compounds containg the more electron-donating substituents have larger $\Delta\nu_{NO}$s (by about 4 cm^{-1}) than the antisymmetric stretches of the compounds containing the more electron-withdrawing substituents.

The compound $[Fe(NO)_2(P(C_6H_5)_3)_2]^+[PF_6]^-$ is known.[30] The ν_{NO} of this compound (ν_{NO} = 1766 cm^{-1} and 1814 cm^{-1}) is, as might expected, comparable to $\mathbf{4}^+$ (ν_{NO} = 1767 cm^{-1} and 1816 cm^{-1})

2.5. Conclusion

We set out to determine how the spectroscopic and electrochemical properties of the $Fe(NO)_2$ group are affected by small changes on the periphery of some dinitrosyliron diphosphine complexes (DNICs). We noted that determining this type of information was important because it will help provide a better understanding of the properties of the $Fe(NO)_2$ moiety. In pursuit of this goal we have successfully prepared a homologous series of six previously unpublished DNICs and characterized them by FTIR and ^{31}P NMR spectroscopy, X-ray crystallography, cyclic voltammetry and fiber-optic infrared spectroelectrochemistry.

Considering all of our results collectively, it was found that relatively small changes on the periphery of the DNICs do indeed have a major effect on their spectroscopic and electrochemical properties. We further report that the solvent system also has a noticeable influence. In addition, IR, ^{31}P NMR spectroscopic and electrochemical data all show evidence of two different classes of $Fe(NO)_2L_2$ compounds (L = phosphine; those with electron withdrawing groups and those with electron donating groups at the phosphine periphery).

Specifically, with FTIR spectroscopy we showed that the ν_{NO}s of our DNICs could be correlated with the phosphine ligand basicity as measured by the Hammett substituent parameter. We showed that in addition to the ligand basicity, the solvent donor and acceptor capacity affected the ν_{NO}s as quantified by the Gutmann donor and acceptor numbers. We also showed that in CH_2Cl_2 and in toluene, the compounds with electron donating groups could be distinguished from those with electron withdrawing groups. Such a distinction could not be made with the coordinating solvent acetonitrile,

which suggested that the three different kinds of solvents interacted differently with each of the two classes of DNICs.

With the ^{31}P NMR data, we showed that the phosphine chemical shifts are affected by the ligand basicity as exhibited by a two-line Hammett plot. Furthermore we obtained a linear relationship between $\delta(^{31}P)$ and the Brown-Okamoto constant suggesting that resonance factors also play some role, however, it is not clear how these factors are related or what other factors may be involved.

Substituent influenced structural differences are evident in the X-ray crystallographic data, but the changes are very small. However, on two extremes (most electron withdrawing substituents versus most electron donating substituents) the differences are quite clear. We were able to show that, among other small changes, the $Fe(NO)_2$ responds to the peripheral substituents by exhibiting an enhanced "*attracto*" conformation with electron withdrawing groups. Larger O•••Fe•••O angles found when electron donating groups are in place.

Lastly, the electrochemistry and the infrared spectroelectrochemistry of the $Fe(NO)_2$ group is dramatically affected by small changes on the periphery of the DNICs. All of the compounds studied exhibit 1-electron oxidations. Reductions were not evident within the solvent potential limit, however, the parent $Fe(NO)_2(CO)_2$ compound was easily reduced in a 1-electron process. Compounds containing the more basic phosphines were easily oxidized at lower *E*°' values while exhibiting a $\Delta\nu_{NO}$ (compared to the neutral compound) of about 100 cm^{-1}. Changing to less basic phosphines with more electron withdrawing substituents (e.g. *p*-F, *p*-Cl, *p*-CF_3) shifted *E*°' values higher eventually leading to the short lived $[Fe(NO)_2(P(C_6H_4\text{-}p\text{-}CF_3)_3)_2]^+$ compound relative to the cyclic

voltammetry time scale employed. Oxidation of **7**, $Fe(NO)_2(P(C_6H_4\text{-}p\text{-}CF_3)_3)_2$, may even release NO as indicated by its infrared difference spectrum.

All of the results herein can be used to emphasize the fact that the environment around DNICs affect their chemistry. This is true even from relatively remote positions on the molecule. As more is learned about the role of DNICs in biological systems including the local environment surrounding them (i.e. ligands), this information may be useful in helping to control their chemical fate and in predicting their derivatives.

2.6. References

1. Shumaev, K. B.; Petrova, N. E.; Zabbarova, I. V.; Vanin, A. F.; Topunov, A. F.; Lankin, V. Z.; Ruuge, E. K., Interaction of Oxoferrylmyoglobin and Dinitrosyl-Iron Complexes. *Biochemistry (Moscow)* **2004,** *69* (5), 569-574.

2. Alencar, J. L.; Vanin, A. F.; Muller, B., Inhibition of Arterial Contraction by Dinitrosyl–Iron Complexes: Critical Role of the Thiol Ligand in Determining Rate of Nitric Oxide (NO) Release and Formation of Releasable NO Stores by S-Nitrosation. *Biochem. Pharmacol.* **2003,** *66*, 2365-2374.

3. Muller, B.; Kleschyov, A. L.; Alencar, J. L.; Vanin, A.; Stoclet, J.-C., Nitric Oxide Transport and Storage in the Cardiovascular System. *Ann. N. Y. Acad. Sci.* **2002,** *962*, 131-139.

4. Vanin, A. F.; Serezhenkov, V. A.; Mikoyan, V. D.; Genkin, M. V., The 2.03 Signal as an Indicator of Dinitrosyl-Iron Complexes with Thiol-Containing Ligands. *Nitric Oxide* **1998,** *2* (4), 224-234.

5. Mulsch, A.; Mordvintcev, P. I.; Vanin, A. F.; Busse, R., Formation and Release of Dinitrosyl Iron Complexes by Endothelial Cells. *Biochem. Biophys. Res. Commun.* **1993,** *196* (3), 1303-1308.

6. Vanin, A. F.; Men'shikov, G. B.; Moroz, I. A.; Mordvintcev, P. I.; Serezhenkov, V. A.; Burbaev, D. S., The Source of Non-Heme Iron that Binds Nitric Oxide in Cultivated Macrophages. *Biochim. Biophys. Acta* **1992,** *1135* (3), 275-279.

7. Vanin, A. F., Endothelium-Derived Relaxing Factor is a Nitrosyl Iron Complex with Thiol Ligands. *FEBS Lett.* **1991,** *289* (1), 1-3.

8. Mulsch, A.; Mordvintcev, P.; Vanin, A. F.; Busse, R., The Potent Vasodilating and Guanylyl Cyclase Activating Dinitrosyl-Iron(II) Complex is Stored in a Protein-Bound Form in Vascular Tissue and is Released by Thiols. *FEBS Lett.* **1991,** *294* (3), 252-256.

9. Li Kam Wah, H.; Postel, M.; Pierrot, M., Structure-Activity Correlation in Iron Nitrosyl Complexes: Crystal Structures of $[Fe(NO)_2(Cl)]_2$(μ-dppe) and $Fe(NO)_2$(dppe). *Inorg. Chim. Acta* **1989,** *165* (2), 215-220.

10. Munyejabo, V.; Guillaume, P.; Postel, M., Activation of Molecular Oxygen by Iron Nitrosyls in the Presence of the Bidentate Phosphines 1,2-Bis(diphenylphosphino)ethane and Ethene. *Inorg. Chim. Acta* **1994,** *221* (1-2), 133-139.

11. Postel, M.; Tomi, F.; Li Kam Wah, H.; Mordenti, L.; Guillaume, P., Decisive Influence of Phosphorus Ligands on Oxygen Oxidations of Alkenes in the Presence of the Iron Nitrato/Iron Nitrosyl Couple. *Phosphorus, Sulfur Silicon Relat. Elem.* **1990,** *49-50* (1-4), 453-457.

12. Tomi, F.; Wah, H. L. K.; Postel, M., Iron-Nitrato/iron-Nitrosyl: A New Redox Couple for the Activation and Transfer of Dioxygen. X-ray Structure of $Fe(NO_3)_2(OPPh_3)_2Cl$. *New J. Chem.* **1988,** *12* (5), 289-292.

13. Li Kam Wah, H.; Postel, M.; Tomi, F., The Iron-Nitrato Iron-nitrosyl Couple in the Presence of Hexamethylphosphoric Triamide and its Relevance to Oxygen Activation and Transfer - X-Ray Structure of $Fe(NO_3)(Cl)_2(HMPA)_2$. *Inorg. Chem.* **1989,** *28* (2), 233-238.

14. Candlin, J. P.; Janes, W. H., The Catalytic Dimerization of Dienes by Nitrosylcarbonyl Transition-metal Compounds. *J. Chem. Soc. C* **1968,** (15), 1856-1860.

15. Gadd, G. E.; Poliakoff, M.; Turner, J. J., Photochemical reaction of $Fe(CO)_2(NO)_2$ and $Co(CO)_3NO$ with 1,3-butadiene in liquid xenon solution: possible intermediates in the catalytic dimerization of dienes. *Organometallics* **1987,** *6* (2), 391-397.

16. Huchette, D.; Nicole, J.; Petit, F., Selective Cyclodimerization of 1,3-Diolefins Catalyzed by "$Fe(NO)_2$" Generated by Electrochemical Reduction of Ferric Chloride in the Presence of Nitric Oxide. *Tetrahedron Lett.* **1979,** (12), 1035-1038.

17. Ballivet-Tkatchenko, D.; Esselin, C.; Goulon, J., EXAFS Study of Soluble Dinitrosyl Iron and Cobalt Complexes Catalyzing Specific Transformations of Olefins. *J. Phys., Colloq.* **1986,** (C8, Vol. 1), C8/343-C8/346.

18. Maxfield, P. L. Dimerization of Diolefins. U.S. Patent 3,377,397, April 9, 1968.

19. Li, L.; Enright, G. D.; Preston, K. F., Synthesis and X-ray Crystal Structure of a Novel Iron Nitrosyl Complex, $Fe(NO)_2PPh_3(\eta^2$-TCNE). *Organometallics* **1994,** *13* (12), 4686-4688.

20. Pellat, C.; Henry, Y.; Drapier, J.-C., IFN-γ-activated Macrophages: Detection by Electron Paramagnetic Resonance of Complexes Between L-Arginine-derived Nitric oxide and Non-heme Iron Proteins. *Biochem. Biophys. Res. Commun.* **1990,** *166* (1), 119-125.

21. Lancaster, J. R.; Hibbs, J. B., EPR Demonstration of Iron Nitrosyl Complex-Formation by Cytotoxic Activated Macrophages. *Proc. Natl. Acad. Sci. U. S. A.* **1990,** *87* (3), 1223-1227.

22. Reddy, D.; Lancaster, J. R.; Cornforth, D. P., Nitrite Inhibition of Clostridium Botulinum: Electron Spin Resonance Detection of Iron-Nitric Oxide Complexes. *Science* **1983,** *221* (4612), 769-770.

23. Cesareo, E.; Parker, L. J.; Pedersen, J. Z.; Nuccetelli, M.; Mazzetti, A. P.; Pastore, A.; Federici, G.; Caccuri, A. M.; Ricci, G.; Adams, J. J.; Parker, M. W.; Lo Bello, M., Nitrosylation of Human Glutathione Transferase P1-1 with Dinitrosyl Diglutathionyl Iron Complex *in Vitro* and *in Vivo*. *J. Biol. Chem.* **2005,** *280* (51), 42172-42180.

24. Toledo, J. C.; Bosworth, C. A.; Hennon, S. W.; Mahtani, H. A.; Bergonia, H. A.; Lancaster, J. R., Nitric Oxide-induced Conversion of Cellular Chelatable Iron into Macromolecule-bound Paramagnetic Dinitrosyliron Complexes. *J. Biol. Chem.* **2008,** *283* (43), 28926-28933.

25. Stadler, J.; Bergonia, H. A.; Disilvio, M.; Sweetland, M. A.; Billiar, T. R.; Simmons, R. L.; Lancaster, J. R., Nonheme Iron-Nitrosyl Complex Formation in Rat Hepatocytes: Detection by Electron Paramagnetic Resonance Spectroscopy. *Arch. Biochem. Biophys.* **1993,** *302* (1), 4-11.

26. Li, L.; Reginato, N.; Urschey, M.; Stradiotto, M.; Liarakos, J. D., The Synthesis and Structural Characterization of Linear and Macrocyclic Bis(dinitrosyliron) Complexes Supported by Bis(phosphine) Bridging Ligands. *Can. J. Chem.* **2003,** *81* (6), 468-475.

27. Eisch, J. J.; King, R. B., Metal Nitrosyl Derivatives. In *Organometallic Syntheses*, Academic Press: New York, 1965; pp 167-168.

28. Shaw, M. J.; Henson, R. L.; Houk, S. E.; Westhoff, J. W.; Jones, M. W.; Richter-Addo, G. B., Fiber-optic Infrared Reflectance Spectroelectrochemistry: Isomerization of a Manganese Pyranyl Complex. *J. Electroanal. Chem.* **2002,** *534* (1), 47-53.

29. McBride, D. W.; Stafford, S. L.; Stone, F. G. A., Chemistry of the Metal Carbonyls. XVI. Synthesis of Dicarbonyldinitrosyliron(0). *Inorg. Chem.* **1962,** *1*, 386-388.

30. Atkinson, F. L.; Blackwell, H. E.; Brown, N. C.; Connelly, N. G.; Crossley, J. G.; Orpen, A. G.; Rieger, A. L.; Rieger, P. H., Synthesis of the 17-Electron Cations $[FeL(L')(NO)_2]^+$ (L, L' = PPh_3, $OPPh_3$): Structure and Bonding in Four-Coordinate Metal Dinitrosyls, and Implications for the Identity of Paramagnetic Iron Dinitrosyl Complex Catalysts. *J. Chem. Soc., Dalton Trans.* **1996,** (17), 3491-3502.

31. van der Sluis, P.; Spek, A. L., BYPASS: an effective method for the refinement of crystal structures containing disordered solvent regions. *Acta Cryst.* **1990,** *46* (3), 194-201.

32. Richter-Addo, G. B.; Legzdins, P., *Metal Nitrosyls*. Oxford University Press: New York, 1992.

33. Munyejabo, V.; Damiano, J.-P.; Postel, M.; Bensimon, C.; Roustan, J. L., Reactivity of a (Fe-NO)-(Fe-NO_3) System in the Presence of a Ferrocene-Ferricinium Group Tethered Nearby via a Ferrocenylphosphine Linkage (FcP_2): Crystal Structures of $[\{Fe(NO)_2Cl\}_2(m\text{-}FcP_2)]$ and $[Fe(NO)_2(FcP_2)]$. *J. Organomet. Chem.* **1995,** *491* (1-2), 61-69.

34. Gerbase, A. E.; Vichi, E. J. S.; Stein, E.; Amaral, L.; Vasquez, A.; Horner, M.; Maichle-Mossmer, C., Preparation, Characterization and Electrochemical Studies of 1,1'-Bis(diphenylphosphino)ferrocene (dppf) Derivatives. Crystal Structure of $[dppfCo(NO)_2][SbF_6]$. *Inorg. Chim. Acta* **1997,** *266* (1), 19-27.

35. Albano, V. G.; Araneo, A.; Bellon, P. L.; Ciani, G.; Manassero, M., Stereochemistry of Tetrahedral Complexes of Group VIII Metals. Crystal and Molecular Structures of Dinitrosylcarbonyl(triphenylphosphine) Iron and of Dinitrosylbis(triphenylphosphine)iron. *J. Organomet. Chem.* **1974,** *67* (3), 413-422.

36. Piazza, G.; Paliani, G., Polarographic Behavior of Transition Metal Nitrosyl Complexes in Nonaqueous Media. III. Dinitrosyl Iron Dicarbonyl and its Mono- and Disubstituted Derivatives with Triphenylphosphine. *Z. Phys. Chem. (Muenchen, Ger.)* **1970,** *71* (1-3), 91-101.

37. Hieber, W.; Fuehrling, H., Metal-Nitrogen Oxide Complexes. XXV. Nitrosylcyano Complexes of Iron Group Metals. *Z. Anorg. Allg. Chem.* **1970,** *373* (1), 48-56.

38. Ballivet, D.; Billard, C.; Tkatchenko, I., A Novel Synthesis of Neutral Dinitrosyl Iron Complexes. Their Catalytic Behavior. *Inorg. Chim. Acta* **1977,** *25* (2), L58.

39. Tsai, F.-T.; Chiou, S.-J.; Tsai, M.-C.; Tsai, M.-L.; Huang, H.-W.; Chiang, M.-H.; Liaw, W.-F., Dinitrosyl Iron Complexes (DNICs) $[L_2Fe(NO)_2]^-$ (L = Thiolate): Interconversion among $\{Fe(NO)_2\}_9$ DNICs, $\{Fe(NO)_2\}^{10}$ DNICs, and [2Fe-2S] Clusters, and the Critical Role of the Thiolate Ligands in Regulating NO Release of DNICs. *Inorg. Chem.* **2005,** *44* (16), 5872-5881.

40. Pignataro, S.; Distefano, G.; Foffani, A., Substitution Kinetics of Paramagnetic Iron(0) Nitrosyl Complexes. Temperature Dependence of the Arrhenius Activation Energy. *J. Am. Chem. Soc.* **1970,** *92* (22), 6425-6429.

41. Bitterwolf, T. E.; Steele, B., Facile Synthesis of $Fe(NO)_2L_2$ compounds, where L = phosphines and phosphites. *Inorg. Chem. Commun.* **2006,** *9* (5), 512-513.

42. Tolman, C. A., Electron Donor-Acceptor Properties of Phosphorus Ligands. Substituent Additivity. *J. Am. Chem. Soc.* **1970,** *92* (10), 2953-2956.

43. Tolman, C. A., Phosphorus Ligand Exchange Equilibriums on Zerovalent Nickel. Dominant Role for Steric Effects. *J. Am. Chem. Soc.* **1970,** *92* (10), 2956-2965.

44. Tolman, C. A., Steric Effects of Phosphorus Ligands in Organometallic Chemistry and Homogeneous Catalysis. *Chem. Rev.* **1977,** *77* (3), 313-348.

45. Allman, T.; Goel, R. G., The Basicity of Phosphines. *Can. J. Chem.* **1982,** *60* (6), 716-722.

46. Lewis, J.; Irving, R. J.; Wilkinson, G., Infrared Spectra of Transition Metal-Nitric Oxide Complexes. I. Complexes Involving Donation from the NO+ Ion. *J. Inorg. Nucl. Chem.* **1958,** *7*, 32-37.

47. Foffani, A.; Poletti, A.; Cataliotti, R., Solvent Effect on C-O and N-O Stretching Modes of Different Symmetry in Transition-Metal Carbonyl-Nitrosyls. *Spectrochim. Acta, Part A* **1968,** *24* (9), 1437-1447.

48. Gutmann, V., Solvent Effects on Metal Carbonyls and Related Compounds. *Monatsh. Chem.* **1977,** *108* (2), 429-435.

49. Horrocks, W. D.; Mann, R. H., Solvent Effects on the Infrared Frequency of Inorganic Carbonyl and Nitrosyl Bands. *Spectrochimica Acta* **1965,** *21* (3), 399-408.

50. Hansch, C.; Leo, A.; Taft, R. W., A Survey of Hammett Substituent Constants and Resonance and Field Parameters. *Chem. Rev.* **1991,** *91* (2), 165-195.

51. Smith, M. B.; March, J., *March's Advanced Organic Chemistry*. 5th ed.; John Wiley & Sons, Inc.: New York, 2001.

52. Hammett, L. P., Some Relations Between Reaction Rates and Equilibrium Constants. *Chem. Rev.* **1935,** *17*, 125-136.

53. Neubrand, A.; Poe, A. J.; van Eldik, R., Activation Parameter Correlations for Nucleophile Addition to $(\mu_2\text{-H})_2Os_3(CO)_{10}$. *Organometallics* **1995,** *14* (7), 3249-3258.

54. Mayer, U.; Gutmann, V.; Gerger, W., The Acceptor Number — A Quantitative Empirical Parameter for the Electrophilic Properties of Solvents. *Monatsh. Chem.* **1975,** *106* (6), 1235-1257.

55. Gutmann, V., Empirical Parameters for Donor and Acceptor Properties of Solvents. *Electrochim. Acta* **1976,** *21* (9), 661-670.

56. Gutmann, V., Solvent Effects on the Reactivities of Organometallic Compounds. *Coord. Chem. Rev.* **1976,** *18* (2), 225-255.

57. Gutmann, V.; Wychera, E., Coordination Reactions in Nonaqueous Solutions. The Role of the Donor Strength. *Inorg. Nucl. Chem. Lett.* **1966,** *2* (9), 257-260.

58. Chipperfield, J., *Non-Aqueous Solvents*. Oxford University Press, Inc.: 1999.

59. Marcus, Y., The Properties of Organic Liquids that are Relevant to their Use as Solvating Solvents. *Chem. Soc. Rev.* **1993,** *22* (6), 409-416.

60. Hedberg, L.; Hedberg, K.; Satija, S. K.; Swanson, B. I., Structure and Bonding in Transition-Metal Carbonyls and Nitrosyls. 1. Gas-phase Electron-diffraction Investigations of Tetranitrosylchromium ($Cr(NO)_4$, Carbonyltrinitrosylmanganese ($MnCO(NO)_3$), and Dicarbonyldinitrosyliron ($Fe(CO)_2(NO)_2$). *Inorg. Chem.* **1985,** *24* (18), 2766-2771.

61. Paris, S. I. M.; Lemke, F. R., Substituent Effects in the Ruthenium Catalyzed Hydrosilylation of *para*-Substituted Phenylacetylenes. *Inorg. Chem. Commun.* **2005,** *8* (5), 425-428.

Chapter 3. The Behavior of 2-Methyl-2-nitrosopropane in Several Solvents: A Kinetics and Equilibrium Study Using ^{1}H NMR Spectroscopy

3.1. Introduction

Nitric oxide, NO, or its activated form reacts with a variety of species to form several different types of derivative compounds. In the first chapter of this thesis, it was mentioned that NO reacts with metals to form nitrosyl (metal-NO) compounds.[1] NO also attaches to some organic fragments to form a variety of nitroso (X-N=O) derivatives that include *N*-nitroso (nitrosamines), *O*-nitroso (alky/aryl nitrites), *S*-nitroso (alkyl/aryl thionitrites) and *C*-nitroso (nitrosoalkanes and nitrosoarenes) compounds (Figure 3.1).[2]

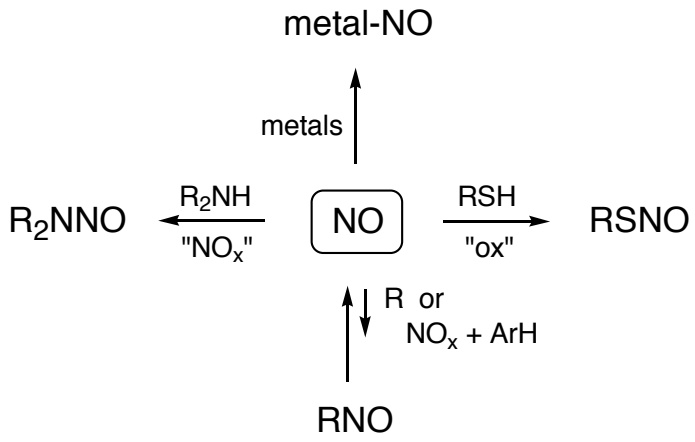


Figure 3.1. Schematic depicting some reactions of nitric oxide with metals and with representative organic fragments.

C-nitroso compounds (RNO) are known to bind to metals.[3-4] They are also occasionally utilized in polymer chemistry.[5] Recent interest in the fundamental properties of this class of compounds has been increasing due to the recognition of the

roles that they play in various biological processes.[3] For example, nitrosoarenes are known to bind to hemoglobin and myoglobin. A hemoglobin complex with Ph-NO is known to be a metabolic product resulting from nitrobenzene poisoning.[3] Under certain physiological conditions some amine containing drugs are metabolized by the enzyme cytochrome P450 to yield *C*-nitroso derivatives, and the activity of cytochrome P450 is also thought to be inhibited by its binding to RNO compounds.[3, 6-8]

Some *C*-nitroso compounds are known to be carcinogens in laboratory animals and in humans while, in contrast, others are thought to have potential as donors of nitric oxide for therapeutic use and may be able to selectively deliver a single redox form of NO to biological targets of interest.[9-10]

Given the biological relevance and the synthetic utility of RNO type compounds, it is of interest to study their fundamental properties and the conditions under which they are active. A number of reviews covering the preparation, coordination chemistry, and history of RNO compounds have been published.[3-4, 11-13]

C-nitroso compounds may exist in monomeric or dimeric form. Dimeric forms are formally azodioxy compounds, that may also be cis/trans dimers. In solution, the dimeric form is in equilibrium with the monomeric form (Figure 3.2) and except in the case of tertiary *C*-nitroso dimers, isomerization to the corresponding oxime (R′CH=NOH) may be possible.[3, 13]

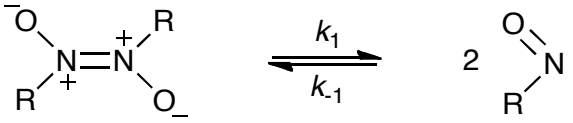


Figure 3.2. General equation for an RNO dimer-monomer equilibrium in solution.

Our interest in the fundamental chemistry of *C*-nitroso compounds has led us to study the equilibrium established by the tertiary dimer 2-methyl-2-nitrosopropane $(tBuNO)_2$. The solid dimer is colorless and in solution the monomer is blue.[14] This equilibrium has previously been studied by various techniques including ^{1}H NMR, ^{14}N NMR, and UV-vis spectroscopy.[15-18] In most cases, however, the data obtained was for a single solvent and at a single temperature.[14-24] In this chapter, we report a kinetics and equilibrium study of the 2-methyl-2-nitrosopropane dissociation reaction involving a series of solvents over a sufficient temperature range to allow for the calculation of thermodynamic data for the dimer-monomer equilibrium. We were particularly interested in establishing the dependence of the equilibrium and rate constants on various solvent parameters.

We thus set out to determine equilibrium and rate constants (K_{eq}, k_1 and k_{-1}) in seven different solvents using ^{1}H NMR spectroscopy. Equilibrium constants were determined over a range of temperatures from 10 to 40 °C as appropriate for the solvent. Rate constants were determined in the range 20 - 30 °C. The dependence of K_{eq}, k_1 and k_{-1} on selected solvent parameters was established and related thermodynamic and kinetic parameters were calculated. We thank Brian G. Gowenlock (United Kingdom) for providing us with a copy of an unpublished manuscript and his request for us to investigate this subject.

3.2. Experimental

3.2.1 Chemicals

The dimer, 2-methyl-2-nitrosopropane, was purchased from Sigma-Aldrich Chemical company (Milwaukee, WI), stored at -10° C, and used as received. Acetone-d_6 (D, 99.9%), acetonitrile-d_3 (D, 99.8%), chloroform-d (D, 99.8%), cyclohexane-d_{12} (D, 99.5%), dichloromethane-d_2 (D, 99.9%), dimethyl sulfoxide-d_6 (D, 99.9%) and ethanol-d_6 (D, 99%, anhydrous) were purchased from Cambridge Isotope Laboratories (Andover, MA). All deuterated solvents (except chloroform) were obtained in single-use ampoules and used as received. Chloroform was drawn from a stock reagent bottle, subjected to at least three freeze-pump-thaw cycles and stored under nitrogen over Grade 514 Type 4A molecular sieves.

3.2.2 Instrumentation

Variable temperature ^{1}H NMR spectra were obtained using a Varian Mercury-VX 300 MHz spectrometer equipped with a four-nuclei autoswitchable pulse field gradient probe. The calibration of the variable temperature unit was checked periodically using the temperature dependence of the chemical shift between the OH resonances and the CH_3 resonances of methanol. Spectra were obtained (as described in Section 3.2.3) using a 45-degree pulse. All chemical shifts (δ, ppm) were referenced to the residual signal of the solvent employed.

3.2.3 Variable Temperature NMR in Different Solvents

A known amount of 2-methyl-2-nitrosopropane (10-15 mg) was added to a dry pre-weighed NMR tube (5 mm OD Precision ASTM Type 1 Class A Borosilicate Glass). The exact weight of the sample was determined by the difference between the weight of the empty NMR tube and the same NMR tube containing the sample. The NMR spectrometer was prepared (i.e., software settings). The variable temperature probe was set to the desired temperature using a dummy sample that consisted of the solvent to be used. After setting appropriate instrument parameters and shimming, the dummy sample was removed. After the temperature was set, the initial time was set (t = 0 s) using a stopwatch while 1.0 mL of solvent was added by syringe to the NMR tube containing the sample (this procedure took 1-3 s). The colorless and clear sample was quickly inverted 2 or 3 times to ensure proper mixing and then placed into the spectrometer probe. A single transient spectrum was taken immediately. Shimming was carried out again if required. The time was again recorded and an arrayed experiment was started taking a single transient spectrum every 1 minute for 2 - 4 hours. (Note: T_1 for the dimer was determined to be ~ 2.1 s in cyclohexane at 20 °C) In all cases, the initial NMR spectra showed a large single resonance corresponding to the dimer downfield relative to another smaller peak corresponding to the monomer. During the course of the experiment the smaller peak due to the monomer became more pronounced while the peak corresponding to the dimer decreased in size. After each experiment the mass of the NMR tube containing the solvent and sample was obtained. This procedure was repeated in triplicate or more for each determination of k_1 at 20, 25 and 30 °C and for each determination of K_{eq} at 10, 15, 20, 25, 30, 35 and 40 °C in the seven different solvents.

3.3. Results

A representative ^{1}H NMR spectrum of 2-methyl-2-nitrosopropane is shown in Figure 3.3.

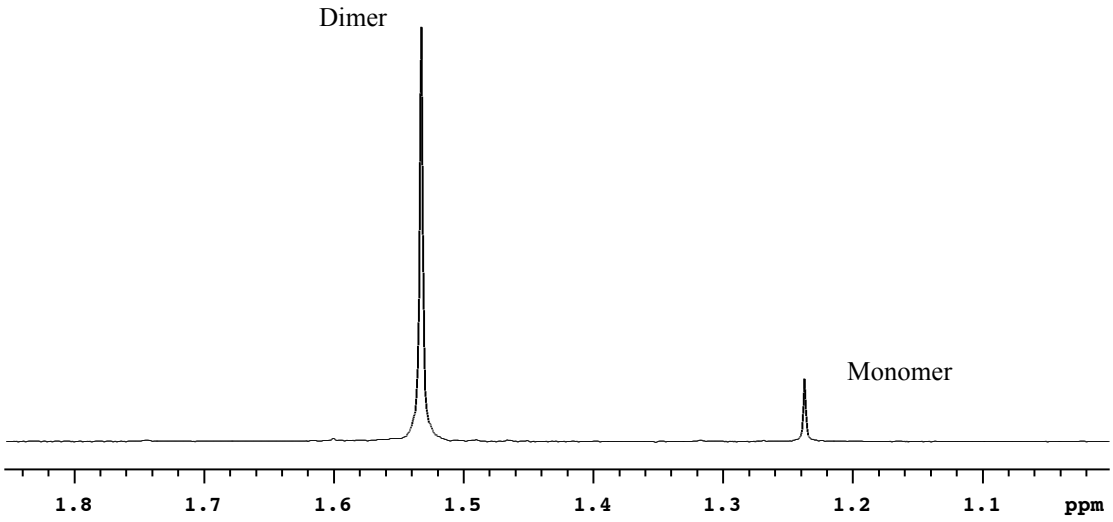


Figure 3.3. ^{1}H NMR spectrum showing peaks for the dimeric and monomeric species at 20 °C in acetonitrile at time 218 s (~3.6 min).

The absolute intensity integrated area was obtained for each peak (A_d and A_m for the dimer and the monomer respectively). The sum of the area under the peaks corresponding to the dimer and to the monomer was normalized to a value of 100. The initial dimer concentration, $[dimer]_o$, was calculated using the exact mass of the solid sample and the density adjusted volume of the solvent.

The concentration of the dimer at time t, $[dimer]_t$, was calculated by

$$[dimer]_t = \frac{A_d(t)}{100}[dimer]_o \tag{1}$$

where $A_d(t)$ is the area under the peak corresponding to the dimer at time t. The concentration of the monomer at time t was calculated by

$$[monomer]_t = \frac{2A_m(t)}{100}[dimer]_o \tag{2}$$

where $A_m(t)$ is the area under the peak corresponding to the monomer at time t.

Representative concentration traces for the monomer and dimer are shown in Figure 3.4. As the concentration of the dimer decreases with time, the concentration of the monomer increases. In this case, after about 8000 s (~ 2.2 h), the concentration no longer changes with time indicating that the system has attained equilibrium.

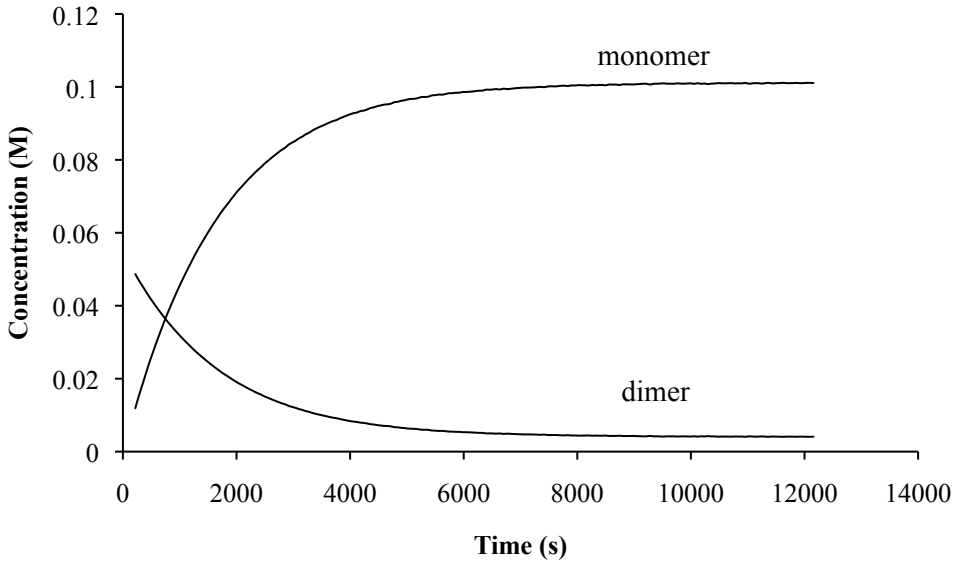


Figure 3.4. Concentration (M) vs. time (s) traces for the monomer and dimer in acetonitrile at 20°C.

As mentioned in the introduction section of this chapter, the dissociation of dimeric 2-methyl-2-nitrosopropane is an example of a dynamic equilibrium.

$$\text{dimer} \underset{k_{-1}}{\overset{k_1}{\rightleftharpoons}} 2\ \text{monomer} \tag{3}$$

The reaction is chemically reversible. Starting initially with only the dimer, the reaction proceeds to the right forming the monomer and the rate of this forward reaction decreases with time. As the concentration of the monomer increases, the rate of the reverse reaction increases.

The first derivative of the concentration vs. time traces depicted in Figure 3.4 are shown in Figure 3.5. The plot in Figure 3.5 depicts the rate of the reaction with respect to the dimer (bottom curve) and the monomer (top curve). The rate of the forward (D → 2M) reaction is given by

$$-\frac{d[\text{dimer}]}{dt} = k_1[\text{dimer}]_t \tag{4}$$

and rate of the reverse (2M → D) reaction is given by

$$\frac{d[\text{monomer}]}{dt} = k_{-1}[\text{monomer}]_t^2 \tag{5}$$

and thus the overall reaction rate is given by

$$\text{overall rate} = k_1[\text{dimer}]_t - k_{-1}[\text{monomer}]_t^2 = -\frac{d[\text{dimer}]}{dt} = \frac{1}{2}\frac{d[\text{monomer}]}{dt} \tag{6}$$

The overall reaction rate can be expressed in terms of either the dimer or the monomer concentrations. It is common practice to express the overall rate such that the numerical value of the rate will be the same regardless of which species is used. For the general reaction aA → bB the overall rate of the reaction is $-1/a\ d[A]/dt$ which is numerically equal to $1/b\ d[B]/dt$. Thus it is necessary to multiply the differential expression for the monomer in Equation 6 by ½ in order to obtain the overall rate.

As the reaction proceeds to equilibrium, the rates of the forward and reverse reactions become equal and the overall reaction rate becomes zero both with respect to the monomer and with respect to the dimer.

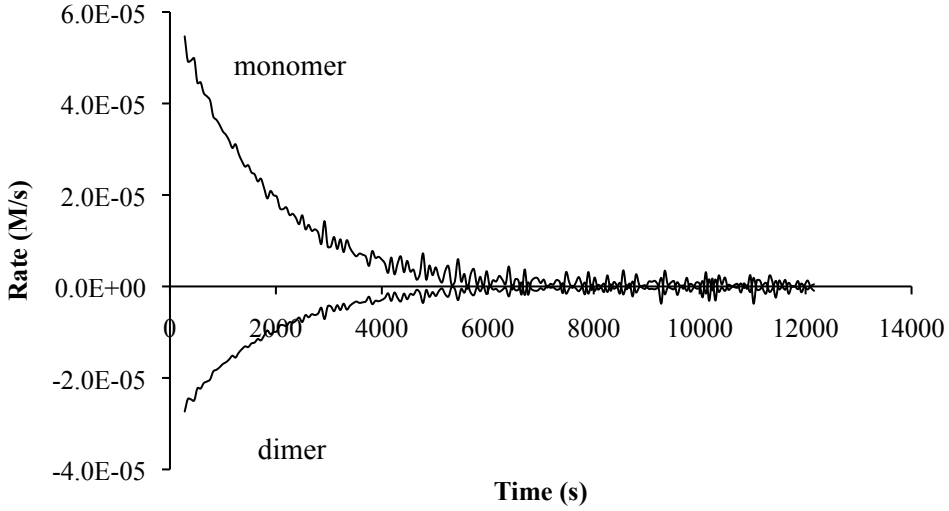


Figure 3.5. First derivative of the concentration (M) vs. time (s) traces for the monomer and dimer in acetonitrile at 20°C. Each curve represents the rate of the reaction with respect to that substance. The overall rate of the reaction = -d[dimer]/dt = ½d[monomer]/dt and approaches zero as equilibrium is attained.

3.3.1 Equilibrium Constants for the Dissociation of the 2-Methyl-2-Nitrosopropane Dimer in Various Solvents

As previously mentioned, once a state of equilibrium is attained the rates of the forward and reverse reactions are equal. Thus, employing equilibrium concentrations, the overall reaction rate is

$$\text{overall rate} = k_1[\text{dimer}]_{eq} - k_{-1}[\text{monomer}]_{eq}^2 = 0 \tag{7}$$

and therefore

$$k_1[\text{dimer}]_{eq} = k_{-1}[\text{monomer}]_{eq}^2 \tag{8}$$

which can be rearranged to give

$$\frac{k_1}{k_{-1}} = \frac{[\text{monomer}]_{eq}^2}{[\text{dimer}]_{eq}} \tag{9}$$

which is the form for the equilibrium constant

$$K_{eq} = \frac{[\text{monomer}]_{eq}^2}{[\text{dimer}]_{eq}} \tag{10}$$

The equilibrium concentrations were determined by averaging the concentrations obtained near the end of each experiment to assure that equilibrium was in place. Typically the last 10 minutes of each experiment was used. The equilibrium constants determined for seven different solvents are provided in Table 3.1. Each value is the average of 3 or more experimental determinations obtained under similar conditions (i.e.

initial concentration of dimer, solvent, temperature). The error reported is the sample standard deviation for each set. In all cases the error was larger at higher temperatures.

It is already known that chemical equilibria are affected by temperature. The results herein are consistent with this fact. Taking the data for acetonitrile as an example, it can be seen that the equilibrium constant is 3.51 ± 0.09 at 25 °C. Decreasing the temperature by 10 °C to 15°C results in a lowering of the equilibrium constant nearly in half to 1.90 ± 0.07. Similarly, raising the temperature 10 °C to 35 °C results in the near doubling of the equilibrium constant to 6.98 ± 0.36. A similar pattern with temperature was observed for all seven solvents used in this study.

In further considering the data in Table 3.1, it is clear that changing the solvent affects the magnitude of the equilibrium constant. Among the solvents used, the largest values were obtained in acetone while the smallest values were obtained in ethanol and chloroform. At 25 °C the equilibrium constant for acetone was 5.14 ± 0.19. For chloroform, the value was 1.47 ± 0.20. Values for the other five solvents fall in between. The reasons for this observed solvent effect are not immediately clear, but will be explored further in the discussion section in terms of solvent properties.

Table 3.1. Equilibrium Constants, K_{eq} (M) for the Dissociation of 2-Methyl-2-Nitrosopropane Dimer in Various Solvents †

		Temperature (°C)						
	Solvent	10	15	20	25	30	35	40
1	Acetone	2.24 ± 0.08	3.03 ± 0.12	3.81 ± 0.20	5.14 ± 0.19	6.88 ± 0.27	--	--
2	Acetonitrile	1.45 ± 0.06	1.90 ± 0.07	2.64 ± 0.13	3.51 ± 0.09	4.88 ± 0.20	6.98 ± 0.36	8.65 ± 0.28
3	Chloroform	0.59 ± 0.05	--	1.03 ± 0.10	1.47 ± 0.20	2.15 ± 0.26	--	--
4	Cyclohexane	0.90 ± 0.04	1.27 ± 0.07	1.85 ± 0.20	2.60 ± 0.32	3.46 ± 0.48	4.76 ± 0.59	6.00 ± 0.64
5	Dichloromethane	--	--	2.00 ± 0.06	2.75 ± 0.35	4.11 ± 0.23	--	--
6	DMSO	--	--	1.13 ± 0.16	1.71 ± 0.20	2.50 ± 0.28	3.32 ± 0.23	3.86 ± 0.59
7	Ethanol	0.61 ± 0.04	0.80 ± 0.06	1.14 ± 0.09	1.52 ± 0.11	2.06 ± 0.13	2.67 ± 0.24	3.31 ± 0.24

† The error reported is the sample standard deviation for each set of at least 3 experimental determinations under similar conditions.

3.3.2 *Rate Constants for the Dissociation of 2-Methyl-2-Nitrosopropane Dimer in Various Solvents*

The dissociation kinetics of 2-methyl-2-nitrosopropane dimer was studied in seven different solvents by ^{1}H NMR spectroscopy. First-order kinetics for the dissociation were determined to be the case for all solvents used.

As mentioned in the previous section (Equation 6), the overall rate of the reaction can be expressed as

$$\text{overall rate} = -\frac{d[\text{dimer}]}{dt} = k_1[\text{dimer}]_t - k_{-1}[\text{monomer}]_t^2 \tag{11}$$

An expression to determine k_1 can be found by using Equation 9 to eliminate k_{-1} from Equation 11. A number of algebraic substitutions can be made in order to obtain an expression with concentration terms on the left and $k_1\,dt$ on the right.[25] After integrating both sides the following rate law with the concentrations of the dimer and monomer as a function of time is obtained. a, b, x, y and q_d are functions of the initial, $[dimer]_o$, and equilibrium, $[dimer]_{eq}$, concentrations of the dimer, and c is the total solution concentration based on monomer units.

$$\ln\left(\frac{x[\text{dimer}]_t + a}{y[\text{dimer}]_t + b}\right) = -q_d k_1 t \tag{12}$$

$c = [\text{monomer}]_t + 2[\text{dimer}]_t$
$a = [\text{dimer}]_{eq}(-c^2 + 4[\text{dimer}]_o[\text{dimer}]_{eq}) = -[\text{dimer}]_{eq}x$
$b = c^2([\text{dimer}]_o - [\text{dimer}]_{eq})$
$x = c^2 - 4[\text{dimer}]_o[\text{dimer}]_{eq}$
$y = 4([\text{dimer}]_{eq}^2 - [\text{dimer}]_o[\text{dimer}]_{eq}) = -4[\text{dimer}]_{eq}\,b/c^2$
$q_d = (c + 2[\text{dimer}]_{eq}) / (c - 2[\text{dimer}]_{eq})$

The values for the forward rate constant k_1 were determined using Equation 12 and by least-squares fitting using COPASI.[26] A plot of the left side of Equation 12 over $-q_d$ versus time gives a slope equal to k_1. The rate constant for the reverse reaction was calculated using Equation 13. The values for k_1 and k_{-1} obtained with Equations 12 and 13 are shown in Table 3.2 and agree with those obtained using COPASI.

$$K_{eq} = \frac{k_1}{k_{-1}} \tag{13}$$

As expected, the rate constants shown in Table 3.2 are affected by temperature. For example, the rate constant for dissociation reaction of the dimer in acetone at 20 °C is 1.06 x 10^{-3} s^{-1}. Increasing the temperature by 5 degrees to 25 °C causes the rate constant to double while increasing the temperature by 10 degrees to 30 °C results in the rate constant increasing by a factor of 4. The same relationship between temperature and k_1 is observed for the other six solvents employed. The reverse rate constants, k_{-1}, for all solvents used were observed to approximately double with a 10-degree increase in temperature. For example, k_{-1} for acetone at 20 °C is 2.79 x 10^{-4} L mol^{-1} s^{-1} while at 30 °C, k_{-1} is 5.71 x 10^{-4} L mol^{-1} s^{-1}.

It is clear that the solvent affects both k_1 and k_{-1} at a given temperature. For example at 25 °C, the forward rate constants range from 5.88 x 10^{-4} s^{-1} in chloroform to 4.50 x 10^{-3} s^{-1} in cyclohexane. At the same temperature, the reverse rate constants range from 3.14 x 10^{-4} L mol^{-1} s^{-1} in dichloromethane and 3.19 x 10^{-4} L mol^{-1} s^{-1} in acetonitrile to 1.73 x 10^{-3} in cyclohexane. Potential explanations for these observations are presented in the discussion section.

Table 3.2. Rate Constants for the 2-Methyl-2-Nitrosopropane Dimer-Monomer Equilibrium in Various Solvents †

	Solvent	Temperature (°C) 20	25	30
		10^4 x k_1 (s^{-1})		
1	Acetone	10.6 ± 0.21	20.3 ± 0.41	39.3 ± 0.57
2	Acetonitrile	5.68 ± 0.16	11.2 ± 0.21	20.9 ± 0.83
3	Chloroform	2.81 ± 0.05	5.88 ± 0.11	11.9 ± 0.48
4	Cyclohexane	24.0 ± 0.35	45.0 ± 2.3	--
5	Dichloromethane	4.70 ± 0.21	8.64 ± 0.30	--
6	DMSO	5.99 ± 0.21	11.8 ± 0.23	--
7	Ethanol	6.89 ± 0.16	13.0 ± 0.02	24.0 ± 1.4
		10^4 x k_{-1} (L mol^{-1} s^{-1})		
1	Acetone	2.79 ± 0.16	3.94 ± 0.17	5.71 ± 0.24
2	Acetonitrile	2.15 ± 0.12	3.19 ± 0.10	4.27 ± 0.24
3	Chloroform	2.73 ± 0.27	4.00 ± 0.55	5.56 ± 0.71
4	Cyclohexane	13.0 ± 1.4	17.3 ± 2.3	--
5	Dichloromethane	2.35 ± 0.13	3.14 ± 0.41	--
6	DMSO	5.30 ± 0.77	6.91 ± 0.82	--
7	Ethanol	6.04 ± 0.50	8.57 ± 0.62	11.7 ± 1.0

† k_1 = forward rate constant and k_{-1} = reverse rate constant for the $D \rightleftharpoons 2M$ equilibrium. The error reported for k_1 is the sample standard deviation for each set of at least 3 experimental determinations under similar conditons. The error in k_{-1} is the propagated error based on the errors in k_1 and K_{eq} where $k_{-1} = k_1/K_{eq}$.

3.3.3 Calculation of Thermodynamic and Kinetic Parameters.

As mentioned in Section 3.3.1, the equilibrium constant for the 2-methyl-2-nitrosopropane dimer-monomer equilibrium is defined as

$$K_{eq} = \frac{[\text{monomer}]_{eq}^2}{[\text{dimer}]_{eq}} \tag{14}$$

where "eq" denotes concentrations determined under equilibrium conditions. Under non-equilibrium conditions, Equation 14 above becomes

$$Q = \frac{[\text{monomer}]_t^2}{[\text{dimer}]_t} \tag{15}$$

which is defined as the reaction quotient.

The overall tendency for the dimer dissociation reaction to occur is governed by the change in Gibbs free energy, ΔG. At any point during the reaction, ΔG is given by

$$\Delta G = \Delta G^\circ + RT \ln Q \tag{16}$$

where ΔG° is the standard Gibbs free energy change, R is the universal gas constant, T is the absolute temperature (given in Kelvin), and Q is the reaction quotient as defined above. Once equilibrium is attained, $\Delta G = 0$ and $Q = K_{eq}$. Thus, at equilibrium, the relationship between ΔG° and K is given by

$$\Delta G^\circ = - RT \ln K_{eq} \tag{17}$$

The values of ΔG° based on the equilibrium constants in Table 3.1 are given in Table 3.3.

Table 3.3. Gibbs Free Energies ($\Delta G°$, kJ mol^{-1}) for the Dissociation of 2-Methyl-2-Nitrosopropane Dimer in Various Solvents †

		Temperature (°C)						
	Solvent	10	15	20	25	30	35	40
1	Acetone	-1.90 ± 0.08	-2.66 ± 0.09	-3.26 ± 0.13	-4.06 ± 0.09	-4.86 ± 0.10	--	--
2	Acetonitrile	-0.87 ± 0.10	-1.54 ± 0.09	-2.37 ± 0.12	-3.11 ± 0.06	-4.00 ± 0.10	-4.98 ± 0.13	-5.62 ± 0.08
3	Chloroform	1.24 ± 0.20	--	-0.07 ± 0.24	-0.96 ± 0.34	-1.93 ± 0.30	--	--
4	Cyclohexane	0.25 ± 0.10	-0.57 ± 0.13	-1.50 ± 0.26	-2.37 ± 0.31	-3.13 ± 0.35	-4.00 ± 0.32	-4.67 ± 0.28
5	Dichloromethane	--	--	-1.69 ± 0.07	-2.51 ± 0.32	-3.56 ± 0.14	--	--
6	DMSO	--	--	-0.30 ± 0.35	-1.33 ± 0.29	-2.31 ± 0.28	-3.07 ± 0.18	-3.52 ± 0.40
7	Ethanol	1.16 ± 0.15	0.53 ± 0.18	-0.32 ± 0.19	-1.04 ± 0.18	-1.82 ± 0.16	-2.52 ± 0.23	-3.12 ± 0.19

† $\Delta G°$ (kJ mol^{-1}) was calculated using Equation 17 and the equilibrium constants provided in Table 3.1. The error reported for $\Delta G°$ is the propagated error based on the error reported for K_{eq}.

$\Delta G°$ is related to the change in enthalpy, ΔH, and to the change in entropy, $\Delta S°$ as given by

$$\Delta G° = \Delta H° - T\Delta S° \tag{18}$$

The contributions from enthalpy and entropy to $\Delta G°$ can be determined experimentally by measuring the equilibrium constant as a function of temperture. By combining equations 17 and 18 it is possible to write

$$\ln K_{eq} = -\frac{\Delta H°}{RT} + \frac{\Delta S°}{R} \tag{19}$$

which is one form of the van't Hoff Equation. Values for $\Delta H°$ and $\Delta S°$ can be determined by a plot of ln K_{eq} versus $1/T$ where the slope of the plot equals $-\Delta H°/R$ and the y-intercept equals $\Delta S°/R$. A representative plot is shown in Figure 3.6.

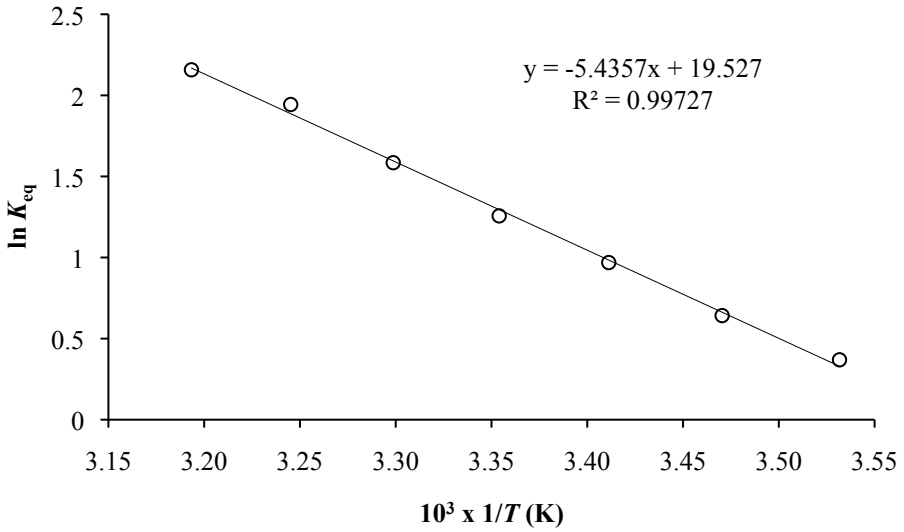


Figure 3.6. A plot of ln K_{eq} versus $1/T$ (Equation 19) for the 2-methyl-2-nitrosopropane dimer-monomer dissociation reaction in acetonitrile. The slope equals $-\Delta H°/R$ and the y-intercept equals $\Delta S°/R$.

Values for $\Delta H°$ and $\Delta S°$ were computed using the slope and the y-intercept from Equation 19 and are shown in Table 3.4.

Table 3.4. Standard Changes in Enthalpy, $\Delta H°$, and Entropy, $\Delta S°$, for the 2-Methyl-2-Nitrosopropane Dimer-Monomer Dissociation Reaction in Various Solvents †

	Solvent	$\Delta H°$ (kJ mol^{-1})	$\Delta S°$ (J mol^{-1} K^{-1})
1	Acetone	39.6 ± 1.1	146.5 ± 3.9
2	Acetonitrile	45.2 ± 1.1	162.4 ± 3.6
3	Chloroform	45.5 ± 3.3	155.9 ± 11.1
4	Cyclohexane	47.3 ± 0.8	166.3 ± 2.8
5	Dichloromethane	53.3 ± 3.9	187.5 ± 13.1
6	DMSO	47.9 ± 4.2	164.9 ± 13.8
7	Ethanol	42.7 ± 0.8	146.5 ± 2.7

† The reported error was calculated using the statistics from the least-squares plot of Equation 19.

It is known that temperature affects the rate of a reaction by affecting the value of the rate constant k. One relationship between temperature and the rate constant of a reaction is given by

$$k = \mathrm{A}e^{-Ea/RT} \tag{20}$$

which is known as the Arrhenius equation. The term E_a is the activation energy which is typically expressed in the units joules/mole. The term A is the pre-exponential or frequency factor which has the same units as k. The other two parameters R and T are the universal gas constant and the absolute temperature.

By taking the natural logarithm of both sides and rearranging Equation 20 into the form for a straight line, the Arrhenius equation can be written as

$$\ln k = \ln \mathrm{A} - \frac{E_a}{R}\frac{1}{T} \tag{21}$$

and in two-point form as

$$\ln \frac{k_2}{k_1} = \frac{E_a}{R}\left(\frac{1}{T_1} - \frac{1}{T_2}\right) \tag{22}$$

Using Equation 21 to plot ln k versus $1/T$ gives a straight line with a slope equal to $-E_a/R$ and a y-intercept equal to ln A. A representative Arrhenius plot is shown in Figure 3.7.

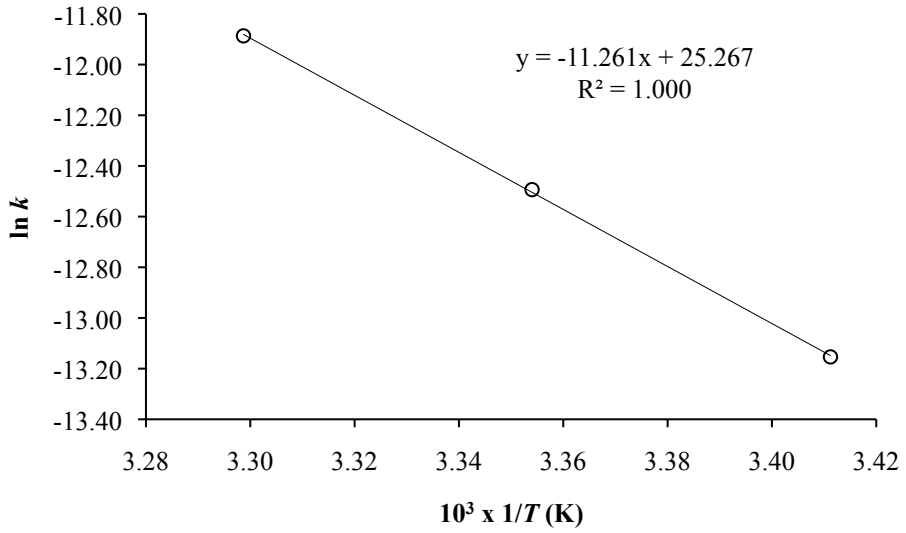


Figure 3.7. A plot of ln k versus $1/T$ (Equation 21) for the 2-methyl-2-nitrosopropane dimer-monomer dissociation reaction in acetonitrile. The slope equals $-E_a/R$ and the y-intercept equals ln A.

Using the data in Table 3.2, E_a was determined for the values of k in each solvent and are given in Table 3.5.

Table 3.5. Activation Energies for the 2-Methyl-2-Nitrosopropane Dimer-Monomer Dissociation Reaction in Various Solvents †

	Solvent	forward (D → 2M)		reverse (2M → D)	
		ln A (s^{-1})	E_a (kJ mol^{-1})	ln A (L mol^{-1} s^{-1})	E_a (kJ mol^{-1})
1	Acetone	32.8 ± 0.6	96.6 ± 1.6	13.5 ± 0.6	52.9 ± 1.5
2	Acetonitrile	32.0 ± 0.6	96.1 ± 1.4	12.4 ± 1.5	50.7 ± 3.7
3	Chloroform	35.7 ± 0.1	106.9 ± 0.2	13.4 ± 0.7	52.6 ± 1.7
4	Cyclohexane	31.5	91.5	10.6	42.0
5	Dichloromethane	28.7	88.6	9.0	42.3
6	DMSO	33.1	98.7	8.3	38.5
7	Ethanol	30.6 ± 0.1	92.4 ± 0.1	12.6 ± 0.5	48.7 ± 1.2

† D = dimer, M = Monomer. The reported error was calculated using the statistics from the least-squares plot of Equation 21.

Considering the data in Table 3.5 obtained from the empirically derived Arrhenius equation, it is clear that there are two factors (the pre-exponential or frequency factor and the activation energy) that may be affected by certain solvent properties and thus affect the rate constant k. At a given temperature, any factor affecting either A or E_a will subsequently affect k. In general, a lower activation energy corresponds to a larger k and a larger activation energy corresponds to a smaller k. This trend is generally reflected in the data obtained as chloroform with the largest E_a (forward) has the smallest forward rate constant and cyclohexane with a relatively small value for E_a (forward) has the

largest rate constant as shown in Table 3.2. The actual values for *k* are of course also dependent on the magnitude of A.

The Arrhenius equation is limited in that it ignores the chemical mechanism. More specifically, the Arrhenius equation ignores the possibility of there being one or more intermediates involved in the conversion of reactions to products. Thus, the use of the activation energy to explain the magnitude of rate constants has been replaced with transition state theory.[27]

Transition state theory has been used widely to examine the effect of solvent on chemical reactions and the model provides a useful means to explain observed effects on the reaction rate constant in terms of specific kinetic parameters (e.g. $\Delta G^{\ddagger}$, $\Delta H^{\ddagger}$ and $\Delta S^{\ddagger}$). The theory states that in order for a reaction to proceed from reactants to products, the reactants must first pass through a higher energy transition state (Figure 3.8).

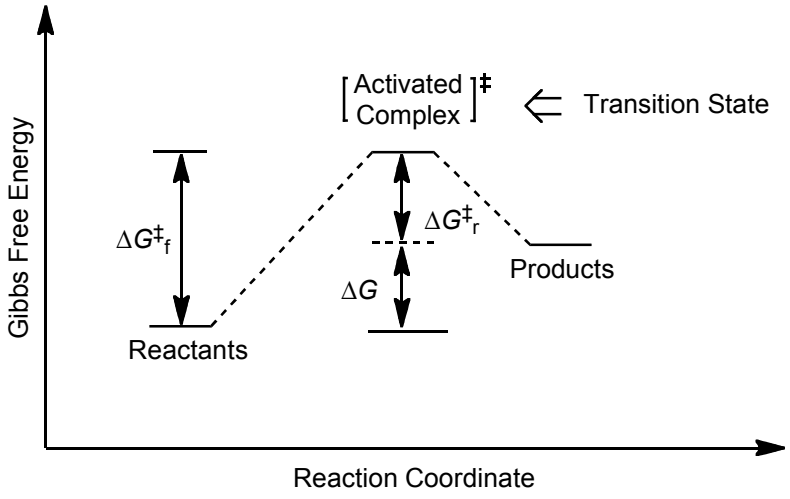


Figure 3.8. Free energy reaction coordinate diagram. $\Delta G^{\ddagger}$ is Gibbs free energy of activation (kJ mol^{-1}) for the forward (f) and reverse reactions (r).

Transition state theory provides another relationship between temperature and the rate constant of a reaction in the form of the Eyring equation which is

$$\ln\left(\frac{k}{T}\right) = \frac{-\Delta H^{\ddagger}}{R}\frac{1}{T} + \ln\left(\frac{k_b}{h}\right) + \frac{\Delta S^{\ddagger}}{R} \qquad (23)$$

where k is the rate constant, T is the absolute temperature, $\Delta H^{\ddagger}$ is the enthalpy of activation, $\Delta S^{\ddagger}$ is the entropy of activation, R is the universal gas constant. k_b is Boltzmann's constant, and h is Planck's constant.

Using the Eyring equation a plot of ln(k/T) versus 1/T was prepared and the activation parameters $\Delta H^{\ddagger}$, and $\Delta S^{\ddagger}$ were determined and are provided in Table 3.6. A representative Eyring plot is shown in Figure 3.9.

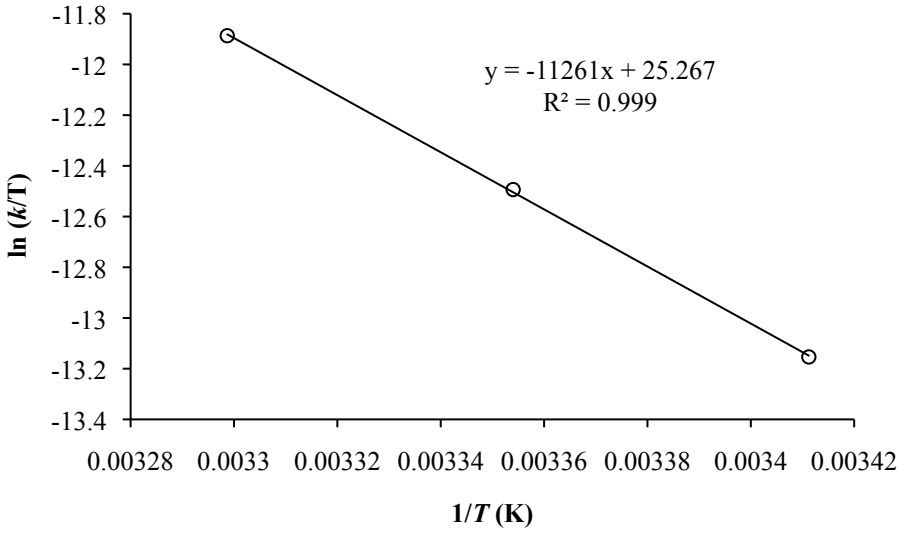


Figure 3.9. A plot of ln (k/T) versus 1/T (Equation 23) for the 2-methyl-2-nitrosopropane dimer-monomer dissociation reaction in acetonitrile. The slope equals -$\Delta H^{\ddagger}$/R and the y-intercept equals [ln (k_b/h) + $\Delta S^{\ddagger}$/R].

Table 3.6. Activation Parameters for the 2-Methyl-2-Nitrosopropane Dimer Monomer Equilibrium in Various Solvents †

	Solvent	forward (D → 2M)		reverse (2M → D)	
		$\Delta H^{\ddagger}$ (kJ mol^{-1})	$\Delta S^{\ddagger}$ (J K^{-1} mol^{-1})	$\Delta H^{\ddagger}$ (kJ mol^{-1})	$\Delta S^{\ddagger}$ (J K^{-1} mol^{-1})
1	Acetone	94.1 ± 1.5	19.3 ± 5.2	50.5 ± 1.5	-140.8 ± 4.9
2	Acetonitrile	93.6 ± 1.4	12.5 ± 4.6	48.3 ± 3.7	-150.2 ± 12.5
3	Chloroform	104.5 ± 0.2	43.5 ± 0.6	50.1 ± 1.8	-142.1 ± 5.9
4	Cyclohexane	89.0	8.6	39.5	-165.2
5	Dichloromethane	86.2	-14.5	39.9	-178.2
6	DMSO	96.3	22.0	36.1	-184.4
7	Ethanol	89.9 ± 0.1	1.3 ± 0.4	46.2 ± 1.2	-148.8 ± 4.2

† D = dimer, M = monomer. The reported error was calculated using the statistics from the least-squares plot of Equation 23.

Transition state theory assumes that a special type of equilibrium with an equilibrium constant $K^{\ddagger}$ exists between the reactants and the activated complex. The rate constant for a reaction is given by

$$k = (k_B T/h)K^{\ddagger} \tag{24}$$

Since $K^{\ddagger}$ is an equilibrium constant, it is possible to write

$$\Delta G^{\ddagger} = -RT \ln K^{\ddagger} \tag{25}$$

which is similar to Equation 17 and where $\Delta G^{\ddagger}$ is Gibbs free energy of activation.

It follows from Equations 24 and 25 that the rate constant is related to $\Delta G^{\ddagger}$ by

$$k = (k_B T/h)\exp(-\Delta G^{\ddagger}/RT) \quad (26)$$

The relationship between $\Delta G^{\ddagger}$, enthalpy and entropy at a given temperature is by

$$\Delta G^{\ddagger} = \Delta H^{\ddagger} - T\Delta S^{\ddagger} \quad (27)$$

$\Delta G^{\ddagger}$ for the forward and reverse reactions was calculated using the data in Table 3.6 and Equation 27 above. The results are provided in Table 3.7. $\Delta G^{\ddagger}$ for both the forward and reverse reactions varies very little with temperature (~0.2 kJ mol^{-1} and ~1.6 kJ mol^{-1} over a ten degree range for the forward and reverse reactions respectively). There is a clear variation with solvent as the non-polar solvent cyclohexane has the lowest $\Delta G^{\ddagger}$ for both the forward and the reverse reactions. Chloroform and acetonitrile, polar aprotic solvents, have among the largest values of $\Delta G^{\ddagger}$. The relationship between $\Delta G^{\ddagger}_f$, $\Delta G^{\ddagger}_r$, and $\Delta G°$ as indicated in Figure 3.8 is confirmed within this data. $\Delta G^{\ddagger}_f - \Delta G^{\ddagger}_r$ in Table 3.7 are approximately equal to the corresponding $\Delta G°$ values presented in Table 3.3.

Lastly, Equation 26 indicates that any factor affecting the Gibbs free energy of activation will ultimately affect k. It should also be noted that since $\Delta G^{\ddagger}$ is composed of enthalpy and entropy components (Equation 27), any factor affecting $\Delta H^{\ddagger}$ and/or $\Delta S^{\ddagger}$ will affect $\Delta G^{\ddagger}$ and thus k.

The effect of the solvent on K_{eq} k_1 and k_{-1} is discussed in terms of various solvation parameters and in terms of the solvent effect on the thermodynamic and activation parameters in the next section.

Table 3.7. Free Energies of Activation for the 2-Methyl-2-Nitrosopropane Dimer Monomer Equilibrium in Various Solvents †

	Solvent	Temperature (°C) 20	25	30
		$\Delta G^{\ddagger}_{f}$ (kJ mol^{-1})		
1	Acetone	88.5 ± 2.2	88.4 ± 2.2	88.3 ± 2.2
2	Acetonitrile	90.0 ± 1.9	89.9 ± 1.9	89.8 ± 1.9
3	Chloroform	91.7 ± 0.3	91.5 ± 0.3	91.3 ± 0.3
4	Cyclohexane	86.5	86.4	86.4
5	Dichloromethane	90.4	90.5	90.6
6	DMSO	89.8	89.7	89.6
7	Ethanol	89.5 ± 0.2	89.5 ± 0.2	89.5 ± 0.2
		$\Delta G^{\ddagger}_{r}$ (kJ mol^{-1})		
1	Acetone	91.7 ± 2.0	92.4 ± 2.1	93.1 ± 2.1
2	Acetonitrile	92.3 ± 5.2	93.1 ± 5.3	93.8 ± 5.3
3	Chloroform	91.7 ± 2.5	92.5 ± 2.5	93.2 ± 2.5
4	Cyclohexane	88.0	88.8	89.6
5	Dichloromethane	92.1	93.0	93.9
6	DMSO	90.1	91.1	92.0
7	Ethanol	89.8 ± 1.7	90.6 ± 1.8	91.3 ± 1.8

† $\Delta G^{\ddagger}_{f}$ and $\Delta G^{\ddagger}_{r}$ are the free energies of activation for the forward (D → 2M) and reverse (2M → D) reactions respectively. The values in this table were calculated using Equation 27. The relationship between $\Delta G^{\ddagger}_{f}$, $\Delta G^{\ddagger}_{r}$ and $\Delta G°$ is $\Delta G° = \Delta G^{\ddagger}_{f} - \Delta G^{\ddagger}_{r}$. $\Delta G°$ values are given in Table 3.3.

3.4. Discussion

Considering the data in Tables 3.1 and 3.2 it is clear that both the equilibrium and rate constants for the 2-methyl-2-nitrosopropane dissociation reaction are dramatically affected by a change in the solvent at a given temperature. In order to explain these observations, it is desirable to determine if there are one or more solvent properties that can be related to the magnitude of K_{eq} and/or k. In addition, since it is known that equilibrium and rate constants are related to various thermodynamic and kinetic parameters, it is also desirable to determine if correlations exists between solvent parameters and these model quantities. Knowing the aforementioned information should assist with making it possible to interpret the solvent dependency of K_{eq} and k in terms of proposed reaction mechanisms.

3.4.1 Solvent Effects on Equilibrium and Rate Constants

The equilibrium constant is affected by the choice of solvent and is related to the free energy of reaction by Equation 17. The degree to which the free energies of the solute molecules in equilibrium are affected by solvation will ultimately affect the value of $\Delta G°$. As $\Delta G°$ changes, the equilibrium composition of the reaction will change and this change is reflected by a change in the equilibrium constant. Generally, the equilibrium is expected to shift with a change in solvent in a way to favor the side most stabilized by solvation.[28]

The rate constants of chemical reactions are also affected by the choice of solvent. A classic example of this is demonstrated by how the rate of an S_N2 reaction is changed depending on whether or not the reaction is carried out in a protic or in a polar aprotic

solvent. The reaction rate is generally slower in protic solvents relative to the rate in polar aprotic solvents because the solvent molecules in protic solvents are capable of forming hydrogen bonds with negatively charged nucleophiles thus lowering their energy level and decreasing reactivity towards electrophiles.[29]

Hughes and Ingold used transition state theory (mentioned in the results section) to qualitatively describe the effect of solvent on the rate of a reaction.[30-32] The main solvent parameter used was that of solvent polarity. It was suggested that if the transition state is more polar than the initial state of the reactants, then an increase in solvent polarity will stabilize the transition state relative to the initial state thus leading to an increase in the reaction rate. The opposite is true if the transition state is less polar than the initial state. An increase in solvent polarity would decrease the reaction rate.

Solvents are, of course, characterized by numerous chemical and physical properties including: boiling point, freezing point, density, vapor pressure, cohesive pressure, dielectric constant, refractive index, dipole moment, polarizability, hydrogen bonding capabilities, donor-acceptor properties, and others.[33] Based on the ideas of Hughes and Ingold and for the purposes of this work, we begin by trying to find correlations with solvent polarity. Solvent polarity along with polarizability, hydrogen bonding capabilities, and donor-acceptor interactions is a major component of what constitutes a solvent's solvation ability which is expected to affect K_{eq} and k.[28]

3.4.2 Solvent Polarity

The polarity of a solvent refers to the attractive and repulsive forces between ionic or dipolar solutes and solvent dipoles.[30, 34] Solvents exerting relatively strong such forces are known as *polar* solvents. While it is common in the chemical literature to employ the relative permittivity, ε_r, (the dielectric constant) or the permanent dipole moment of a solvent molecule to quantify solvent polarity, it is best to think of solvent polarity as the sum of all the molecular properties (excluding those leading to a chemical change) responsible for the interactions between solvent and solute molecules (i.e. solvation).[30, 34] Such properties include Coulombic, inductive, dispersion, hydrogen bonding, and electron pair donor (EPD)/electron pair acceptor (EPA) interaction forces.

Several different scales are used to quantitatively assess solvent polarity. As mentioned above, the permanent dipole moment of the solvent molecule and the relative permittivity are two such scales. Cohesive pressure and refractive index have also been applied.[30, 35] In addition, several empirically derived scales have been developed based on the solvatochromic response of chemical probes to a solvent's overall solvation ability. Such scales include the Z scale, the $E_T(30)$ scale and its normalized version the E_T^N scale.[34, 36-40] The Gutmann donor and acceptor number scales have been used to quantify solvent electron pair donor and acceptor interactions with the solute.[41-44] Some of the most widely used scales are provided in Table 3.8.

In the following subsections, the relationship between K_{eq}, k_1 and k_{-1} for the 2-methyl-2-nitrosopropane dissolution reaction and solvent polarity using several of the aforementioned scales will be examined starting with relative permittivity.

Table 3.8. Relative Permittivity, Viscosity and Various Empirical Scales of Solvent Polarity †

		ε_r [a]	Z [b]	E_T^N [c]	DN [d]	AN [e]	Kamlet-Taft Parameters [f]			η [g]
	Solvent		kcal mol^{-1}		kcal mol^{-1}	kcal mol^{-1}	π*	α	β	cP
1	Acetone	20.56	65.7	0.355	17	12.5	0.62	0.08	0.48	0.322
2	Acetonitrile	35.94	71.3	0.460	14.1	18.9	0.66	0.19	0.40	0.362
3	Chloroform	4.89	63.2	0.259	4	23.1	0.69	0.20	0.10	0.566
4	Cyclohexane	2.02	60.1	0.006	0	0	0.00	0.00	0.00	0.973
5	Dichloromethane	8.93	64.2	0.309	1	20.4	0.73	0.13	0.10	0.437
6	DMSO	46.45	70.2	0.444	29.8	19.3	1.00	0.00	0.76	2.146
7	Ethanol	24.55	79.6	0.654	32	37.1	0.54	0.86	0.75	1.162

† (a) relative permittivity or dielectric constant measured at 25 °C, (b) Kosower's *Z* scale, (c) normalized energy of transition for Reichardt's betaine dye, (d) Gutmann donor number, (e) Gutmann acceptor number, (f) Kamlet-Taft general polarity, hydrogen bond donor, and hydrogen bond acceptor parameters (π*,α & β respectively), (g) solvent viscosity measured at 20 °C. The data in this table were obtained from references.[30, 33, 35, 41, 45-46]

3.4.3 Correlations with Relative Permittivity, ε_r, (the dielectric constant)

The dielectric constant, ε_r, of a solvent is a measure of how well the solvent can separate opposing charges (i.e. a measure of polarization).[35] If the solvent is placed between two oppositely charged plates in an electric field, E_o, the field strength in a vacuum, will be lowered to E as a result of the solvent molecules, with permanent or induced dipoles, aligning themselves with the field in an ordered arrangement. The dielectric constant is defined as

$$\varepsilon_r = E_o/E \tag{28}$$

As mentioned previously, the dielectric constant tends to mirror solvent polarity as molecules with large molecular dipoles, large molecular polarizabilities and/or hydrogen bonding sites tend to have larger dielectric constants.[27]

A plot of the log K_{eq} versus ε_r for the 2-methyl-2-nitrosopropane dissociation reaction is shown in Figure 3.10. (the identities of solvents 1-7 are defined in Table 3.8)

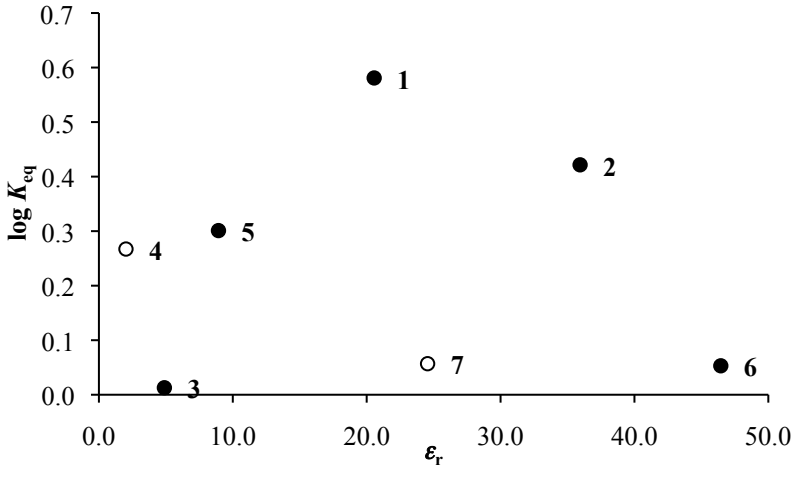


Figure 3.10. Plot of log K_{eq} (20 °C) versus ε_r.

An interesting relationship between the equilibrium constant and the dielectric constant of the polar aprotic solvents used in this study was found. Starting with chloroform **3**, an increase in the dielectric constant was accompanied with an increase in the equilibrium constant to a maximum and then by a decrease. This trend suggests that the solvent's ability to separate charges has little effect on dissociation reaction when the dielectric constant is small, but once the dielectric constant is large enough (which represents greater ability to separate charges), the solvent begins to stabilize the dimer and this stabilization is reflected by a decrease in the equilibrium constant. Cyclohexane **4**, a non-polar solvent, and ethanol **7**, a polar-protic solvent, do not fall directly within this trend. (indicated by open circles on the plot) More solvents of those respective types would need to be included in order to reveal any potential relationships.

A plot of the k_1 versus ε_r for the 2-methyl-2-nitrosopropane dissociation reaction is shown in Figure 3.11.

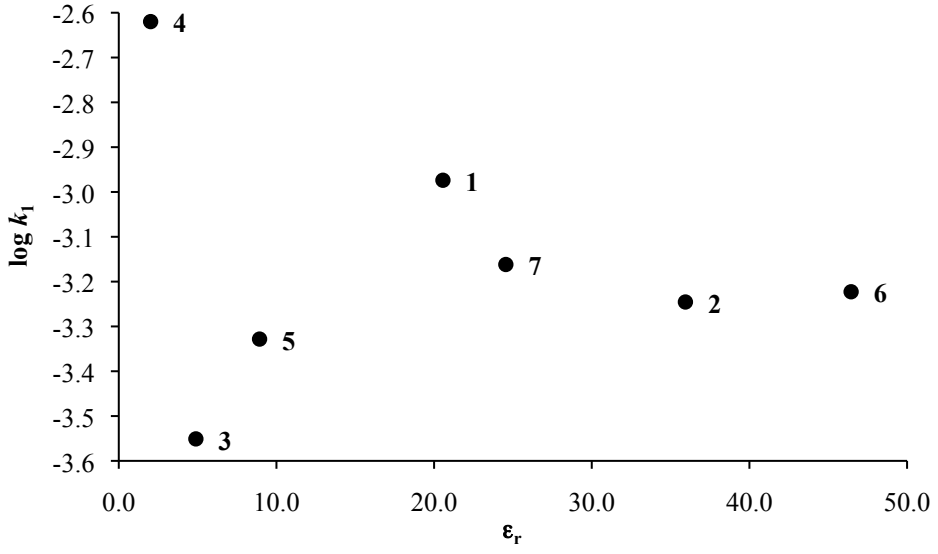


Figure 3.11. Plot of log k_1 (20 °C) versus ε_r.

No single trend exists incorporating all seven solvents studied. However, some useful observations are apparent. The largest rate constant correlates with the least polar (in this case non-polar) solvent, cyclohexane **4**. The smallest rate constants correlate with the two most polar solvents acetonitrile **2** and DMSO **6**. The two chlorinated solvents, chloroform and dichloromethane (**3** & **5** respectively), which contain polarizable chlorine atoms, appear as outliers and do not follow any particular trend. If the plot is examined leaving out the two chlorinated solvents and ethanol **7**, which is the only solvent in the group with strong hydrogen bonding capabilities, a linear trend emerges including solvents **4**, **1**, **2** and **6** ($r^2 = 0.93$). Assuming ε_r is a true measure of solvent polarity, this analysis indicates that the dimer is stabilized by polar solvents. In addition, this analysis indicates that the polarizable chlorinated solvents and the hydrogen bonding solvent interact in a significantly different way with the dimer than do the other non-polar and polar aprotic solvents. The former two categories of solvents have additional interacting forces (*i.e.* significant polarizability and hydrogen bonding capability) that apparently affect k_1 in addition to those forces quantified by the dielectric constant. At this point, it should be noted that the dielectric constant is a bulk solvent property and that its value in the vicinity of a particular solute molecule is lower than that for the bulk solvent because those molecules existing in the solvation shell are less free to orientate themselves in a direction imposed by the charged plates used to measure ε_r.[30] This means that the bulk value of ε_r may not correlate with properties that depend on solute/solvent interactions. Presumably, the molecular ε_r is required to obtain satisfactory trends. Lastly, no useful trends between k_{-1} and relative permittivity were found.

3.4.4 Solvatochromism

Solvatochromism is a change in the electronic absorption or emission spectrum of a chromophore or fluorophore induced by the solvent.[47] Typically the change occurs in response to a change in solvent polarity. This phenomenon has been exploited to develop empirical scales of solvent polarity.[34, 48] Two of the most popular such scales are the *Z* scale and the $E_T(30)$ scale.[34, 36-40]

3.4.5 Correlations with the Kosower Z scale

Kosower's *Z* scale was developed based upon the spectrum of *N*-ethyl-4-methylcarboxypyridinium iodide.[27] Following excitation, the system undergoes a charge-transfer from the iodine ion to the pyridinium moiety forming a neutral radical species. The excited state has a smaller dipole than the ground state. Thus, in polar solvents the ground state is stabilized relative to the excited state. As a result, the energy required for excitation in polar solvents increases (a blue shift). Parameters for the *Z* scale are correlated to λ_{max} (nm) for the excitation in a particular solvent according to Equation 29.

$$Z\ (\text{kcal mol}^{-1}) \equiv hcN_A/\lambda_{(max)} \tag{29}$$

where *h* is Plank's constant, *c* is the speed of light in a vacuum, N_A is Avogadro's number.

The relationship between the equilibrium constant and Kosower's Z scale is similar to the one described for the dielectric constant in the last section except the relative positions of two solvents have switched. A plot of log K_{eq} versus Z is shown in Figure 3.12. (the identities of solvents 1-7 are defined in Table 3.8)

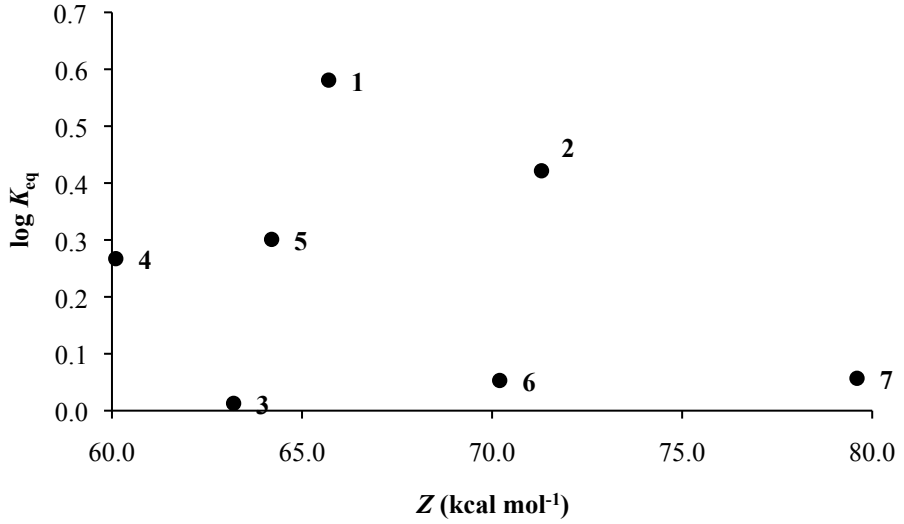


Figure 3.12. Plot of log K_{eq} (20 °C) versus Z.

Ethanol **7** is the most polar solvent on the Z scale. As a result, the curious trend described for K_{eq} versus ε_r is not duplicated here. For K_{eq} versus ε_r, it was possible to remove the non-polar and the polar-protic solvents from the set revealing a possible (albeit curious) trend among the polar aprotic solvents. Here, however, there is no clear way to separate the solvents into groups that will reveal any obvious pattern between K_{eq} and Z. Assuming that both ε_r and Z are measures solvent polarity, one of the scales is accounting for a specific or non-specific factor not included in the other. While the two

scales partially agree, this likely accounts for why the most polar solvent on the two scales is different.

A plot of log k_1 versus Z for the 2-methyl-2-nitrosopropane dissociation reaction is shown in Figure 3.13.

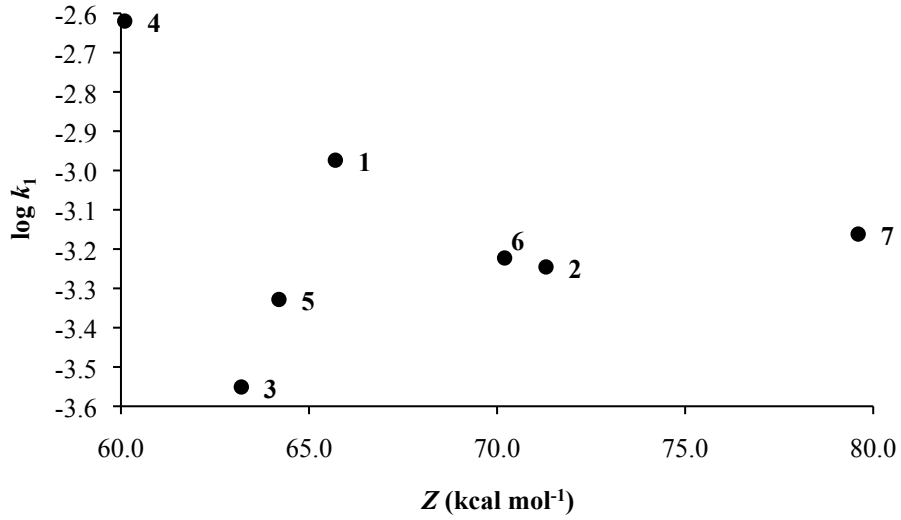


Figure 3.13. Plot of log k_1 (20 °C) versus Z.

The plot in Figure 3.13 is similar to the plot in Figure 3.11 which depicts log k_1 versus the dielectric constant. The largest rate constant again correlates with the least polar solvent and the smallest rate constants correlate with the two most polar solvents. The two scales, however, differ about which solvent is the most polar. The most polar based on ε_r is DMSO **6** while the most polar based on Z is ethanol **7**. Examining the plots closely it can be seen that the positions of the two solvents (DMSO and ethanol) are swapped.

Once again the chlorinated solvents (**3** & **5**) appear as outliers and do not follow any particular trend. As with ε_r, if we accept that *Z* is a ranking of solvent polarity, the analysis indicates that polar solvents stabilize the dimer and that the polarizable chlorinated solvents and the hydrogen bonding solvent interact differently with the dimer. In fact, based on the *Z* scale, the hydrogen-bonding factor is quite pronounced as ethanol appears as an outlier. If we consider the plot without ethanol and without the two chlorinated solvents a linear correlation results with solvents **4**, **1**, **6**, and **2** ($r^2 = 0.99$). Both ε_r and *Z* scales include the same solvents in a linear trend albeit in a slightly different order. Lastly, as with relative permittivity, no useful trends between k_{-1} and the *Z* scale were found.

3.4.6 Correlations with the $E_T(30)$ and E_T^N scales

Using a procedure similar to that described for establishing the *Z* scale, the $E_T(30)$ scale was developed using the longest wavelength electronic absorption band of the solvatochromic dye 2,6-diphenyl-4-(2,4,6-triphenylpyridinio)phenolate (also known as *Dimroth-Reichardt's betaine*).[34, 39-40, 48-49] The visible transition for this dye leads to a less polar excited state as a result the compound exhibits a hypsochromic shift (a blue shift) as solvent polarity is increased which is the basis for the $E_T(30)$ scale. A modern normalized version of the scale referred to as the E_T^N scale has also been developed.[27] The $E_T(30)$ scale is probably the most popular among the solvatochromic scales. A number of undergraduate experiments have been developed using it.[50-52]

The relationship between K_{eq} and E_T^N is nearly identical to that described for the Z scale. The positions of the solvents relative to each other are the same on both scales. This is may be because both scales were developed similarly. A plot of log K_{eq} versus E_T^N is shown in Figure 3.14.

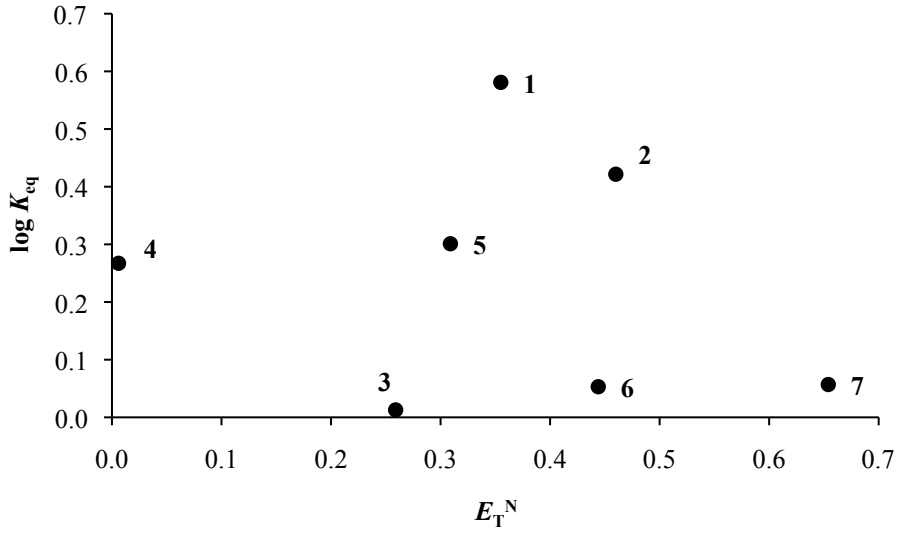


Figure 3.14. Plot of log K_{eq} (20 °C) versus E_T^N.

As with the Z scale, no linear trend exists and there is no obvious way to group the solvents revealing any particularly useful pattern.

A plot of log k_1 versus the E_T^N scale for the 2-methyl-2-nitrosopropane dissociation reaction is shown in Figure 3.15.

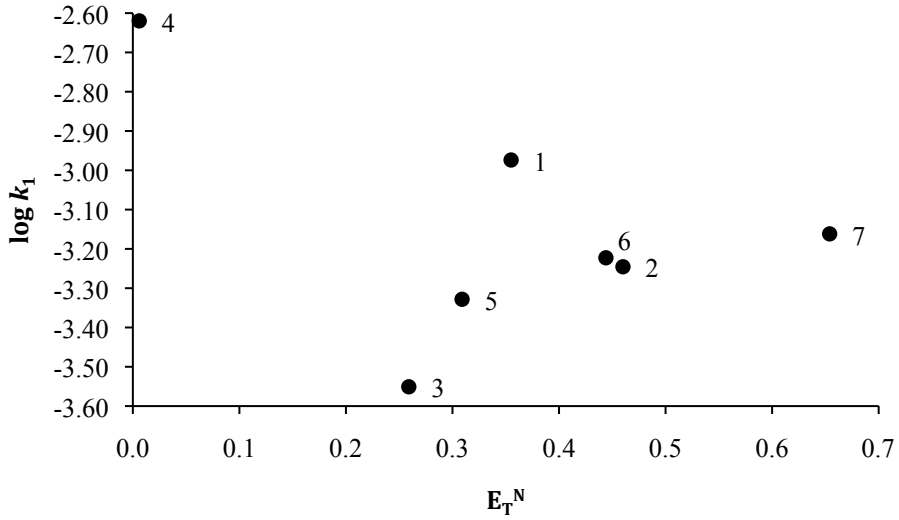


Figure 3.15. Plot of log k_1 (20 °C) versus E_T^N.

The plot depicted in Figure 3.15 is also essentially the same as Figure 3.13 that described for the Z scale suggesting that both scales empirically measure the same types of intermolecular forces affecting solvation. Indeed a plot of Z versus E_T^N (not shown) for the solvents used in this study is linear ($r^2 = 0.9$). No useful trends between k_{-1} and the E_T^N scale were found.

3.4.7 Correlations with the Gutmann Donor Number

The donor number (DN) is a measure of a solvent's Lewis basicity (i.e. the ability of the solvent to donate a pair of electrons).[42-44] Developed by Gutmann, the DN is defined as the negative enthalpy of reaction of a base (the donor solvent, S) with the Lewis acid antimony pentachloride, $SbCl_5$ in dilute dichloroethane solution.

$$S: + SbCl_5 \rightarrow S\text{-}SbCl_5 \qquad \Delta H° / \text{kcal mol}^{-1} \equiv DN \qquad (30)$$

No apparent relationship exists between the donor number and K_{eq}. However there may be a relationship within two different groups of solvents (coordinating and non-coordinating). A plot of log K_{eq} vs DN is shown in Figure 3.16.

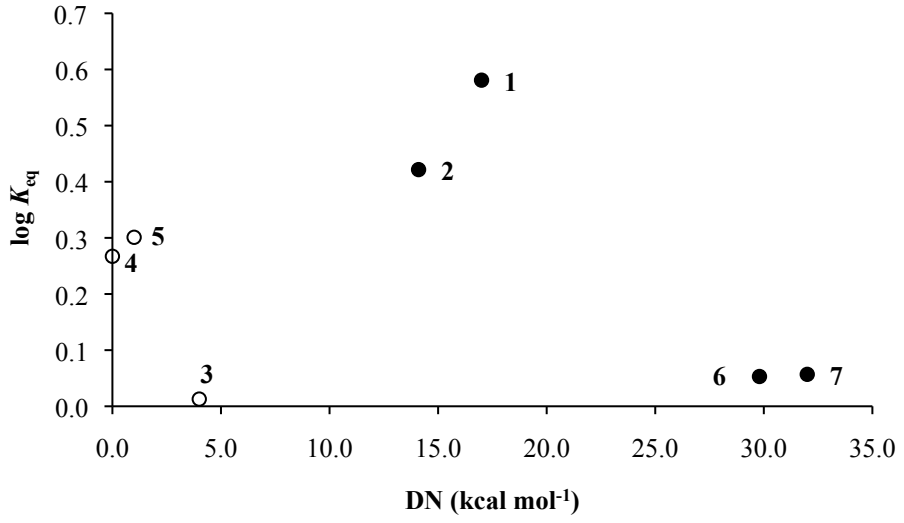


Figure 3.16. Plot of log K_{eq} (20 °C) versus DN.

Solvents **3**, **4** and **5** are all non-coordinating solvents and appear grouped on the left side of the plot. There is a general decrease in K_{eq} with increasing DN among this small group. Solvents **2**, **6**, **1**, and **7** are grouped on the right side of the plot. Taking a line from **1** and **2** down to **6** and **7**, there is a general decrease in K_{eq} with increasing DN. More of each type of solvent (non-coordinating and coordinating) would be necessary to fully confirm these trends. In hindsight, both of these groups exists on the previous plots describing log K_{eq} versus ε_r, Z and E_T^N however, the groups are not as apparent because the points are not as tightly grouped. The DN scale clearly accounts for an interaction not completely accounted for in the previous scales.

A plot of log k_1 versus the Gutmann donor number is depicted in Figure 3.17.

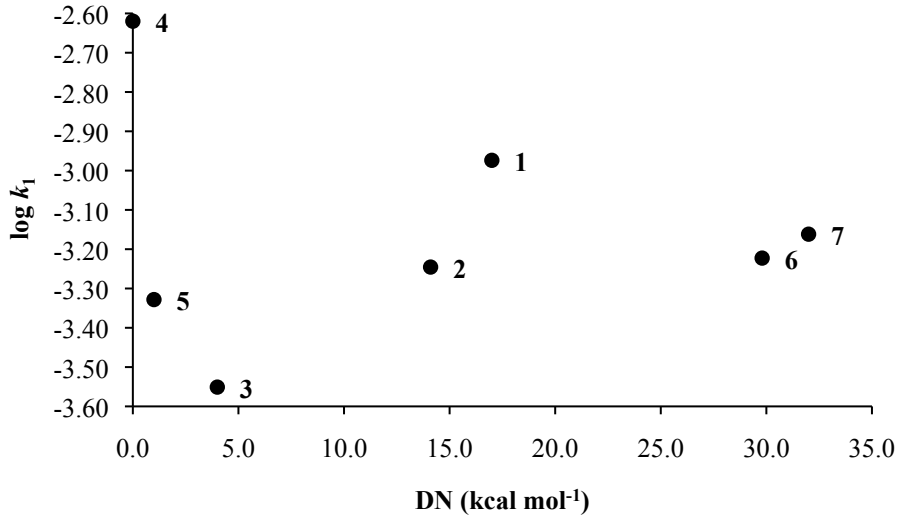


Figure 3.17. Plot of log k_1 (20 °C) versus DN.

There is no one trend incorporating all seven solvents used in this study. There appears, however, to be a trend involving solvents **4**, **1**, and **6**. The trend mirrors the one observed with the Z and E_T^N scales except in this case the hydrogen bonding solvent ethanol **7** is not far removed from the trend line. Acetonitrile **2** appears as an outlier. As with all of the previous analyses both of the chlorinated solvents are outliers and do not appear to fit the trend. Since the donor number is a measure of a solvent's Lewis basicity, with the exception of the outliers, from this analysis it appears that as basicity (ability to donate electron density) of the solvent increases, k_1 decreases. This probably occurs due to the stabilization of the dimer.

Alternatively, there are two different groups of solvents on the plot. Solvents **4**, **5** and **3** are all non-coordinating solvents and appear grouped on the left side of the plot. As DN increases, k decreases. This trend is also generally observed among the remaining solvents which are all coordinating solvents. Taking a line from **1** and **2** over to **6** and **7**, there is a small general decrease in k_1 with increasing DN.

It should be noted that the trends described with the DN are not clear. There appears to be more than one way of interpreting the plot suggesting, unsurprisingly, that other factors are involved. More solvents of the three different types would need to be plotted against DN to potentially gain more insight.

There appears to be a useful relationship between the donor number and k_{-1}. A plot of log k_{-1} versus DN is shown in Figure 3.18.

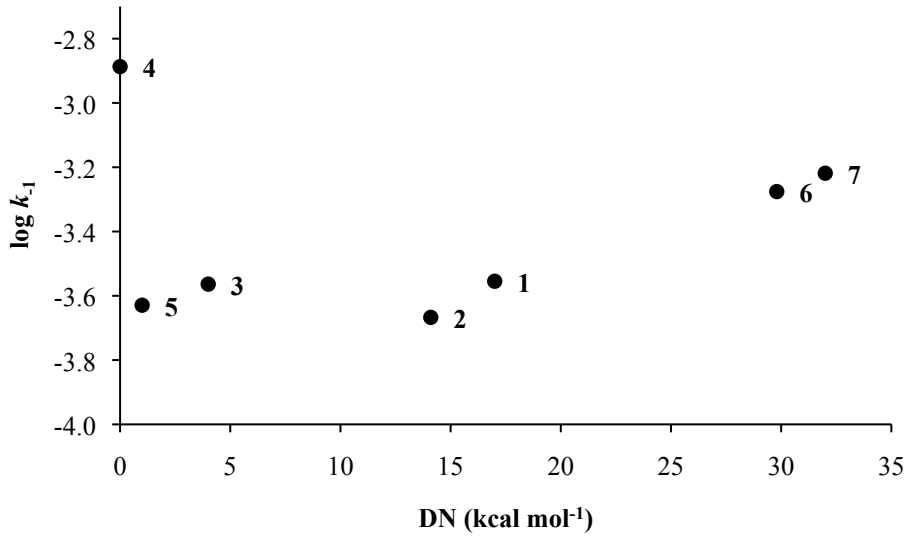


Figure 3.18. Plot of log k_{-1} (20 °C) versus DN.

The non-polar solvent, cyclohexane **4** along with the two chlorinated solvents dichloromethane **5**, and chloroform **3**, appear on the left side of the plot. Cyclohexane is clearly and outlier and does not seem to fit any trend. More non-polar solvents would need to be included to make meaningful comparisons. Dichloromethane **5**, and chloroform **3**, appear on a line parallel to a line composed of coordinating solvents **2**, **1**, **6**, and **7**. For both of these lines, as the donor number increases, k_{-1} increases. The trend is roughly opposite of that observed between k_1 and DN. Since the donor number is a measure of a solvent's Lewis basicity, with the exception of the outliers, from this analysis it appears that as basicity of the solvent increases, k_{-1} increases.

3.4.8 Correlations with the Gutmann Acceptor Number

The acceptor number (AN) of a solvent (also developed by Gutmann and co-workers) is a measure of the solvent's Lewis acidity (i.e. the ability of the solvent to accept a pair of electrons).[41-43] The AN scale is based on ^{31}P chemical shift measurements of triethylphosphine oxide dissolved in the solvent of interest. The ^{31}P resonance of triethylphosphine oxide acts as a highly sensitive probe towards a change in solvent because the oxygen atom of the PO moiety interacts differently with different solvents.

A plot of log K_{eq} versus the acceptor number is shown in Figure 3.19.

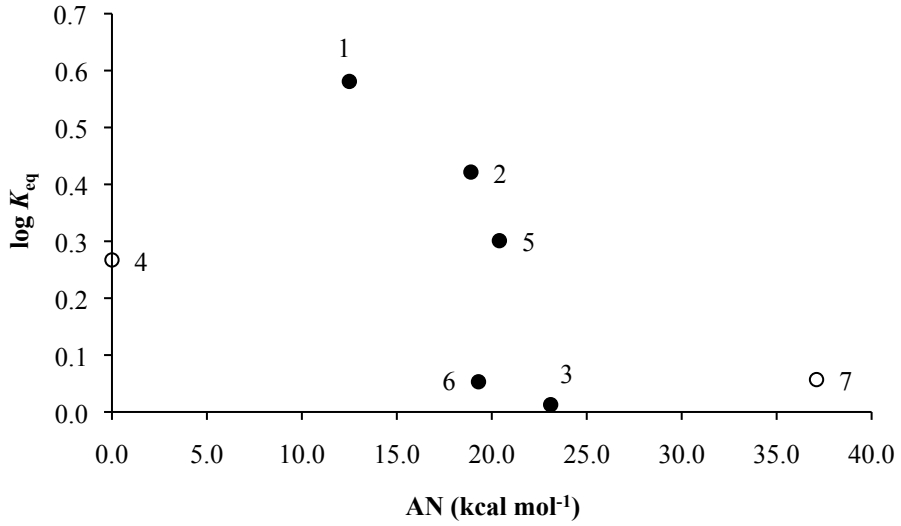


Figure 3.19. Plot of log K_{eq} (20 °C) versus AN.

The solvent acceptor number seems to be generally related to K_{eq}. The plot of log K_{eq} versus AN can be divided into 3 separate groups. The non-polar solvent cyclohexane **4** is on the left side of the plot and the strong hydrogen bonding solvent ethanol **7** is on

the right side of the plot. More solvents of each type would need to be included in order to reveal any trends among the groups. The polar aprotic solvents appear in the center of the plot in what appears to be a general trend. With the exception of DMSO **6**, as the solvent acceptor number increases K_{eq} decreases. The fact that DMSO falls outside this trend suggest that some factor involving this particular solvent is not accounted for by the AN scale. Based on this trend the ability of the solvent to accept electron density from the dimer stabilizes the dimer thus lowering the equilibrium constant.

A plot of log k_1 versus the acceptor number is shown in Figure 3.20.

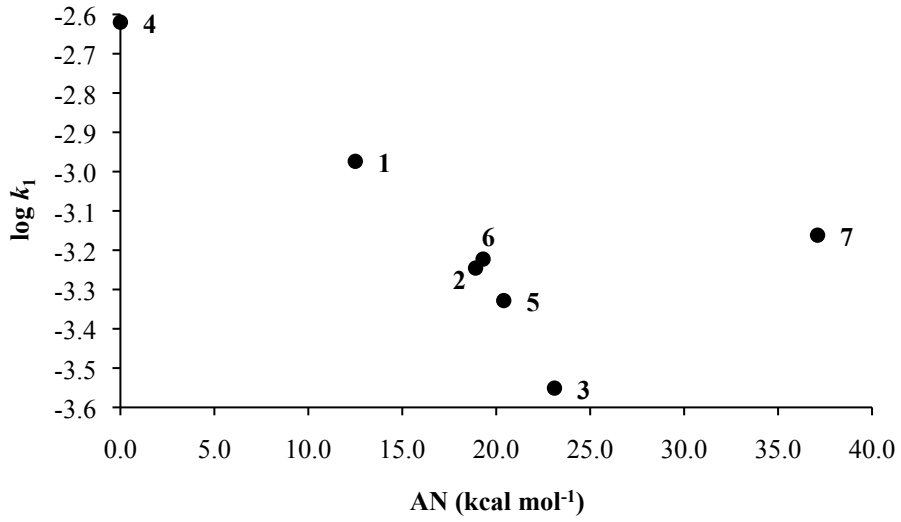


Figure 3.20. Plot of log k_1 (20 °C) versus AN.

The plot of log k_1 versus AN has the strongest trend observed thus far. As the acceptor number increases k_1 decreases linearly (r^2 = 0.95 w/o **7**; r^2 = 0.99 w/o **3, 5** & **7**) This analysis suggests that the solvent's ability to accept electron density is a major factor in stabilizing the dimer. As with each of the previous analyses, the strong hydrogen

bonding solvent ethanol is an outlier suggesting that it interacts with the dimer in a very different way compared to the other solvents.

There is some evidence for a relationship between the acceptor number and k_{-1}. A plot of log k_{-1} versus AN is shown in Figure 3.21.

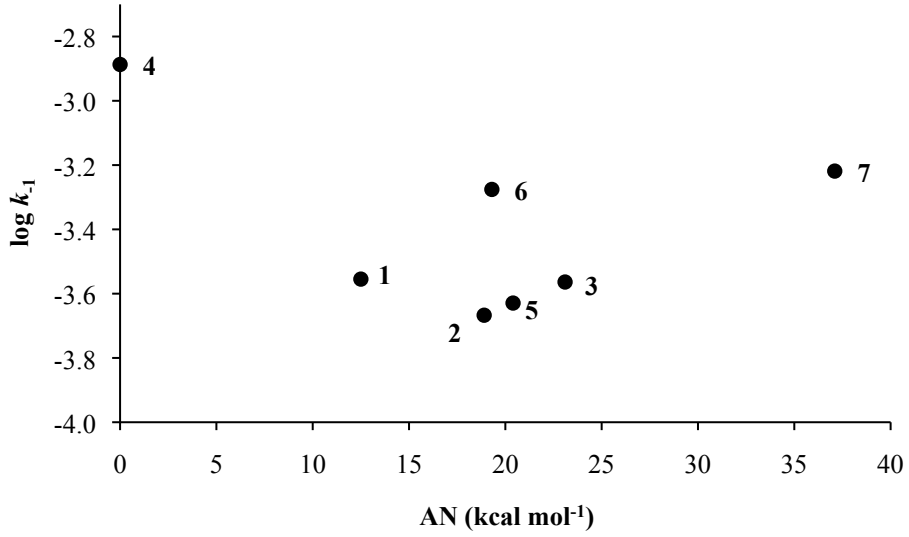


Figure 3.21. Plot of log k_{-1} (20 °C) versus AN.

The non-polar solvent cyclohexane **4** appears on the left side of the plot. There are no other non-polar solvent in the group so the only meaningful comparison that can be made is that changing solvent types from non-polar to polar is accompanied by a decrease in k_{-1}. It should be noted however that this comparison is being made with only one non-polar solvent and that more would need to be included in order to reveal any trends. There is a trend, however, starting with acetone **1** and going to the right. Acetone and DMSO **6** appear on a line parallel to a line including solvents **2**, **5**, **3** and **7**. It appears

that as the AN increases, k_{-1} increases. This trend is the opposite of the one described between k_1 and AN.

3.4.9 Kamlet-Taft Analysis

The analyses thus far reveal that a single solvent parameter does not yield fully useful correlations with the reaction equilibrium or rate constant. This is not entirely surprising because when changing from one solvent to another one necessarily changes multiple properties some of which may have an effect on K_{eq} or k. Different scales account for different solvent parameters. The question is to what extent do individual solvent parameters affect K_{eq} or k.

The Kamlet and Taft method is one of several linear solvation energy relationships (LSER) which divide different aspects of solvent polarity or solvation ability into several different parameters which when regressed into a linear relationship can be used to correlate and predict solvent dependent variables in a useful way.[53-56] The Kamlet-Taft parameters include π^*, α, β, δ, δ_H and ζ and are available in tables for numerous solvents.

The π^* parameter is based on the solvatochromic response of multiple dyes, not just one as is the case with the Z and $E_T(30)$ scales mentioned earlier. The π^* parameter is a measure of the general polarity/polarizability of the solvent. The scale was intentionally developed in such a way that it does not include hydrogen bonding effects. The α parameter represents the solvent hydrogen bond donor (HBD) ability or acidity.

The β parameter represents the solvent hydrogen bond acceptor (HBA) ability or Lewis basicity. The δ parameter is an empirical polarizability correction term needed for polychlorinated and aromatic solvents. For non-chlorinated aliphatic solvents δ = 0.0. For polychlorinated aliphatic solvents δ = 0.5 and for aromatic solvents δ = 1.0. The δ_H and ζ parameters are the Hildebrand solubility parameter and a coordinate covalency index. Neither of these last two parameters will be used or discussed further here. With the π*, α, β, and δ parameters, the most familiar form of the Kamlet-Taft equation is expressed as

$$\log k = \log k_o + s(\pi^* + d\delta) + a\alpha + b\beta \qquad (31)$$

The coefficents s, d, a and b express the extent (magnitude) to which that particular solvent property contributes to k. k_o is the value of k in a reference solvent. The Kamlet-Taft parameters for the solvents used in this study are provided in Table 3.8.

A linear regression was carried out on the data set of k_1 for each solvent at 20 °C to determine the coefficents s, d a and b using Microsoft® Excel and the StatPlus® statistical analysis tool. The resulting equation follows ($r^2 = 0.94$)

$$\log k_1 = -2.61 - 1.41\,(\pi^* - 0.249\delta) - 0.712\alpha + 1.08\beta \qquad (32)$$

The standard errors for the intercept, s, d, a and b are ±0.12, ±0.60, ±0.55, ±0.37 and ±0.80 respectively.

The Kamlet-Taft analysis successfully provides a relationship between the forward rate constant and solvent parameters for polarity/polarizability, hydrogen bond donor ability, and hydrogen bond acceptor ability. Ideally, with this information, it should be possible to predict the forward rate constant in any solvent for which Kamlet-Taft parameters are known.

A plot of log k_1 (experimental) versus log k_1 (calculated), which was determined with Equation 32, is shown in Figure 3.22.

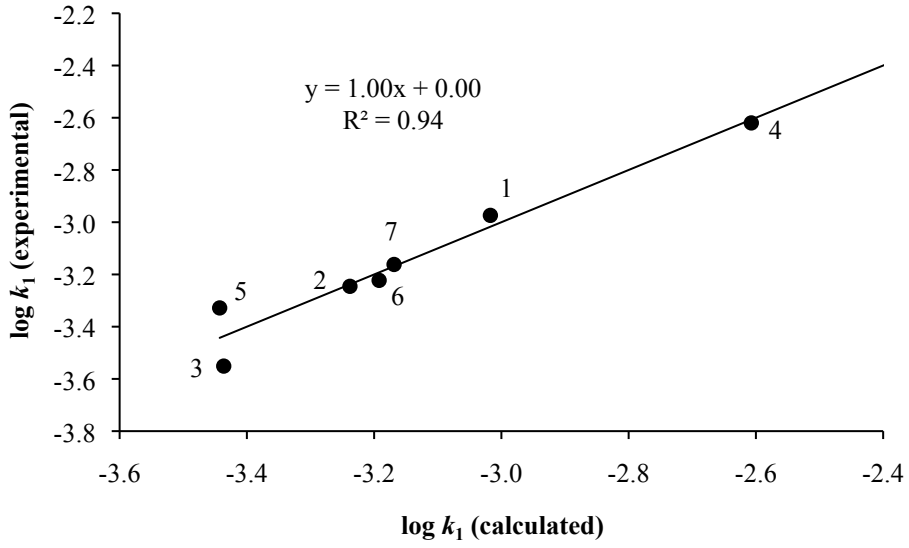


Figure 3.22. Plot of the experimentally determined log k_1 versus the calculated value.

The Kamlet-Taft multiparameter equation (Equation 32) is able to estimate the rate constants for all seven solvents used in the study. The percent difference between the experimental rate constants and the calculated values is less than 1.0% for all solvents except acetone (-1.45%), chloroform (-3.28%) and dichloromethane (-3.38%).

The Kamlet-Taft analysis indicates that the largest contribution to the rate comes from the solvent's polarity/polarizability (-1.41π*) followed by contributions from hydrogen bond acceptor (HBA) ability or basicity (+1.08β) and hydrogen bond donor (HBD) ability or acidity (-0.712α). An optimal fast rate of dissociation would thus be attained in a solvent with low polarity/polarizability, low acidity and a higher ability to accept hydrogen bonds with the relative importance of these factors indicated by the coefficients in the Kamlet-Taft equation.

As shown in Figure 3.22, the correlation of log k_1 (experimental) versus log k_1 (calculated) gives a linear relationship with a slope of 1.00 and a correlation coefficient of r = 0.97. The coefficient of variance, r^2 = 0.94 which suggests that 94% of the experimental results can be explained by Equation 32. The overall significance of the regression model (Equation 32) was tested using the *F* statistic where β_k represents the k^{th} regression coefficient. The null hypothesis for the test is H_0: $\beta_1 = \beta_2 = \ldots \beta_k = 0$. The alternative hypothesis is that at least one of the regression coefficients is not equal to zero. The *F* value for this test was determined to be 8.34 with $p = 0.11$. The significance of the model is improved somewhat by choosing to neglect the δ parameter which, in this case, is non-zero for and thus only relevant for the two chlorinated solvents. Leaving the δ term out gives an *F* value of 15.0 with $p = 0.03$ which is a clear rejection of the null hypothesis suggesting an acceptable correlation. The revised equation is

$$\log k_1 = -2.61 - 1.14\pi^* - 0.568\alpha + 0.727\beta \qquad (33)$$

The standard errors for the intercept, s, a and b are ±0.10, ±0.17, ±0.17 and ±0.19 respectively. All coefficients in Equation 33 were found to be statistically significant with *t*-stat values being -26.3224 (p = 0.0001), -3.3623(p = 0.0384), 3.8569(p = 0.0263) and -6.5624(p = 0.0058) for the intercept, s, a and b respectively. A plot of log k_1 (experimental) versus log k_1 (calculated) for Equation 33 gives a linear relationship with a slope of 1.00 and a correlation coefficient of r = 0.97. The coefficient of variance, r^2 = 0.94 which as with Equation 32 suggests that 94% of the experimental results can be explained by Equation 33.

A Kamlet-Taft analysis was also carried out with k_{-1} and with K_{eq}. The results were mixed. The analysis involving K_{eq} gave a poor correlation with r^2 = 0.19. The analysis with k_{-1} was more useful with r^2 = 0.62, but certainly not significant. Therefore, it was not possible to find a useful Kamlet-Taft expression with either k_{-1} or K_{eq} suggesting that there are other factors affecting these two quantities.

Recalling that the reverse reaction involves the coming together of two solvated monomer units, it was thought that the solvent viscosity, η, might play a roll in determining the reverse reaction rate constant k_{-1}. A plot of log k_{-1} (20 °C) versus the viscosity of the solvent is shown in Figure 3.23.

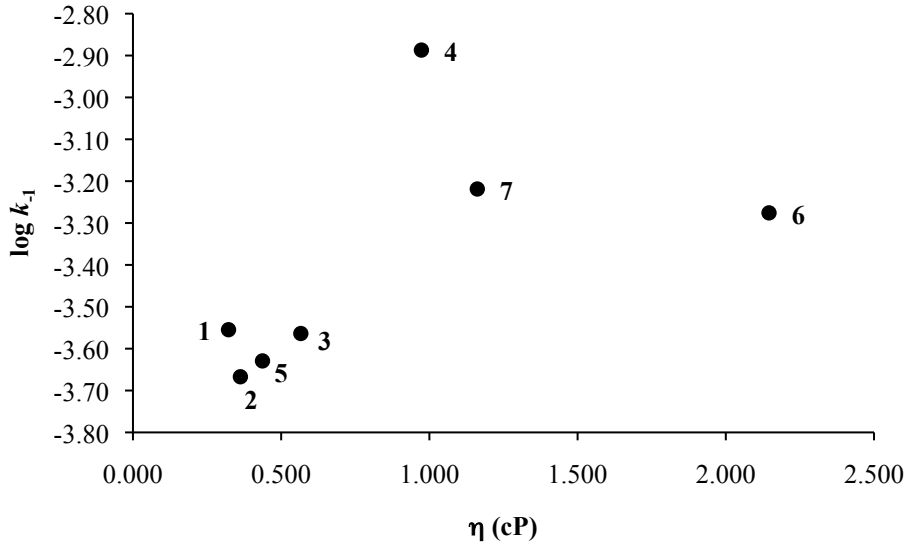


Figure 3.23. Plot of log k_{-1} (20 °C) versus the solvent viscosity.

The relationship between log k_{-1} and the solvent viscosity appears promising. There is a clear trend incorporating solvents **2**, **5**, **3** and **7**. This general result suggests that the more viscous solvents provide a greater opportunity for the monomer units to interact whereas they are more able to escape contact in the less viscous solvents. Solvent **1,** acetone, along with cyclohexane **4** and DMSO **6** do not follow the trend suggesting that another parameter is involved. Encouraged by these results involving the viscosity and k_{-1}, an attempt was made to construct a multiparameter equation involving the Kamlet-Taft parameters and the solvent viscosity. As can be seen in Figure 3.24, a useful trend was established. The multiparameter equation for the calculated value of log k_{-1} follows ($r^2 = 0.99$)

$$\log k_{-1} = -3.22 + 0.0197\alpha + 0.0112\beta - 0.800\pi^* + 0.340\eta \qquad (34)$$

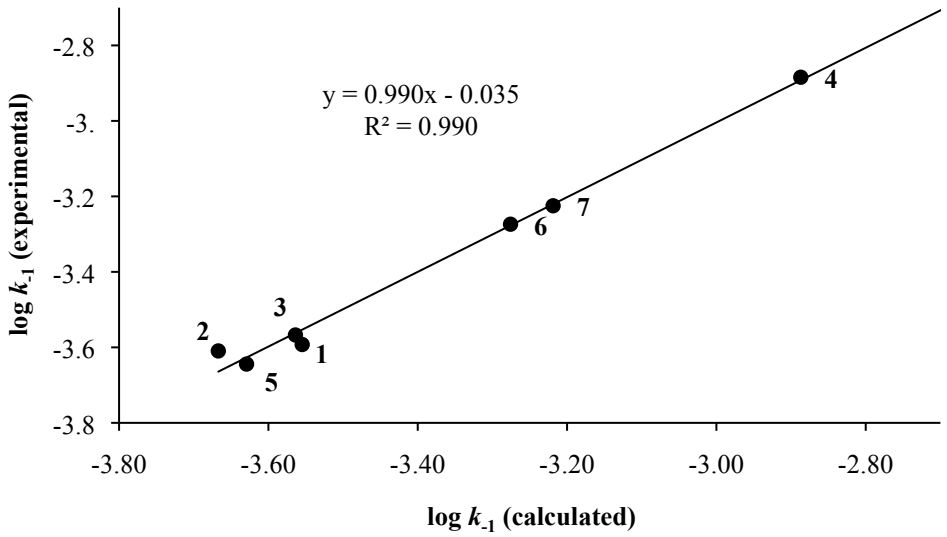


Figure 3.24. Plot of the experimentally determined log k_{-1} versus the calculated value.

The standard errors for the intercept, a, b, s, and C (the coefficient for η) in Equation 34 are ±0.054, ±0.087, ±0.114, ±0.086 and ±0.041 respectively. An examination of the statistical data reveals that the overall correlation is significant with an *F* value of 47.8 with $p = 0.02$. As with k_1, the largest contribution to the rate constant comes from the solvent polarity/polarizabilty (-0.800π*) followed by a relatively large contribution from the solvent viscosity (+0.340η). Note that the contribution from the solvent viscosity is positive which supports the earlier observation with the single parameter trend. The last two contributions come from the α and β terms (hydrogen bond donating (+0.0197α) and hydrogen bond accepting (+0.0112β) abilities). The contributions from these two parameters are quite small. In fact, the statistical analysis shows that they are not significant having coefficients with *t*-stat values of 0.2259 (p =

0.991) and 0.0979 (p = 0.999). However, the p values for the coefficients of π* and η are both less than 0.05 indicating that they are statistically significant.

Given the fact that the α and β terms were not statistically significant in the multiparameter equation for the calculated value of log k_{-1} (Equation 34), the analysis was repeated without them which yielded an improved result. The revised equation is

$$\log k_{-1} = -3.21 - 0.792\pi^* + 0.343\eta \qquad (35)$$

The standard errors for the intercept, s and C (the coefficient for η) are ±0.035, ±0.051 and ±0.024 respectively. Equation 35 is very similar to Equation 34, but over all significance of the model is improved. The F value for the regression is 178.4 with p = 0.0001. The t-stat values for the coefficients of the intercept, π* and η were -91.2889 (p = 0.), -15.5025 (p = 0.0001) and 14.4271 (p = 0.0001) all being statistically significant.

Encouraged by the fact that statistically significant multiparameter equations were found for both k_1 and k_{-1}, another effort was made to find a relationship with K_{eq}. It seemed reasonable that solvent effects on K_{eq} would involve all those factors affecting k_1 and k_{-1}, thus a regression was carried out using π*, α, β and η. The resulting equation is

$$\log K_{eq} = 0.614 - 0.362\eta - 0.605\alpha + 0.754\beta - 0.357\pi^* \qquad (36)$$

The standard errors for the intercept and the coefficients of η, α, β and π* are ±0.12, ±0.087, ±0.19, ±0.25 and ±0.18 respectively. Unfortunately, the model was not found to be statistically significant in that it has an F value of 5.42 with $p = 0.16$. Nevertheless the results suggest that contributions from all four parameters affect log K_{eq} with the largest contribution coming from the hydrogen bond acceptor ability of the solvent (+0.754β) followed by the hydrogen bond donating ability (-0.605α), the solvent viscosity (-0.362η) and finally the solvent polarity/polarizability (-0.357π*). These results suggest that increasing η, α or π* will tend to decrease K_{eq} shifting the equilibrium left. This is reasonable in that increasing any of these three parameters would tend to stabilize the dimer. Apparently an increase in the solvent's Lewis basicity would tend to shift the equilibrium to the right. This may, in part, explain why Acetone **1**, and Acetonitrile **2**, have the highest equilibrium constants of the solvents studied in this work. They are not the most basic solvents used in this study. They have donor numbers of 17 and 14.1 respectively. They do, however, have relatively low viscosities, which tend to favor the reaction shifting to the right. On the other hand, DMSO **6**, and Ethanol **7** both have large viscosities of 2.146 cP and 1.162 cP respectively. Perhaps the viscosity of these solvents is more important than the larger donor numbers of 29.8 and 32 respectively and this explains why they have lower equilibrium constants relative to acetone and acetonitrile. A plot of the experimentally determined log K_{eq} versus the calculated value is shown in Figure 3.25. While, as stated above, the predictive value of this model is not statistically significant, the resulting trend is encouraging and warrants further study with more solvents of varied types (e.g. polarities, donor/acceptor abilities and viscosities).

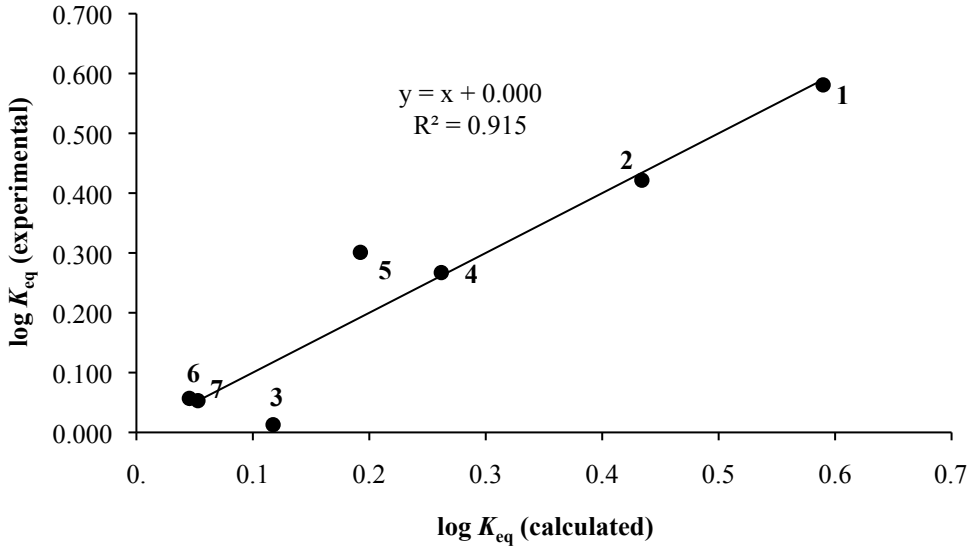


Figure 3.25. Plot of the experimentally determined log K_{eq} versus the calculated value.

3.4.10 Correlations with thermodynamic and kinetic parameters

Table 3.4 summarizes the standard changes in enthalpy and entropy for the dissociation reaction. The enthalpy values do not vary much from solvent to solvent. The largest variation is evident in the values for $\Delta S°$ and thus at a given temperature it is the entropy term controlling the value of $\Delta G°$ and thus the value of K_{eq} via Equation 17. The values of $\Delta H°$ and $\Delta S°$ are linearly related with a positive slope. No correlations with ε_r, Z, E_T^N, DN or AN were found.

Equation 26 gives the relationship between $\Delta G^‡$ and the rate constant. Equation 27 gives the relationship between $\Delta G^‡$ and the other two activation parameters, $\Delta H^‡$ and $\Delta S^‡$. As mentioned in the results section, factors that affect the Gibbs free energy of activation will ultimately affect k. Attempts were made to correlate the activation

parameters with ε_r, Z, E_T^N, DN and AN with little success. It was found that $\Delta H^{\ddagger}$ and $\Delta S^{\ddagger}$ are linearly related ($r^2 = 0.93$) as has been observed previously in similar compounds.[57]

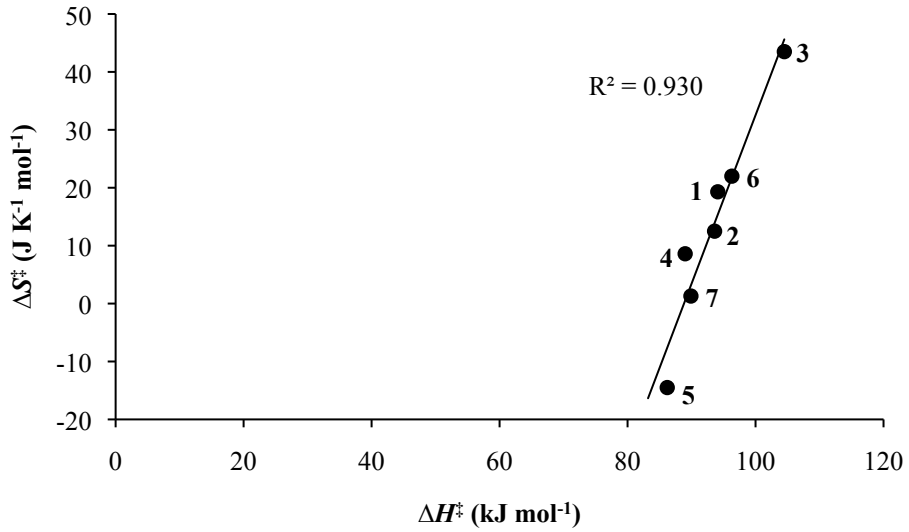


Figure 3.26. Plot of the entropy of activation versus the enthalpy of activation.

As with $\Delta H°$, $\Delta H^{\ddagger}$ does not vary much with solvent, however $\Delta S^{\ddagger}$ varies significantly making the $T\Delta S^{\ddagger}$ the important factor affecting $\Delta G^{\ddagger}$. No particularly useful correlations were found between either $\Delta H^{\ddagger}$ or $\Delta S^{\ddagger}$ with ε_r, Z, E_T^N, DN or AN. However, the AN correlated well with $\Delta G_f^{\ddagger}$ as shown in Figure 3.27 below. As the acceptor number increases, $\Delta G_f^{\ddagger}$ increases linearly. Ethanol, **7** appears as an outlier on the right side of the plot. This plot is the mirror image of the plot of log k_1 versus the acceptor number in Figure 3.20 which might have been expected since $\Delta G^{\ddagger}$ and k are related by Equation 26.

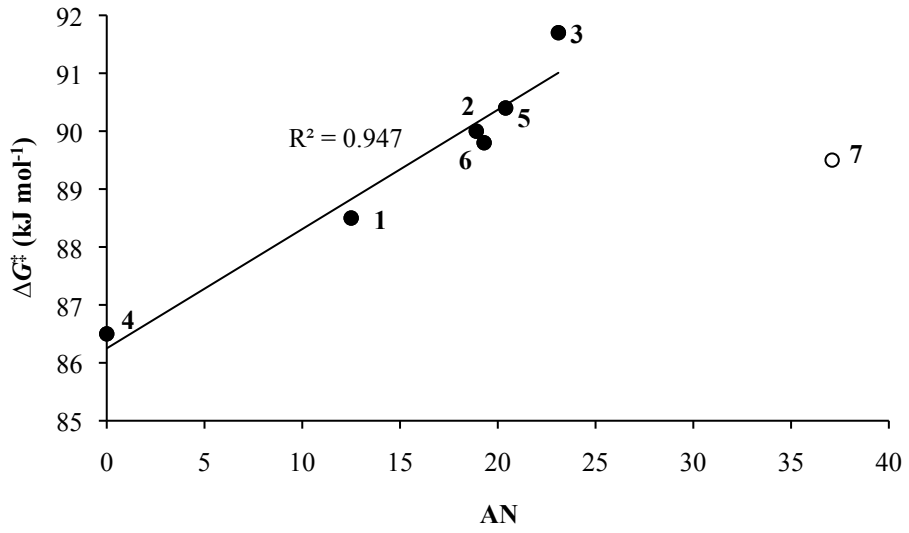


Figure 3.27. Plot of Gibbs free energy of activation versus the solvent acceptor number.

3.5. Conclusion

With this study the equilibrium constants and the forward and reverse rate constants for the 2-methyl-2-nitrosopropane dissociation reaction were successfully determined over a range of temperatures. Related thermodynamic and kinetic parameters for the reaction in each solvent were determined. The dependence of the rate and equilibrium constants on various solvent parameters was successfully established. The results of this project show that the effect of solvent on the dissociation reaction is dramatic. Attempts were made to correlate the magnitude of the equilibrium and rate constants with some commonly used solvent polarity scales each of which measures slightly different aspects of solvent polarity. Limited success was attained in that some

trends with a subset of the solvents were found, but no trends were found which could encompass the whole range of solvents used.

It was found that the solvent acceptor number is a major factor in determining the magnitude of both the equilibrium constant and the forward rate constant. The acceptor number was found to be linearly related with Gibbs free energy of activation with the exception of the strongly hydrogen bonding solvent ethanol appearing as an outlier.

The Kamlet-Taft multiparameter approach was successfully employed to express a complete relationship between the forward rate constant and specific solvent parameters. Solvent polarity followed by hydrogen bond acceptor ability or basicity and hydrogen bond donor ability or acidity were found to be the most important factors in determining the forward rate constant. The contribution to the rate constant from polarity/polarizability, hydrogen bond acceptor (HBA) ability or basicity, and hydrogen bond donor (HBD) ability or acidity was suggested by the individual correlations with ε_r, Z, E_T^N, DN and AN. However, the relative importance of each of these parameters is different for each solvent making it difficult to find single parameter correlations. The Kamlet-Taft analysis made it possible to determine the relative contribution of each parameter.

A general relationship between solvent viscosity and k_{-1} was found. As the solvent viscosity increased k_{-1} increased. By modifying the Kamlet-Taft equation to include solvent viscosity as a parameter, a multiparameter equation was found to include all seven solvents used in this study. Solvent polarity and viscosity were determined to be the major parameters affecting the value of k_{-1}.

Finally, using what was learned about the effects of various solvent parameters on k_1 and k_{-1}, a multiparameter equation was found relating solvent properties to K_{eq}. The major factors affecting the value of K_{eq} were determined to be (in order of decreasing contribution) the solvent's hydrogen bond accepting ability, hydrogen bond donating ability, viscosity and solvent polarity/polarizability.

3.6. References

1. Richter-Addo, G. B.; Legzdins, P., *Metal Nitrosyls*. Oxford University Press: New York, 1992.

2. Richter-Addo, G. B., Binding of Organic Nitroso Compounds to Metalloporphyrins. *Acc. Chem. Res.* **1999,** *32* (6), 529-536.

3. Lee, J.; Chen, L.; West, A. H.; Richter-Addo, G. B., Interactions of Organic Nitroso Compounds with Metals. *Chem. Rev.* **2002,** *102* (4), 1019-1065.

4. Cameron, M.; Gowenlock, B. G.; Vasapollo, G., Coordination Chemistry of C-Nitroso-Compounds. *Chem. Soc. Rev.* **1990,** *19* (4), 355-379.

5. Grishin, D. F.; Semyonycheva, L. L.; Kolyakina, E. V., 2-Methyl-2-nitrosopropane as a New Regulator of the Polymer Chain Growth. *Mendeleev Commun.* **1999,** (6), 250-251.

6. Schenkman, J. B.; Wilson, B. J.; Cinti, D. L., Diethylaminoethyl 2,2-Diphenylvalerate HCl (SKF 525-A) - *In vivo* and *in vitro* Effects of Metabolism by Rat Liver Microsomes - Formation of an Oxygenated Complex. *Biochem. Pharmacol.* **1972,** *21*, 2373-2383.

7. Franklin, M. R., The Formation of a 455 nm Complex During Cytochrome P-450-Dependent *N*-Hydroxyamphetamine Metabolism. *Mol. Pharmacol.* **1974,** *10* (6), 975-985.

8. Mansuy, D.; Beaune, P.; Cresteil, T.; Bacot, C.; Chottard, J.-C.; Gans, P., Formation of Complexes Between Microsomal Cytochrome. *Eur. J. Biochem.* **1978,** *86*, 573-579.

9. Chakrapani, H.; Bartberger, M. D.; Toone, E. J., C-Nitroso Donors of Nitric Oxide. *J. Org. Chem.* **2009,** *74* (4), 1450-1453.

10. Wang, P. G.; Xian, M.; Tang, X.; Wu, X.; Wen, Z.; Cai, T.; Janczuk, A. J., Nitric Oxide Donors: Chemical Activities and Biological Applications. *Chem. Rev.* **2002,** *102*, 1091-1134.

11. Gowenlock, B. G.; Richter-Addo, G. B., Preparations of C-Nitroso Compounds. *Chem. Rev.* **2004,** *104* (7), 3315-3340.

12. Gowenlock, B. G.; Richter-Addo, G. B., Dinitroso and Polynitroso Compounds. *Chem. Soc. Rev.* **2005,** *34* (9), 797-809.

13. Gowenlock, B. G.; Richter-Addo, G. B., The First 85 Years of C-Nitroso Compounds: A Survey of the Salient Features. *J. Chem. Educ.* **2008,** *85* (9), 1243-1245.

14. Stowell, J. C., *tert*-Alkylnitroso compounds. Synthesis and dimerization equilibriums. *J. Org. Chem.* **1971,** *36* (20), 3055-3056.

15. Guang-Zhi, X.; Jian-Wei, Z.; Yu-Xiang, Z.; Jing-Lain, K., Study of Dimer-Monomer Reversible Reaction of 2-Methyl-2-nitrosopropane. *Acta Chim. Sinica.* **1985,** *43*, 192-194.

16. Witanowski, M.; Sitkowski, J.; Biernat, S.; Kamienski, B.; Hamdi, B. T.; Webb, G. A., A Quantitative Nitrogen-14 NMR Study of the Dimerization Equilibria of 2-Methyl-2-nitrosopropane. *J. Magn. Reson.* **1985,** *63*, 354-359.

17. Homer, S. R.; McKinnon, S. J.; Whittenburg, S. J., A Series of Experiments with 2-Methyl-2-nitrosopropane. *J. Chem. Educ.* **1986,** *63*, 1103-1104.

18. Leenson, I. A., Thermodynamics and Kinetics of Chemical Equilibrium in Solution. Multipurpose Experiment in the Physical Chemistry Course. *J. Chem. Educ.* **1986,** *63*, 437-441.

19. Sergeev, G. B.; Leenson, I. A., Spectrophotometric Study of the Kinetics and the Thermodynamics of the Monomer-Dimer Equilibrium in Solutions of 2-Methyl-2-nitrosopropane. *Russ. J. Phys. Chem.* **1978,** *52* (3), 312-315.

20. Joshi, A.; Moss, H.; Riesz, P., ESR Study of the Post-Radiolysis Growth of Spin-Trapped Radicals in γ-Irradiated Aqueous Solutions of Thymine. *Int. J. Radiat. Biol. Relat. Stud. Phys., Chem. Med.* **1978,** *34*, 165-176.

21. Riesz, P.; Rustgi, S., Aqueous Radiation Chemistry of Protein and Nucleic Acid Constituents: ESR and Spin-Trapping Studies. *Radiat. Phys. Chem.* **1979,** *13*, 21-40.

22. Ohkuma, T.; Kirino, Y.; Kwan, T., Some Physicochemical Properties of 2-Methyl-2-nitrosopropane, Phenyl *N*-*tert*-Butyl Nitrone, 5,5-Dimethylpyrroline-*N*-oxide, and 2,5,5-Trimethylpyrroline-*N*-oxide and the Feasibility of their Use as Spin Traps in Aqueous Solution. *Chem. Pharm. Bull.* **1981,** *29* (1), 25-28.

23. Sergeev, G. B.; Batyuk, V. A.; Shabatina, T. I., Reactions in Liquid-Crystals - Thermodynamics and Kinetics for Establishment of the Monomer Dimer Equilibrium of 2-Methyl-2-nitrosopropane. *Kinet. Catal.* **1983,** *24* (3), 455-458.

24. Kimura, Y.; Yoshimura, Y.; Nakahara, M., Chemical-Reactions in the Medium Density Fluid - Anomaly in the Volume Profile of the Dimerization Reaction of 2-Methyl-2-nitrosopropane in Carbon-Dioxide. *Chem. Lett.* **1987,** (4), 617-620.

25. Orrell, K. G.; Stephenson, D.; Rault, T., NMR Study of the Monomer-Dimer Equilibria of Dimethylnitrosobenzenes in Solution. Identification of Mixed Azodioxy Dimeric Species. *Magn. Reson. Chem.* **1989,** *27* (4), 368-376.

26. Hoops, S.; Sahle, S.; Gauges, R.; Lee, C.; Pahle, J.; Simus, N.; Singhal, M.; Xu, L.; Mendes, P.; Kummer, U., COPASI — a COmplex PAthway SImulator. *Bioinformatics* **2006,** *22*, 3067-3074.

27. Dougherty, E.; Anslyn, E. V.; Anslyn, D. A., *Modern Physical Organic Chemistry*. University Science Books: 2005.

28. Isaacs, N., *Physical Organic Chemistry*. 2nd ed.; John Wiley & Sons: New York, 1995.

29. Pine, S. H., *Organic Chemistry*. McGraw-Hill: New York, 1987.

30. Reichardt, C., *Solvents and Solvent Effects in Organic Chemistry*. 3rd ed.; VCH: Weinheim, Federal Republic of Germany, 2003.

31. Hughes, E. D.; Ingold, C. K., Mechanism of Substitution at a Saturated Carbon Atom Part IV A Discussion of Constitutional and Solvent Effects on the Mechanism, Kinetics, Velocity, and Orientation of Substitution. *J. Chem. Soc.* **1935**, 244-255.

32. Hughes, E. D., Mechanism and Kinetics of Substitution at a Saturated Carbon Atom. *Trans. Faraday Soc.* **1941,** *37*, 603-631.

33. Yaws, C. L., *Chemical Properties Handbook: Physical, Thermodynamics, Engironmental Transport, Safety and Health Related Properties for Organic and Inorganic Chemical*. McGraw-Hill Professional Publishing: 1998.

34. Reichardt, C., Empirical Parameters of Solvent Polarity as Linear Free-Energy Relationships. *Angew. Chem., Int. Ed.* **1979,** *18* (2), 98-110.

35. Chipperfield, J., *Non-Aqueous Solvents*. Oxford University Press, Inc.: 1999.

36. Kosower, E. M., The Effect of Solvent on Spectra. I. A New Empirical Measure of Solvent Polarity: Z-Values. *J. Am. Chem. Soc.* **1958,** *80*, 3253-3260.

37. Kosower, E. M., The Effect of Solvent on Spectra. II. Correlation of Spectral Absorption Data with Z-values. *J. Am. Chem. Soc.* **1958,** *80*, 3261-3267.

38. Kosower, E. M., The Effect of Solvent on Spectra. III. The Use of Z-Values in Connection with Kinetic Data. *J. Am. Chem. Soc.* **1958,** *80*, 3267-3270.

39. Reichardt, C., Solvatochromic Dyes as Empirical Indicators of Solvent Polarity. *Chimia* **1991,** *45* (10), 322-324.

40. Reichardt, C., Solvatochromism, Thermochromism, Piezochromism, Halochromism, and Chiro-Solvatochromism of Pyridinium *N*-Phenoxide Betaine Dyes. *Chem. Soc. Rev.* **1992,** *21* (3), 147-153.

41. Mayer, U.; Gutmann, V.; Gerger, W., The Acceptor Number — A Quantitative Empirical Parameter for the Electrophilic Properties of Solvents. *Monatsh. Chem.* **1975,** *106* (6), 1235-1257.

42. Gutmann, V., Empirical Parameters for Donor and Acceptor Properties of Solvents. *Electrochim. Acta* **1976,** *21* (9), 661-670.

43. Gutmann, V., Solvent Effects on the Reactivities of Organometallic Compounds. *Coord. Chem. Rev.* **1976,** *18* (2), 225-255.

44. Gutmann, V.; Wychera, E., Coordination Reactions in Nonaqueous Solutions. The Role of the Donor Strength. *Inorg. Nucl. Chem. Lett.* **1966,** *2* (9), 257-260.

45. Connors, K. A., *Chemical Kinetics: The Study of Reaction Rates in Solution*. VCH Publishers, Inc.: New York, 1990.

46. Marcus, Y., The Properties of Organic Liquids that are Relevant to their Use as Solvating Solvents. *Chem. Soc. Rev.* **1993,** *22* (6), 409-416.

47. Buncel, E.; Rajagopal, S., Solvatochromism and Solvent Polarity Scales. *Acc. Chem. Res.* **1990,** *23* (7), 226-231.

48. Reichardt, C., Solvatochromic Dyes as Solvent Polarity Indicators. *Chem. Rev.* **1994,** *94* (8), 2319-2358.

49. Johnson, B. P.; Gabrielsen, B.; Matulenko, M.; Dorsey, J. G.; Reichardt, C., Solvatochromic Solvent Polarity Measurements in Analytical Chemistry: Synthesis and Applications of ET-30. *Anal. Lett.* **1986,** *19* (9-10), 939-962.

50. Osterby, B. R.; McKelvey, R. D., Convergent Synthesis of Betaine-30, a Solvatochromic Dye: An Advanced Undergraduate Project and Demonstration. *J. Chem. Educ.* **1996,** *73* (3), 260-261.

51. Deng, T.; Acree, W. E., Selection of an Analysis Wavelength: An Interesting Example Involving Solvatochromism and the Zwitterionic Dimroth-Reichardt's Betaine ET-30 Dye. *J. Chem. Educ.* **1999,** *76* (11), 1555-1556.

52. Vitha, M. F., Determining the Percent Water in Organic Solvents Using the Zwitterionic Dimroth-Reichardt Betaine ET-30 Dye. An Industrially Relevant Application of a Previously Published Laboratory Experiment. *J. Chem. Educ.* **2001,** *78* (3), 370-372.

53. Kamlet, M. J.; Abboud, J. L. M.; Abraham, M. H.; Taft, R. W., Linear Solvation Energy Relationships. 23. A Comprehensive Collection of the Solvatochromic Parameters, π^*, α, and β, and Some Methods for Simplifying the Generalized Solvatochromic Equation. *J. Org. Chem.* **1983,** *48* (17), 2877-2887.

54. Taft, R. W.; Kamlet, M. J., The Solvatochromic Comparison Method. 2. The α-Scale of Solvent Hydrogen-Bond Donor (HBD) Acidities. *J. Am. Chem. Soc.* **1976,** *98* (10), 2886-2894.

55. Kamlet, M. J.; Abboud, J. L.; Taft, R. W., The Solvatochromic Comparison Method. 6. The π* Scale of Solvent Polarities. *J. Am. Chem. Soc.* **1977,** *99* (18), 6027-6038.

56. Kamlet, M. J.; Taft, R. W., The Solvatochromic Comparison Method. I. The β-Scale of Solvent Hydrogen-Bond Acceptor (HBA) Basicities. *J. Am. Chem. Soc.* **1976,** *98* (2), 377-383.

57. Batt, L.; Gowenlock, B. G., Kinetic and Structural Studies of trans-Dimeric 3-Methyl-3-Nitrosobutan-2-one. *J. Chem. Soc.* **1960**, 376-380.

Epilogue

The ultimate goal of any research project is to disseminate the results in a way that will benefit society, be it through publication in peer reviewed journals, through oral presentations or through teaching. One of my original goals for this work was to take graduate level research and introduce and incorporate it into an undergraduate educational setting. It is well known that many of the experiments currently used in typical undergraduate laboratories are dated. While they are useful for some teaching purposes, they do not directly relate to the state of the scientific art, and as a result often do not engage student learning in a way that makes them excited about science and want to learn more. In this modern age when scientific based television and the internet are quite compelling, many students expect to take science courses that at least somewhat resemble what they are exposed to by the media

In the early days of my graduate work at OU, I contributed to a paper for the *Journal of Electroanalytical Chemistry* which involved the monitoring of electrogenerated species on the surface of an electrode with a newly-designed (in our laboratory) fiber-optic probe system. This work involved the combination of two classic technologies (infrared spectroscopy and electrochemistry) put together in a new way to make what had been a more cumbersome approach (the use of optically transparent thin layer electrodes; OTTLEs) more straightforward and "undergraduate friendly". I found working on this project compelling and it occurred to me that this technology could be used as an exciting teaching tool in the undergraduate laboratory setting. I was also convinced that it could be a useful method around which I could design undergraduate *research* projects.

Many undergraduates experience research for the first time when they are enrolled in their discipline's Senior Capstone course. The projects in this dissertation lend themselves well to being starting points for multiple undergraduate research experiences and/or Capstone projects. The varied concepts involved in both of these projects are a combination of (i) those covered in the typical undergraduate course curriculum, and (ii) new ones that have not yet found their way into typical undergraduate-level courses and laboratories. The experience of learning these concepts in a research environment will be very valuable to the students and will allow them to gain access to advanced techniques and instrumentation which will make learning much more engaging.

In the Summer 2005, Summer 2008, and Fall 2008 semesters, I had the opportunity to teach the General Chemistry sequence here at OU. Having had those experiences and the experience of participating in guest electrochemistry lectures at Langston University in 2009 and 2010 (where I incorporated some of my dissertation work into the guest lectures), I am more convinced than ever that developing unique and engaging research experiences for undergraduates will help promote student learning.

The DNIC project (Chapter 2) and the RNO project (Chapter 3) in this dissertation have the potential to be expanded by instructors of chemistry into experiences for undergraduates that will be much more compelling than the current slate of experiments used. That, in part, is my desire for the future of this work.